STUDIES IN RADIOCARBON GEOCHEMISTRY

A

THESIS

SUBMITTED FOR THE DEGREE OF

DOCTOR OF PHILOSOPHY

IN THE

UNIVERSITY OF GLASGOW

BY

NINA D. DRNDARSKI

DEPARTMENT OF CHEMISTRY

AUGUST 1977

ProQuest LLC.
789 East Eisenhower Parkway
P.O. Box 1346
Ann Arbor, MI 48106 – 1346

ACKNOWLEDGEMENTS

Here, I wish to express my deepest gratitude to my supervisor, Dr M.S. Baxter, for his guidance throughout this project and particularly for constructive and indispensable criticism of the thesis in manuscript. I would also warmly thank my colleagues John Campbell, Ian McKinley, David Swan and Ron Crawford, with whom I have had many professional discussions that are precious to me, and who encouraged me to persist in this work. I am also grateful to Jack Baldwin for his help in patiently transforming my manuscript into typescript. Finally, I express my thanks to numerous other individuals who have contributed in various ways to the completion of my thesis.

LIST OF CONTENTS

PART ONE: ATMOSPHERIC RADIOCARBON AND THE 11-YEAR SOLAR CYCLE

LIST OF FIGURES

PART ONE

Chapter 1.

Chapter 2.

LIST OF TABLES

Chapter 4.

SUMMARY

This study relates to two discrete areas of radiocarbon geochemistry:

(1) Recent work has questioned the assumed constancy of natural radiocarbon concentrations over short time intervals of 11 years and has thus implied the reduced effectiveness of present calibration curves in the age-correction of short-lived dating samples. Annual atmospheric C-14 concentrations have therefore been studied through analysis of single tree rings. Natural radiocarbon fluctuations over the 11-year sunspot cycle cannot be unambiguously identified but statistical treatment of all available data suggests that cycles of variable period and amplitude may occur.

(2) In the Clyde sea area a large excess of fossil carbon from fuels and industrial wastes has been deposited, thus diluting natural C-14 concentrations and producing abnormally old ages near surface sediments. Radiocarbon analysis of sediments enables fossil carbon pollution indices to be estimated for the Clyde sea area. In addition, points of radiocarbon inversion in sediment profiles are consistent with commencement of large-scale industrial pollution of the area around 200 years ago. A source of natural fossil carbon in the area is also evident.

In Loch Lomond the natural sedimentation rate is estimated to be 0.40 ± 0.12 mm y^{-1}. A marine incursion into Loch Lomond is dated at 6500 y B.P.

PART ONE

ATMOSPHERIC RADIOCARBON AND THE 11-YEAR SOLAR CYCLE

CHAPTER 1. INTRODUCTION.

In 1946, W.F. Libby postulated that it should be possible to detect the radioactivity emitted by the cosmogenic radionuclide carbon-14 in samples taken from the atmosphere or in terrestrial samples which have exchanged with carbon dioxide from the atmosphere. Libby and his co-workers, Anderson, Weinhouse, Reid, Kirschenbaum and Grosse (1947) then proceeded to prove by experiment that the radioactivity of carbon-14 could be detected and suggested its use as a method of dating.

The application to age determination depends on the fact that all living matter acquires a minute proportion of the radioactive isotope of carbon, C-14, along with the atmospheric carbon dioxide assimilated by living vegetation. The proportion of the radioactive isotope in living tissue should, therefore, be the same as in atmospheric carbon dioxide. From the moment of death the radioactive carbon fixed in vegetation decays at known (exponential) rate, without replenishment. After about 5730 years (Godwin, 1962) the radiocarbon activity falls to half the original value; after a further lapse of 5730 years (the half-life of radiocarbon) the inventory is halved again, etc. The approximate date of death can therefore be estimated by accurate assay of the radioactivity still remaining in any sample. However, it is only in rare cases that a sample will have aged some multiple of 5730 years. Therefore, for realistic age calculations it is necessary to apply the equation which relates

the C-14 activity to time or:

$$A_t = A_o e^{-\lambda t}$$

This equation states that the activity, (A_t), in the tissue at any given time, t, after formation is equal to the original specific activity (A_o), times e (the base of the natural logarithmic system) to the power $-\lambda t$, where λ is the decay constant of carbon-14 which is related to the radioactive half-life, $t_{1/2}$, by the equation:

$$\lambda = \frac{\ln 2}{t_{1/2}}$$

Thus knowing A_o, the initial specific activity, and λ, it is possible to calculate the age, t, of a sample - the time during which decay of carbon-14 has taken place - from the measurement of its residual activity, A_t,:

$$t = 8200 \ln \frac{A_o}{A_t}$$

Age estimates obtained in this way depend on the fundamental assumption of radiocarbon dating that the minute proportion (ca. 10^{-10}%) of radioactive carbon in atmospheric carbon dioxide is always and everywhere the same, and that it has been so over the last 40,000 years - the period for which samples still contain enough radioactivity for measurement. (At an age of $\sim$ 40,000 years, less than 1% of the original carbon-14 atoms remain.)

Radioactive carbon atoms originate in the upper atmosphere. As galactic cosmic ray primary particles (mostly protons) enter the earth's atmosphere, they continually produce showers of

secondary radiation, including neutrons, at high altitude (up to 1.6 km). Most of the neutrons collide and react with nitrogen atoms (nitrogen gas makes up 80% of the atmosphere); few survive to reach ground level.

A neutron entering a nitrogen-14 nucleus can effectively replace a proton according to the reaction:

$$^{1}_{0}n + ^{14}_{7}N \longrightarrow ^{14}_{6}C + ^{1}_{1}H$$

The product ^{14}C atom, tending to have a neutron excess, is radioactive by negatron decay, according to:

$$^{14}_{6}C \longrightarrow ^{14}_{7}N + ^{0}_{-1}\beta$$

The decay of a carbon-14 atom can therefore be detected via the ionisation produced in a gas or liquid by the ejected beta particle. This is the basic principle of modern radiocarbon counting methods.

Production rate and decay of carbon-14.

A small number of radiocarbon atoms are produced in the atmosphere each second for each square centimetre of the earth's surface. Lingenfelter and Ramaty (1970) have calculated the production rates of radiocarbon from measured energy spectra and cosmic ray flux data in the high atmosphere at solar minima and solar maxima. The latitude dependence of the neutron and carbon-14 production rates by galactic cosmic rays is quantified in Table 1.1. Including data records from the Cheltenham ionisation chamber back to 1937, Lingenfelter and Ramaty found a three solar cycle average (1937-1967) production rate of

TABLE 1.1 COSMIC-RAY NEUTRON AND C-14 PRODUCTION RATES

(N AND C-14 CM^{-2} SEC^{-1})

	SOLAR MINIMUM, 1953-1954		SOLAR MAXIMUM, 1957-1958	
GEOMAGNETIC LATITUDE	NEUTRON	C-14	NEUTRON	C-14
0	1.37	0.91	1.31	0.86
10	1.42	0.94	1.35	0.89
20	1.72	1.13	1.61	1.07
30	2.56	1.70	2.28	1.51
40	4.27	2.80	3.46	2.27
50	6.53	4.20	4.95	3.19
60	7.92	4.88	5.61	3.50
70-90	3.81	4.99	5.61	3.50
GLOBAL AVERAGE	3.81	2.42	2.99	1.93

(AFTER LINGENFELTER AND RAMATY, 1970)

2.2 ± 0.4 carbon-14 atoms per cm^2 per second. Furthermore, the same workers (Lingenfelter and Ramaty, 1970) later estimated an additional solar flare contribution to carbon-14 production. Thus, the solar flare carbon-14 production rate averaged over the 11-year solar cycle lies between 0.31 and 0.12 carbon-14 atoms per cm^2 per second, between 14 per cent-6 per cent of the cosmic ray carbon-14 production. The production rates, normalised to an incident solar-particle flux of 1 proton cm^{-2} sec^{-1} of energy greater than 30 MeV, are shown in Table 1.2.

Assuming a steady state model for the carbon cycle, the global average rate of radiocarbon disintegration should be balanced by the above rate of formation. By determining the activity of modern wood over a wide range of both latitude and altitude, Anderson (Libby, 1965) showed in the early days that within the then relatively wide experimental limits there were no major differences in carbon-14 specific activity (Table 1.3). Their mean value for the carbon-14 decay rate, however, differs outside error with the more recently accepted value of 13.56 ± 0.07 disintegrations per minute per gram of carbon (Karlen et al., 1964). Furthermore, a specific activity of 13.56 dpm/g carbon corresponds to a mean global carbon-14 decay rate of 1.63 dps cm^{-2}, considerably below the estimated production rate of 2.2 ± 0.4 atoms C sec^{-1} cm^{-2}. Therefore the decay and production rates of radiocarbon appear to be imbalanced. Possibly, the present day production rate is

TABLE 1.2 SOLAR FLARE C-14 PRODUCTION

SOLAR FLARE	φ_p (>30MEV) $p\ CM^{-2}\ SEC^{-1}$	P_o (MV)	YEARLY AVER. PROD. RATE OF C-14 $CM^{-2}\ SEC^{-1}$	
			NORMAL CUT OFF	20% NORMAL CUT OFF
1956 FEB.23	6.5X10	325	0.860	2.330
1957 JAN.20	3.0X10	60	0.006	0.015
1958 MAR.23	2.0X10	55	0.004	0.009
JULY 7	3.0X10	55	0.005	0.0013
1959 MAY 10	7.0X10	60	0.013	0.034
JULY 10	8.8X10	90	0.039	0.098
JULY 14	1.1X10	70	0.030	0.072
JULY 16	8.1X10	110	0.055	0.140
1960 NOV.12	1.4X10	145	0.180	0.450
NOV.15	5.2X10	135	0.056	0.140
1961 JULY 12	1.0X10	50	0.002	0.004
JULY 18	2.1X10	135	0.023	0.057

(AFTER LINGENFELTER AND RAMATY, 1970)

TABLE 1.3 SPECIFIC ACTIVITY FOR C-14 FROM DIFFERENT GEOMAG. LATITUDES

SOURCE	LATIT.	ACTIVITY (dpm/gC)
WHITE SPRUCE, YUKON	60° N	14.84±0.30
NORWEG. SPRUCE, SWEDEN	55° N	15.37±0.54
ELMWOOD, CHICAGO	53° N	14.72±0.54
FRAXIMUS EXCELSION, SWITZ.	49° N	15.16±0.38
HONEYSUCKLE LEAV., OAK RIDGE	47° N	14.60±0.30
PINE TWIGS, NEW MEXICO	44° N	15.82±0.47
BIAR N.AFRICA	40° N	14.47±0.44
OAK, PALESTINE	34° N	15.19±0.40
WOOD, IRAN	28° N	15.57±0.31
FRAXIMUS MANDSHURICA, JAPAN	26° N	14.84±0.30
WOOD, PANAMA	20° N	15.94±0.51
CHLOROPH. EXCELSA, LIBERIA	11° N	15.08±0.34
STERCULIA EXC., COPACABANA	1° N	15.47±0.50
IRON WOOD, BOLIVIA	0	14.53±0.60
WOOD, CEYLON	2° S	15.29±0.67
BEECHWOOD, TIERRADEL FUEGO	45° S	15.37±0.49
EUCALYPTUS, NSW AUSTRALIA	45° S	16.31±0.43
SEAL OIL, ANTARTICA	65° S	15.69±0.30
AVERAGE		15.30±0.10

significantly higher than the average production rate over the last 8,200 years (the mean life of carbon-14) so that the present day inventory does not correspond to the equilibrium value but is increasing (Lal and Suess, 1968). Alternatively, Damon & Wallick (1971) have suggested that if 1.1 x 10^{15} grams of carbon are stored as sediment each year (a much higher sedimentation flux than values proposed by earlier workers) then the above discrepancy is removed.

Distribution of carbon-14

On production, radiocarbon is readily oxidised to appear as a minute contribution to the atmospheric carbon dioxide inventory (Libby 1946; 1955). Thereafter incorporation of carbon-14 into the various carbon reservoirs occurs via the well-known carbon cycle (Figure 1.1). As shown in Figure 1.1 the reservoirs within the carbon cycle may be subdivided into a dynamic system, in which carbon is exchanged on time scales short relative to the carbon-14 half-life, and a sedimentary system, which includes rock weathering and precipitation/dissolution of carbonaceous sediments in the oceans. The sedimentary system of the carbon cycle is estimated to turnover carbon once every 10^5 years (Brown, 1957), during which time radiocarbon initially present decays to negligible levels.

The oceans themseleves do not represent a uniformly mixed reservoir. A surface layer which extends to a depth of approximately 100 metres is well mixed by the action of wind and waves and contains the majority of marine life. The deep

Fig. 1.1 The Carbon Cycle

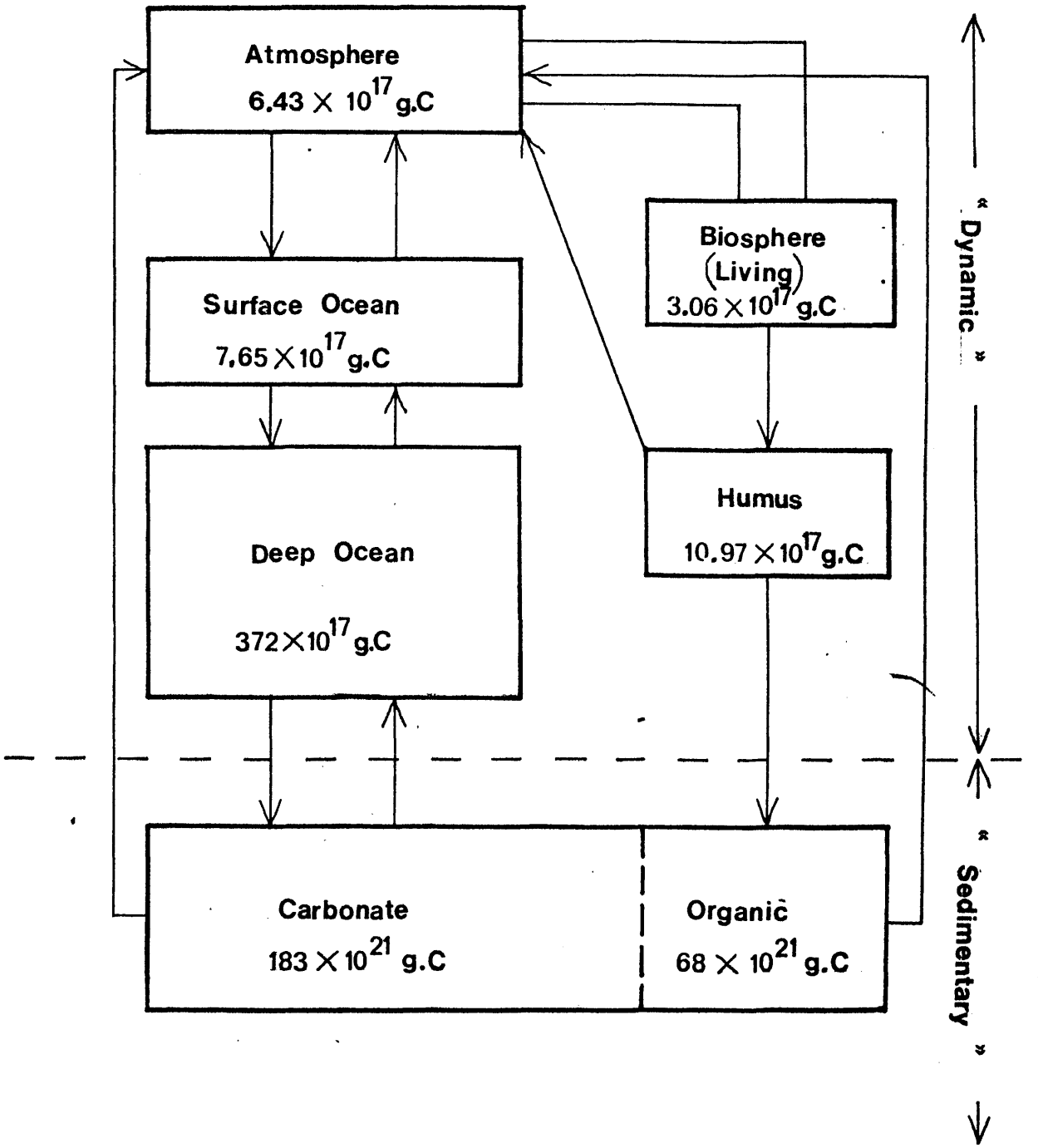

ocean, however, mixes very slowly on a time scale in the order of a thousand years.

The first estimate, based on radiocarbon, of the residence time of carbon dioxide in the atmosphere was calculated by Revelle and Suess (1957) to be about 10 years. However, using carbon-14 produced by nuclear explosions, Hagemann, Gray, Machta and Turkevich (1959) calculated a mean atmosphere residence time of 5 years. Rafter and O'Brien (1970) later defined the mean residence time of carbon-14 in the troposphere to be 9.4 years and taking into consideration an 18 per cent loss to the biosphere, the mean transfer time between the troposphere and the ocean was estimated to be 12 years. These workers also calculated that the mean residence time of a carbon-14 atom in the surface ocean before being mixed into the deep ocean is around 4.5 years.

In comparison with time constants for atmosphere/ocean and surface/deep ocean exchange processes, the mixing of the atmosphere is a fast process. From observations on artificial activities it was shown that tropospheric mixing between the hemispheres requires about 18 months (Nydal, 1966), while the exchange time between the atmosphere and vegetation is also rapid (Broecker & Walton, 1959). Thus, the carbon-14 activity of grasses and cereals is the same as the carbon-14 activity of the atmosphere during their respective growth periods.

Application of carbon-14

Because of its convenient half-life and of the common and

world-wide occurence of material containing carbon, the radiocarbon dating method has been used extensively in the fields of archaeology and anthropology. More recently the method has been used to evaluate rates of marine and freshwater sedimentation, late Pleistocene geology and climate and, also, the dates of meteorite falls. Furthermore, carbon-14 is so far the only cosmic-ray produced radioisotope which has been shown to follow time-dependent changes in atmospheric concentration during the last 10,000 years (Suess, 1965). Therefore, both natural and artificial fluctuations of atmospheric carbon-14 are significant in geochemistry and geochronology because they offer an opportunity to evaluate rates and mechanisms of carbon exchange and distribution.

1.1 Natural fluctuations of atmospheric carbon-14 concentration.

Differences between historical and radiocarbon dates of archaeological specimens were observed early in the development of radiocarbon dating. These led many investigators to study in detail the variations in radiocarbon concentration which have occurred during the past millenia. Indeed, the information gathered over the last 20 years shows that the C-14/C-12 ratio has been far from constant with time (de Vries, 1958; Willis et al., 1960; Suess, 1965; Dyck, 1965; Damon et al., 1966; Stuiver, 1967; Stuiver, 1970; Lerman et al., 1970; Suess, 1970; Vogel, 1970; Baxter and Walton, 1971; Damon et al., 1973; Lavrukhina et al., 1973; Alekseyev et al., 1974; Dergachev et al., 1974; Kocharov et al., 1974; Cain and Suess, 1976; Stuiver, 1976).

A deviation of 1 per cent in atmospheric carbon-14 concentration alters the subsequent radiocarbon age by about 80 years. Thus, as the fluctuations represent deviations from the basic assumption of the radiocarbon dating method, a documented record of the main trends of secular carbon-14 variations is of the utmost importance. Furthermore, a knowledge of the magnitude and deviations of carbon-14 variations could improve the understanding of the geochemical and geophysical processes which control carbon-14 production and distribution.

To measure past carbon-14 levels the dendrochronologically dated annual growth rings of long-lived trees are analysed. In particular, for this purpose and associated calibration of the radiocarbon timescale, the bristlecone pine tree ring chronology, as established by Ferguson (1969), has been applied. This chronology covers more than 8,000 years (Ferguson, 1968, 1969). More recently, European tree ring sequences have been assembled from oak trees excavated from river gravel beds and from peat bogs. Continuous tree ring chronologies have been derived, covering the time from the present back to about 350 B.C. (Becker, 1975), as well as so called "floating" tree ring sequences embracing several hundred years each, from periods dating back to late glacial times.

The detection of past fluctuations of atmospheric carbon-14 can also be achieved by radiocarbon analysis of lake sediments. The Swedish varve clay chronology of de Geer (1940) has been used in the measurement of carbon-14 contents back to

12,500 years B.P. (Tauber, 1970). The other major varve series used for this purpose is from Lake of the Clouds, Minnesota. Direct measurements on the organic matter present (Stuiver, 1970; 1970A) have provided data on carbon-14 levels during the past 10,000 years. The method is, however, less sensitive than wood assay because of the chemically open nature of the sediments.

1.1.1. Long-term fluctuations of atmospheric carbon-14 concentration

Variations in the content of carbon-14 in atmospheric carbon dioxide may be caused by:

1. changes in the production rate of radiocarbon as a consequence of variations in cosmic-ray flux through modulation of its galactic component by the dipole moment of the earth.
2. changes associated with climate variations i.e. changes in geochemical exchange and transfer rates of carbon between its reservoirs.

Geomagnetic field intensity modulated cosmic-rays

Low-energy cosmic-ray particles are subjected to greater deflection in magnetic fields than those of higher energy. Thus, when the earth's magnetic field is enhanced, a reduced flux of cosmic-ray particles reaches the upper atmosphere where carbon-14 production occurs. Therefore, a decrease in the earth's magnetic dipole field intensity (i.e. the dipole moment) is followed by an increase in cosmic-ray flux at the

earth and thus by a consequent increase in the production rate of radiocarbon (Elsasser et al., 1956). According to the hydromagnetic theory the earth's magnetic field is defined by movements in the liquid core. Westward drift of the non-dipole magnetic field, evidence that part of the earth's core is liquid, is estimated to be due to the different angular velocities of rotation of the mantle and upper core. Thus, ascending and descending convective fluid motions on the boundary between core and mantle may induce increases and decreases of the non-dipole field and cause changes of the earth's magnetic moment (Bucha 1963, 1967). Bucha (1970) has calculated that a deviation of 1 per cent in carbon-14 production rate corresponds to a causal change of 0.645×10^{25} gauss cm^3 of the earth's magnetic moment. Figure 1.2 compares the geomagnetic moment changes (curve a) with carbon-14 deviations, based on the 5730 year half-life, (according to Suess, 1969, curve b) using a slightly different constant for carbon-14 specific activity (15.84 dpm/gC than that which Libby used (1955); c is the smoothed sinusoidal curve for both geomagnetic-moment changes and carbon-14 deviations. Its period is approximately 8900 years; d is the sinusoidal curve for carbon-14 deviations (5568 half-life). The geomagnetism curve has its maximum around 400 B.C. when the intensity of the magnetic field reached 1.6 times its present value, and its minimum around 4000 B.C., when the intensity decreased to around 0.5 times its present value. Furthermore, the increase of

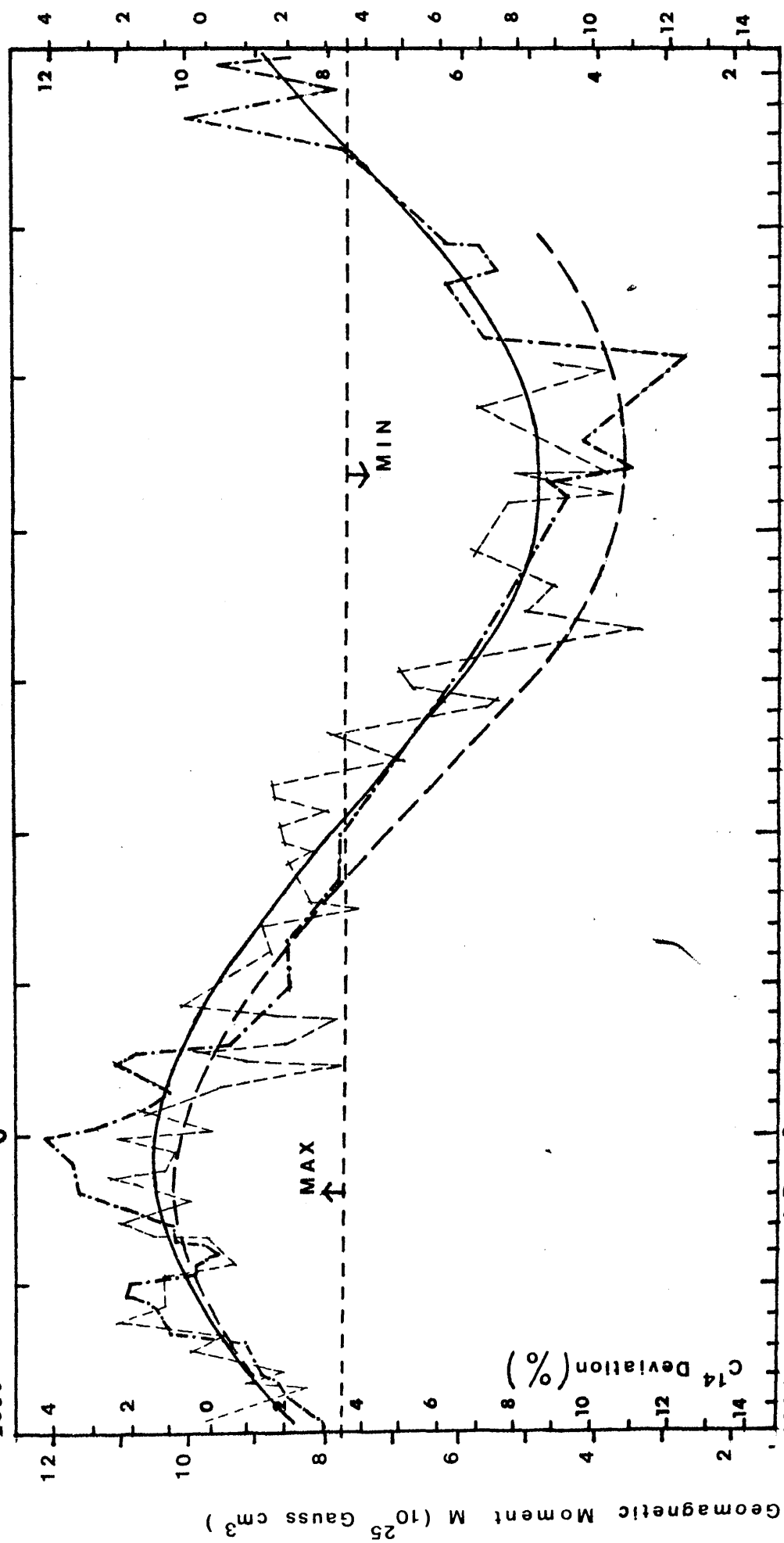

Fig. 1.2 Variations of the Geomagnetic Moment and Atmospheric Carbon-14 Concentrations in the past. (After Bucha, 1970)

magnetic moment around 900 A.D. and A.D. 1200 as well as between 1 A.D. and 700 B.C., are accompanied by decreases in carbon-14 levels (Bucha, 1970).

Suess (1970) has implied that the long-term carbon-14 variation represented by the sine wave agrees quantitatively with the expected change in production rate of carbon-14 resulting from the changes in geomagnetic dipole moment as given by Bucha. Furthermore, the relative carbon-14 production rates could be obtained from Bucha's paleomagnetic data, assuming that these rates are proportional to the geomagnetic dipole moment to the power -0.52 as derived by Elsasser et al. (1956). Suess (1970) calculated, using the computer programme of Houtermans, that the period of the sine wave is 8000 years, which corresponds to the period of 10,350 years obtained for the long-term carbon-14 variation. The amplitude of the sine wave is 33 per cent i.e. the carbon-14 production rate was a factor of 2.0 higher during the time of minimum geomagnetic moment (5260 B.C.) than during its maximum around 330 B.C.

Stuiver (1970) has similarly shown that changes in the earth's magnetic dipole moment and atmospheric carbon-14 concentration seem correlated, especially for the carbon-14 maximum at 6000 years B.C. The earth's magnetic dipole moment increased by at least a factor of 1.8 between 6000 and 1500 B.C.; such a change should have resulted in an approximately 30 per cent reduction in the carbon-14 production rate.

Furthermore, Damon (1968) has found that the average deviation of atmospheric carbon-14 from the A.D. 1890 standard, rises to +9 to +12 per cent around 4000 B.C., but falls back to the modern level around 6500 B.C., to -9 per cent around 8000 to 9000 B.C. and to -5 per cent near 10,000 B.C.

The characteristics of the earth's magnetic field during the past 40,000 years can be found by archaeomagnetic measurements on sedimentary rocks (loesses) (Bucha, 1970). Damon (1970) pointed out that if it is assumed that the total geomagnetic intensity was at a maximum around 500 B.C. in accordance with Bucha's data, there is rather a good correspondence between carbon-14 and geomagnetic data.

Climatic changes

Many authors have pointed out that climatic conditions can influence the carbon-14 distribution between atmosphere and ocean bicarbonates (de Vries, 1958; Damon, 1968; Suess, 1968; Labeyrie et al., 1970; Lal and Venkatavaradan, 1970). The mean global temperature determines the carbon dioxide concentration in the atmosphere as well as the extent and position of the thermocline i.e. the layer of high temperature gradient which separates ocean surface waters from deep waters.

Therefore, a decrease in mean global temperatures will lead to a decrease in the partial pressure of carbon dioxide in the atmosphere due to its approximately 10 ppm excess solubility per ^{o}C fall in temperature (Lal and Venkatavaradan

1970; Suess, 1970). Furthermore, such a decrease in temperature will also weaken the thermocline layer of the oceans and will lead to an increase in area of the high latitude oceans where the thermocline layer is absent. This must tend to bring to the surface more water from the ocean deep which has been long out of contact with the atmosphere and, therefore, deficient in carbon-14. For this reason the exchange of carbon dioxide between atmosphere and ocean should initiate a decrease rather than an increase of carbon-14 in the atmosphere (Lal and Venkatavaradan, 1970; Suess, 1970). Furthermore, if the long-term variation in carbon-14 content on a time-scale of 10,000 years is attributed to the climatic optimum between 6000 and 3000 B.C. (Damon, 1968), then it can be calculated that during the climatic optimum the radiocarbon transfer into the oceans must have been slower than it is at present by a factor of 1.5 (Suess, 1970). However, Suess (1970) estimated that it is unlikely that a difference in mean temperature of about 2 to 3 degrees could have a profound change in transfer rate. However, the observed carbon-14 variations indeed show a correlation with the more general patterns of climatic change (Lamb, 1961; Lamb et al., 1966). Thus during the "little Ice Age" the carbon-14 content of the atmosphere was rising during the 15th and 17th centuries. Furthermore, Schell et al. (1965) have shown that world-wide melting of glaciers may have caused the long-term decrease of $\sim$10 per cent in atmospheric carbon-14 from ca. 8000 B.C.

through both an increase in ocean volume and a contribution of old carbon locked in the ice.

Labeyrie et al. (1970) have suggested that the very important warm period at the end of the Würm which started at about 15,000 B.C. and lasted till 10,000 B.C. (the temperature variation was about 15 times more important than those which have occurred since 10,000 B.C.) was too slow to induce an important carbon-14 change. Furthermore, the short Alleröd warm oscillation, characterised by an abrupt increase in temperature between about 12,000 and 11,500 B.C. followed by a rapid decrease from 11,500 to 11,000 B.C. and a subsequent increase from about 10,800 to 10,500 B.C. may have caused an inverse fluctuation of several per cent in atmospheric carbon-14. However, the tree-ring chronology stops at about 7000 B.C. and the lake-varve chronology (Stuiver, 1967) is too imprecise to show it.

It seems likely therefore that the geomagnetic and climatic perturbations are superimposed. Thus many accurate measurements are needed to evaluate the important second-order climatic effect so that limits can be set on the factors governing the stability of the ambient carbon-14 reservoirs (Damon, 1970).

1.1.2 Short-term fluctuations of atmospheric carbon-14 concentration

The terrestrial incidence of cosmic rays is reduced at times of solar disturbance, probably through their enhanced

deflection from the earth by powerful, though temporary, magnetic fields associated with streams of solar corpuscles (which produce at the same time great disturbances of the earth's magnetic field known as geomagnetic storms). Direct measurement of cosmic-ray intensity over the last three solar cycles (Lingenfelter, 1963, 1970) has confirmed this empirically derived relationship. A solar cycle model constructed by Grey (1969), based on sunspot numbers estimated by Schove (1955) for the period 1200 A.D. to 1600 A.D., shows excellent agreement between experimentally observed carbon-14 fluctuations and those calculated from solar cycle data (Figure 1.3). It has been proved that solar modulation of the galactic cosmic-ray flux can produce variations in the carbon-14 production rate (about 30 per cent) sufficient to cause short-term carbon-14 variations of duration 50 to 200 years, amplitude 2 to 3 per cent and in negative correlation with sunspot number (Willis et al., 1960; Stuiver, 1961; Lingenfelter, 1963; Suess, 1965; Stuiver, 1965; Houtermans, 1966). Indeed, repeated careful radiocarbon measurements by Willis (1960) and subsequently by Suess (1965) on materials of known age have shown that between about A.D. 1300 and 1800 samples are generally rich in carbon-14 by 1 to 3 per cent (Figure 1.4), thus implying a weakened output of corpuscular streams from the sun during much of that time. That there may be a connection between the periods of implied quiescence of solar flare activity and the cold climatic period between about 1430 and 1850 A.D. is indicated by a

Fig.1.3 Observed and Calculated Atmospheric Carbon-14 Concentrations

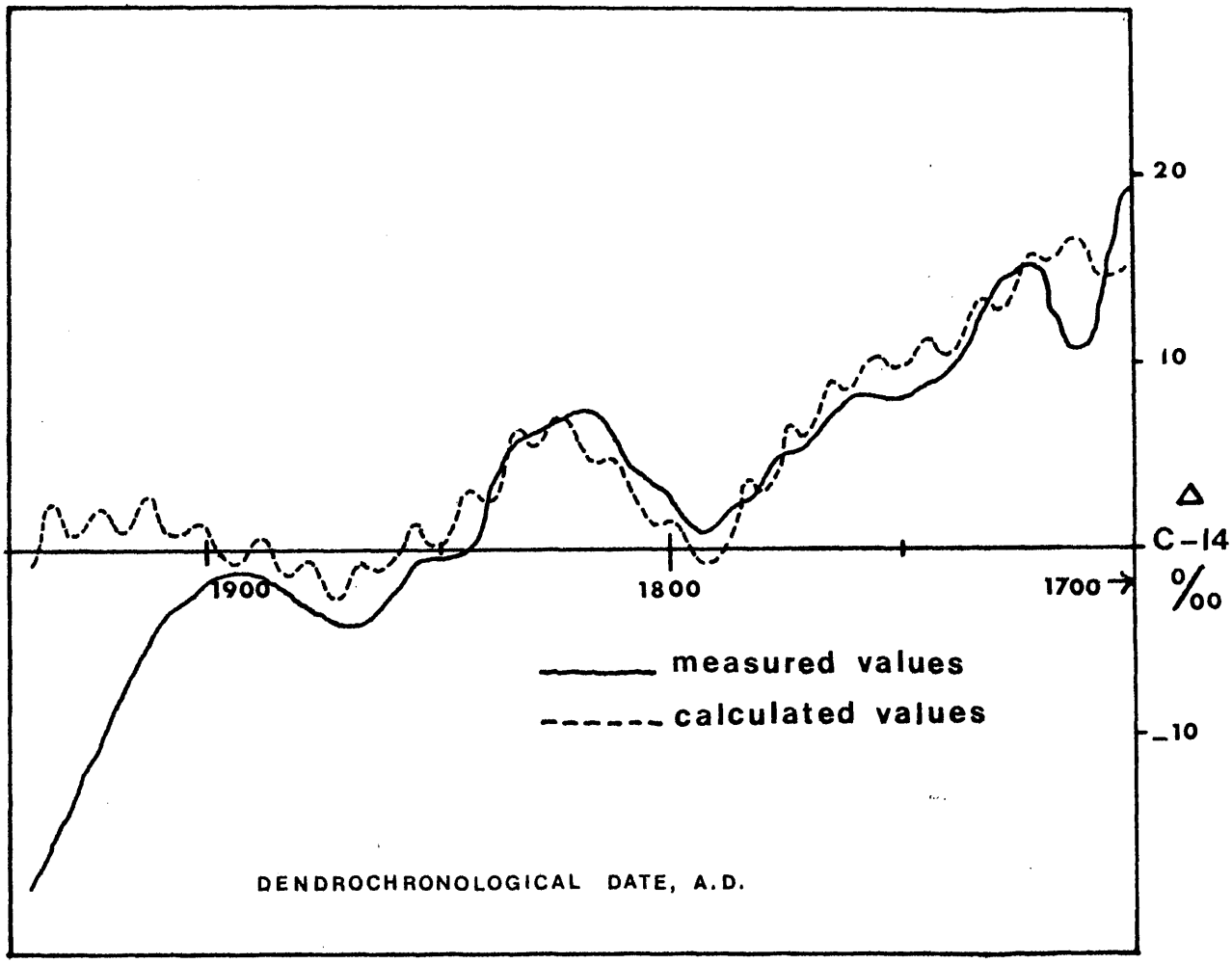

Fig. 1.4 Variations of Carbon-14 Content in the Atmosphere Since 1100 BC.

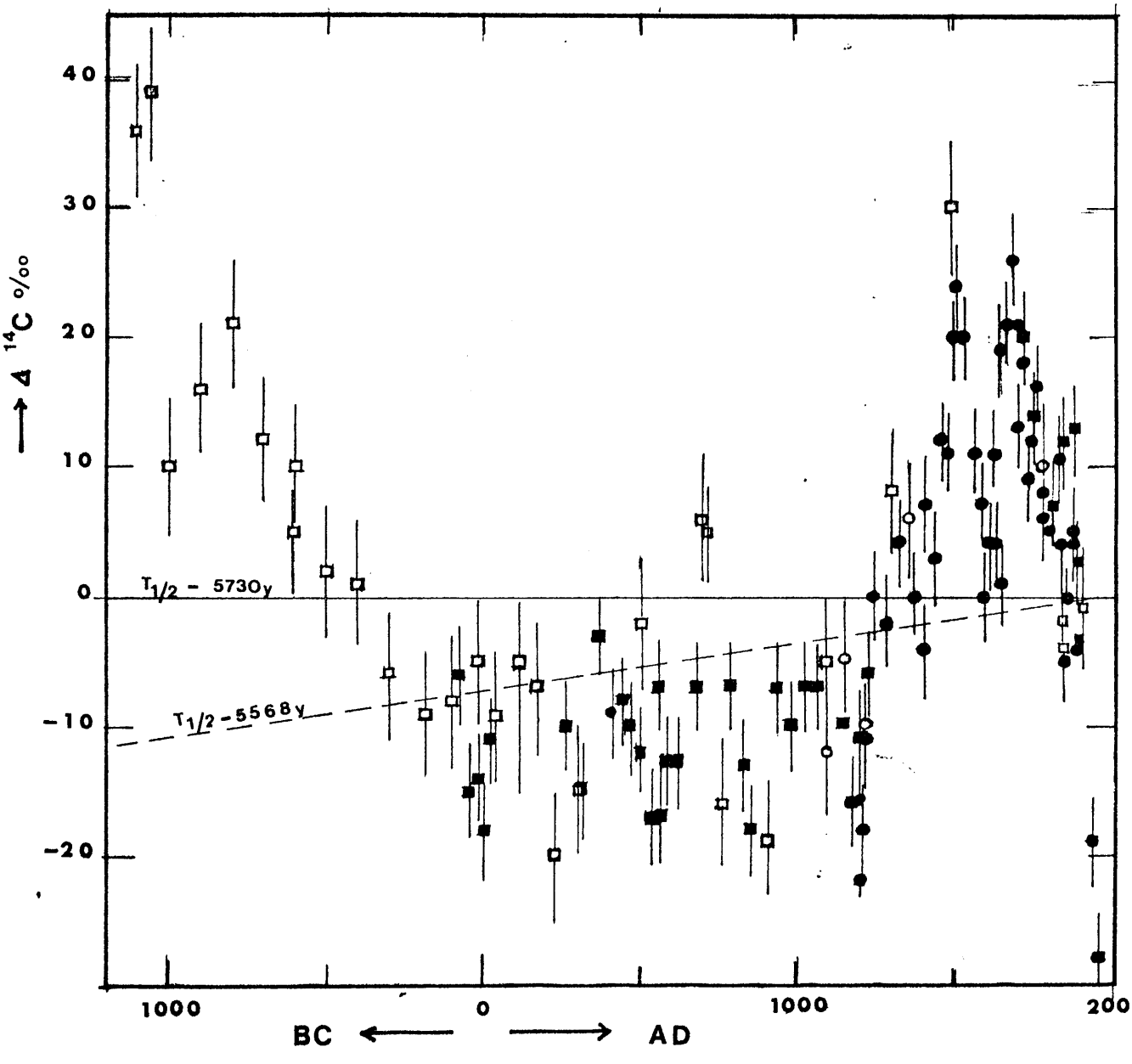

● DENOTES EUROPEAN TREES COUNTED FOR TWO DAYS.

● .. .. FOUR ..

■ DENOTES AMERICAN TREES COUNTED FOR TWO DAYS.

■ .. .. FOUR ..

(AFTER SUESS, 1965)

correlation coefficient of -0.80 between successive 50 year mean values of carbon-14 and temperatures prevailing in England a century and a half later, both series extending over 1150 years since A.D. 650 and A.D. 800 respectively (Lamb, 1965) (Figure 1.5). Suess (1968) has indicated that other marked increases of radiocarbon in the atmosphere occurred for a few centuries around 1000 B.C. and at some earlier times (about 3300 B.C.) - similar to that around A.D. 1500-1700 - which may have been associated with the fluctuation towards sharply colder climates. An approximately 200 year oscillation of considerable amplitude ($\sim$ 1 to 3 per cent) in the inventory of radiocarbon appears to be a constant feature throughout the record, though possibly replaced by a 400 year oscillation in the earlier millenia B.C. (Suess, 1968).

The theory that these short-term regular variations of atmospheric carbon-14 are initiated by variations in solar disturbance has been strengthened by computations by Bray (1967). A crude solar disturbance index, which should be roughly equivalent to average sunspot number in the years of maximum in each 11-year cycle, was constructed from available data on sunspots and aurorae from 527 B.C. to 1964 A.D. Throughout these centuries, sequences of three or four 11-year cycles of high solar disturbance (maximum yearly sunspot numbers over 100) alternated with runs of three or four cycles of low solar disturbance (maximum yearly sunspot numbers below 100); and in all but two of the twenty-four solar transformations for which

Fig.1.5 Average Temperatures in England and Variation in Carbon-14 Content in the Atmosphere Since A.D. 600.

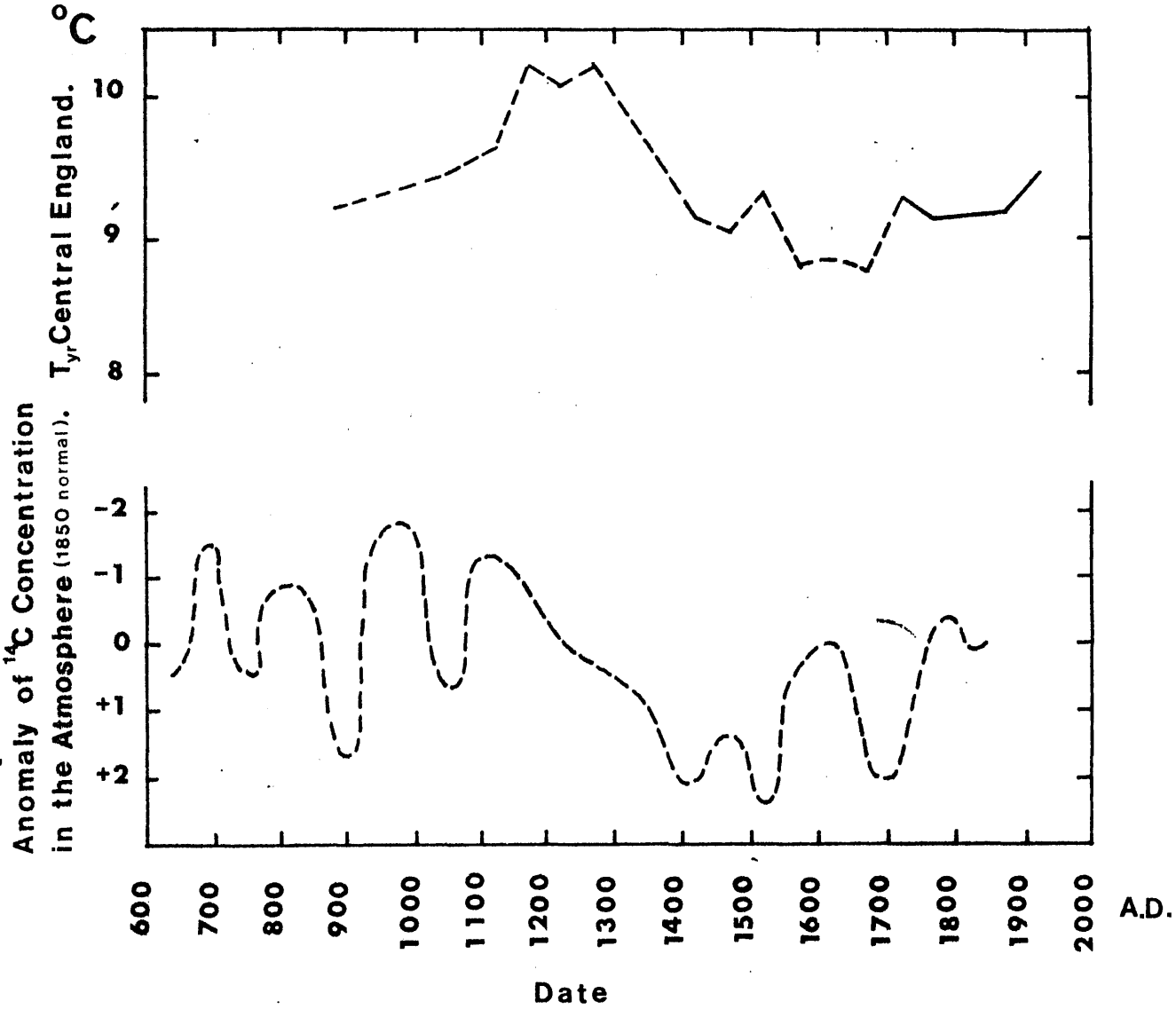

(After Willis et al. 1960; Lamb, 1965)

adequate carbon-14 data before and after could be compared, the carbon-14 content of the atmosphere changed in the opposite sense to that of solar activity. In one of the two exceptions there was no change in carbon-14; in only one case did a carbon-14 change occur in the same direction as that of solar activity (Bray, 1965, 1966, 1967).

1.1.3 Annual fluctuations of atmospheric carbon-14 concentration

Recent investigations (Baxter and Walton, 1971; Farmer and Baxter, 1973) have questioned the constancy of natural carbon-14 concentration over even shorter time periods of 1 to 10-20 years and have thus implied the inadequacy of present calibration curves to the age-correction of short-lived dating samples. It has been suggested by others that such variations could have their origin in supernova explosion (Konstantinov and Kocharov, 1965), in phenomena like the Tunguska meteorite catastrophe (Cowan et al., 1965; Vinogradov et al., 1966) or in the 11-year sunspot cycle itself (Dyck, 1965; Dolctov, 1968; Lavrukhina et al., 1973). While the 11-year solar cycle does exist it is not possible to attribute small variation (~2 to 3%) of the atmsopheric carbon-14 content to production rate variations alone. Baxter and Walton (1971) attributed the 20th-century annual carbon-14 variations to a combination of isotope production rate modulation by solar activity and of variable injection of radiocarbon from its stratospheric source into the troposphere. They suggested, on the basis of their correlation

between sunspot numbers and carbon-14 activity, that maximum input of carbon-14 to the troposphere occurs on average within the 2 year period following sunspot maximum when measured radiocarbon concentrations increase most rapidly. Thus maximum carbon-14 concentration is attained about 1 year before sunspot minimum. The actual physical mechanism involved a combination of intensified atmospheric circulation (and hence of stratosphere/troposphere exchange) and tropopause height variations as a result of the high energy fluxes of UV and corpuscular radiation associated with solar maximum.

Furthermore, Farmer and Baxter (1973) observed cyclic fluctuations of 2% in atmospheric carbon-14 levels for the time interval between 1829 and 1865. These were significantly correlated with the 11-year sunspot cycle (Figure 1.6). This finding suggested a possible relationship with 11-year solar cycle, perhaps analogous to that previously postulated by Baxter and Walton (1971). Thus both studies clearly provide evidence of significant variations of 2-3 per cent in atmospheric carbon-14 concentrations over periods of a decade.

However, between the two sets of Glasgow data, there appears to be a difference in the phase shift of maximum correlation e.g. during the period 1829-1865 (Figure 1.6), maximum carbon-14 levels are attained 5 years after sunspot minimum or 1 year before sunspot maximum. Because of this 180^{o} difference in phase shift, it is unlikely that the theory

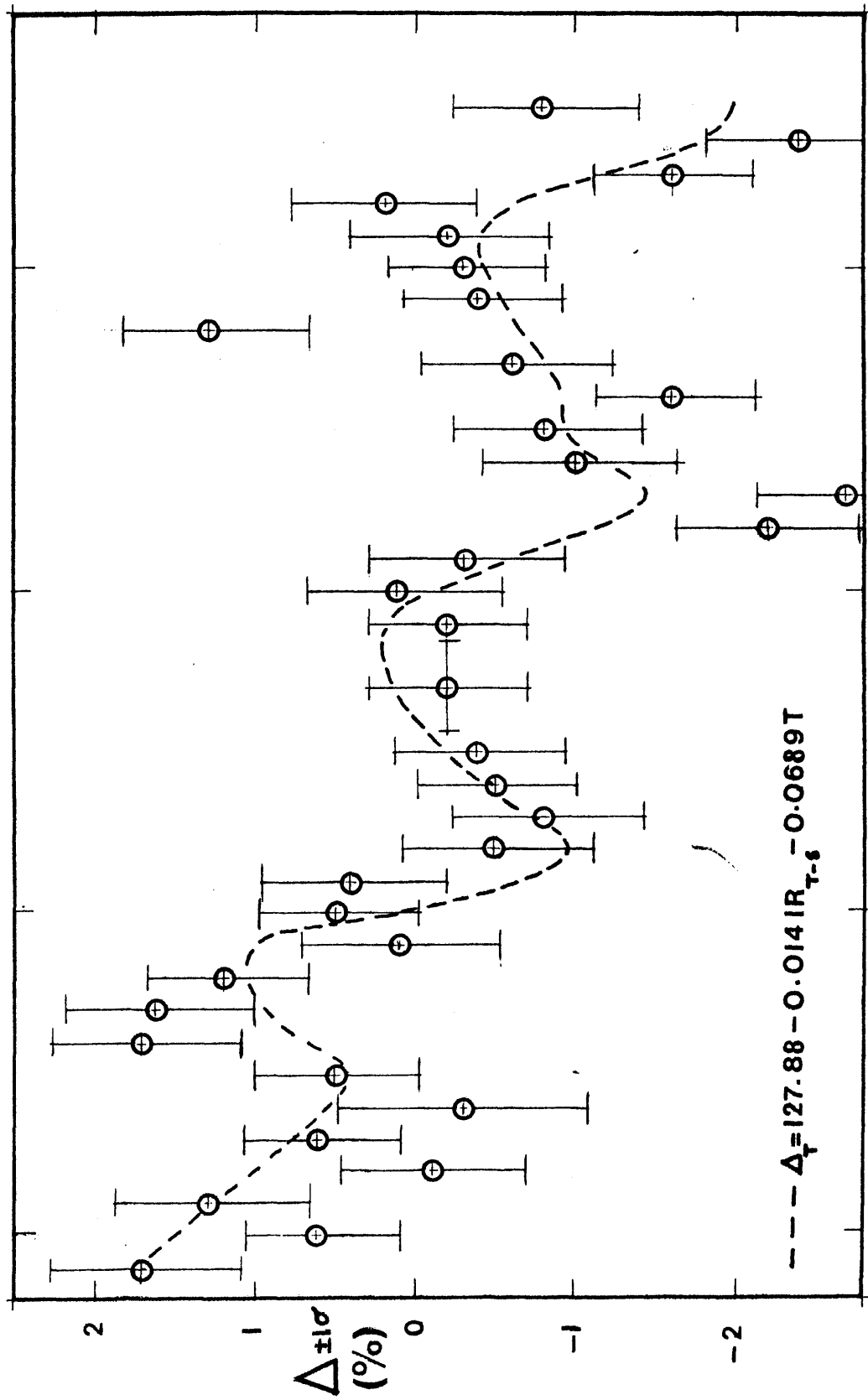
ATMOSPHERIC ^{14}C CONCENTRATIONS (1829–65)
(RELATIONSHIP WITH SUNSPOT NUMBERS R)
$\Delta_T = 127.88 - 0.014 IR_{T-5} - 0.0689T$
$\Delta \pm 1\sigma$ (%)
2
1
0
-1
-2
1830
1840
1850
1860
YEAR A.D.

Fig. 1.6

postulated by Baxter and Walton (1971) can directly account for the carbon-14 fluctuations observed during 1829-1865 unless temporal variations of the solar-sensitive stratosphere/troposphere exchange mechanism can occur.

Damon et al. (1973) used Douglas fir for the 15-year period from A.D. 1940 to 1954 in an attempt to provide further experimental evidence on this topic. This 15-year period is contemporaneous with some agricultural products previously measured by Baxter and Walton (1971). The computer analysis of their experimental results indicated a ca. 3°/oo peak to trough oscillation with an increase of about 5°/oo between 1952 and 1954. The radiocarbon maximum lagged the sunspot minimum by approximately 2 years and, likewise, the radiocarbon minimum lagged the sunspot maximum by about the same amount. The ca. 3 per mil. amplitude variation during the 11-year solar cycle was atributed to attenuation of radiocarbon fluctuations by the atmosphere through its function as a low pass filter. The rise of about 5°/oo from 1952 to 1954 was in agreement with the expected increase resulting from nuclear tests (Broecker and Walton, 1959).

Recently Cain & Suess (1976) have reported that major deviations from global average radiocarbon content, by up to 10°/oo, may be caused by local meteorological conditions which prevent rapid atmospheric mixing, such as persistant inversion layers along the Pacific coast. Thus, such local conditions may also explain the oscillations in radiocarbon

concentration with a period of 11 years which have been observed by Baxter and Walton (1971), Farmer and Baxter (1973), but not by Damon et al. (1973).

1.2 Artificial fluctuations of atmospheric carbon-14 concentration

Twentieth-century atmospheric radiocarbon levels have been significantly influenced by two of man's activities:

a) the burning of fossil fuels ("Suess effect")

b) the testing of nuclear weapons ("bomb effect")

a) "Suess effect"

The "Suess effect" is the decrease in atmospheric carbon-14 concentrations caused by combustion of large quantities of radiocarbon-free fossil fuels. It originated with the industrial revolution but did not become significant until the late 19th century. Since then, this effect was estimated to have caused a depression of about 3 per cent in northern hemisphere atmospheric carbon-14 levels by 1950 and, by extrapolation, about 4.2 per cent by 1970 (Suess, 1955). Alternatively, Fergusson (1958) obtained a corresponding value of 2 per cent for the southern hemisphere. Baxter and Walton (1970) calculated that the "Suess effect" would amount to -8.6 per cent, -16.0 per cent and -31.1 per cent in 1980, 2000 and 2025. Furthermore, Brannon et al. (1957) suggested a decrease in the carbon-14 concentration of the surface ocean by about 1 to 2 per cent as a result of the "Suess effect".

The annual input of fossil fuel CO_2 to the atmosphere can be calculated from the records of the production of coal, petroleum, lignite, natural gasoline and natural gas. The rate of input has risen rapidly since 1860 with a doubling time of 15 to 20 years, except for a noticeable slowing during the economic depression and the two world wars. The present atmosphere contains about 320 ppm CO_2 compared with 290 ppm in 1890 (Callender, 1958; Bolin and Bischof, 1970). The acceleration in the consumption of fossil fuels implies an atmospheric concentration of about 375 ppm by the end of the 20th century (Revelle, 1965; Bolin & Bischof, 1970; Baxter and Walton, 1970). Since carbon dioxide acts as a strong absorber and back-radiator of infra-red radiation, especially in the wavelength range 12-18μ, an increase of atmospheric carbon dioxide could cause an increase in global surface temperature (Callender, 1938; Plass, 1956; Kaplan, 1960). However, the evaluation of this effect is rather difficult because of associated changes in cloud cover and atmospheric dust levels and further study is required.

b) <u>"Bomb effect"</u>

The "bomb effect" is the result of the addition to the atmosphere of considerable quantities of carbon-14 produced through the reaction of atmospheric nitrogen atoms with "bomb" neutrons released during nuclear weapon tests. The majority of the artificial carbon-14 was injected into the northern hemisphere stratosphere (Table 1.4). The highest levels of

TABLE 1.4 ARTIFICIAL CARBON-14 INVENTORY

TIME PERIOD (Y)	TOTAL C-14 PRODUCTION ($X10^{27}$ C-14 ATOMS)
1945-1951	0.1
1952-1954	6.0
1955-1956	3.8
1957-1958	14.2
1959-1960	-
1961	24.0
1962	43.4
1963	-
1964-1970	4.0
1971-1973	2.3
TOTAL	98.0

northern tropospheric concentration occurred in 1963 and 1964, about 2 years after the period of maximum production. Since the maximum levels were attained, carbon-14 concentrations have gradually decreased through mixing with the southern troposphere and absorption by the oceans and biosphere. This exchange of "bomb" traces carbon-14 has afforded an opportunity for determination of the exchange parameters controlling carbon distribution and the carbon-14 levels in the atmosphere have therefore been monitored extensively as a fluctuation of latitude and altitude (Broecker and Walton, 1959; Machta, 1959; Broecker and Olson, 1960; Tauber, 1960; Willis, 1960; Fergusson, 1963; Nydal, 1963; Rafter, 1965A, 1965B; Lal and Rama, 1966; Münnich and Roether, 1967; Young and Fairhall, 1968; Walton et al., 1970; Telegades, 1971). Artificial carbon-14 has interesting applications in other fields of research - as plants and animals living after 1962 should reflect the large increase in carbon-14 in tropospheric air. Thus the suitability of a particular material (e.g. tree-ring component) as an indicator of atmospheric carbon-14 levels can be tested (Baxter and Walton, 1970; Farmer, 1972). Interesting studies have also been performed using "bomb" carbon-14 as a tracer of carbon turnover and transport in human tissues (Stenhouse and Baxter, 1976), soil systems (Jenkinson, 1966; Rafter and Stout, 1970) and ground waters (Brinkmann et al., 1959).

The carbon-14 concentration fluctuations in the northern hemisphere troposphere produced by both artificial effects are

shown in Figure 1.7. The decrease in carbon-14 concentration caused by the Suess effect is apparent up to 1954 but thereafter is masked by the bomb effect. Tropospheric carbon-14 activities in the northern troposphere rose to 100 per cent above the pre-bomb level in late 1963, one year after the end of large scale nuclear testing. The maximum carbon-14 concentration reached in the southern hemisphere corresponds to only 65 per cent of the northern maximum 3 years earlier, as shown also in Figure 1.7.

Before the discovery of the "Suess effect", several laboratories used samples of 20th-century organic material as reference standards to represent the steady-state atmsopheric C-14/C-12 ratio maintained by all living materials (de Vries, 1958). This method introduced errors of up to 120 years in resultant radiocarbon dates (Baxter & Walton, 1971). The larger perturbation caused by the bomb effect further emphasised the need for a reference standard based on a time period outwith the artificial disturbances and resulted in the distribution to radiocarbon dating laboratories of a new standard material - The National Bureau of Standards (NBS) Oxalic Acid Standard. The carbon-14 activity of this reference material (A_{STD}) is accurately related to the age-corrected activity of 1890 (pre-industrial) wood (A_o) by the relationship $A_o = 0.95 \times A_{STD}$ (Broecker & Olson, 1959).

1.3 Aim of research project.

The recent preliminary discovery of 2 to 3 per cent

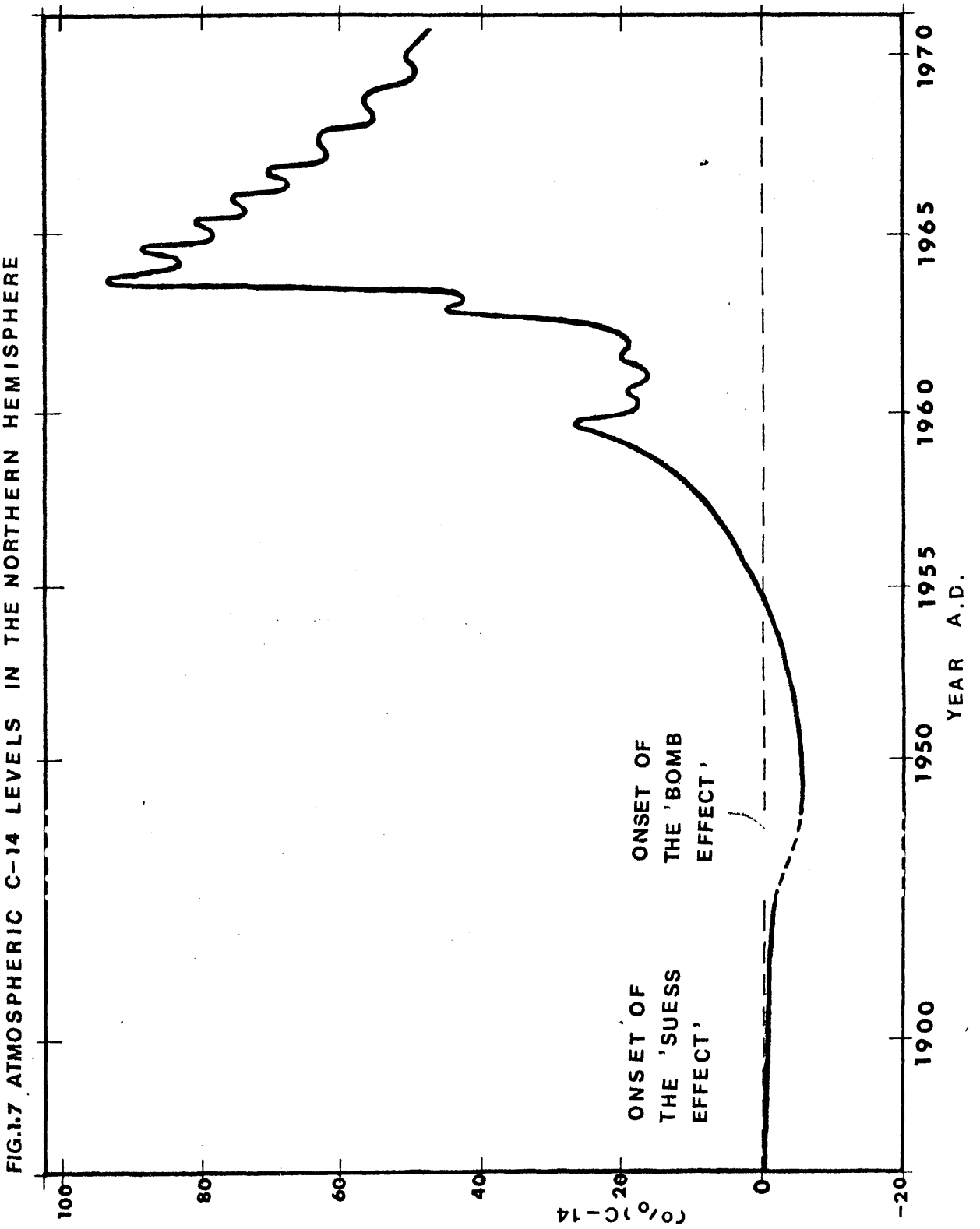

FIG.1.7 ATMOSPHERIC C-14 LEVELS IN THE NORTHERN HEMISPHERE

fluctuations in the atmospheric carbon-14 concentration over the 11-year solar (Baxter and Walton, 1971; Farmer and Baxter, 1973) conflicts with the traditional view shared by many radiocarbon chronologists that deviations of this magnitude are impossible on a time-scale of 11 years. Thus, the need for an investigation of past annual radiocarbon concentration, preferably during a period undisturbed by artificial influences such as the "Suess" and "bomb" effects, is of immediate concern and relevance to the radiocarbon dating method. Only on the basis of a large number of careful measurements can an authoritive pronouncement on an 11-year low-level effect be attempted. Thus, the basic objectives of the research were a) to measure pre-industrial and pre-bomb single tree-rings, after careful chemical pretreatment, for at least 50,000 ^{14}C decays (to decrease statistical errors) and thereafter b) to interpret the results with regard to the annual constancy of atmospheric radiocarbon concentrations, thereby contributing further to this important issue.

CHAPTER 2. Experimental methods in radiocarbon assay.

2.1 Introduction.

Carbon-14 assay requires highly rigorous physical and chemical preparation techniques followed by specialised low level counting. The counting system must possess the following characteristics:

1) high beta detection efficiency

2) low background count rate

3) long-term stability of performance.

The first two properties are essential as a result of the low carbon-14 activity of natural materials relative to normal background count rates in unprotected counters. In addition it is necessary to minimise/eliminate absorption losses of the weak carbon-14 beta particles. This latter necessity demands that the sample be converted into a form in which it can be placed intimately in contact with the detection system e.g. as a gas within a gas proportional counter or as a liquid intimately mixed with scintillant.

Long-term stability of performance is essential if small variations in carbon-14 content between samples are to be measurable. In addition, counting times are long ($\sim$ 24 hours) to reduce statistical counting errors so that stable conditions are necessary. Furthermore, conventional radiocarbon determinations involve precise intercomparison of modern standard and sample activities. The reference samples and background are counted only intermittently.

Thus experimental data may be applied to gross sample activities only if counting conditions remain constant both during and between individual counting periods.

The early counting systems (Anderson et al., 1947; Libby, 1955) involved the coating of the inner wall of a screen-wall Geiger counter with elemental carbon prepared from the sample. Since carbon-14 beta absorption was considerable in this solid matrix total detection efficiency was only 5 per cent. However, with the onset of the nuclear era it was apparent that the solid carbon counting technique would involve a major contamination risk from radioactive fall-out from weapon tests.

Internal gas and liquid scintillation counting are the two major techniques currently employed for radiocarbon assay. Internal gas proportional counting has long been accepted as the optimal method for low level measurements on radiocarbon and tritium (de Vries and Barendsen, 1953; Fergusson, 1955; Burke and Meinschein, 1955; Fairhall et al., 1961). Counting efficiencies above 90 per cent for radiocarbon are readily achieved, with backgrounds in the counts per minute range. From the N.B.S. oxalic acid-derived CO_2 content within the active volume of the counter and assuming the absolute activity of oxalic acid to be 14.27 ± 0.07 disintegration per minute, Stuiver et al. (1974) have calculated that 95.96 per cent of electrons emitted in the active volume are detected.

To minimise background count rate both a shielding assembly and anticoincidence guard counters are employed. Noise and cosmic radiation can be detected by guard counters as efficiently as by sample detectors and effective cancellation of simultaneous pulses performed electronically.

In addition, long-term stability and reproducibility of background and sample data are outstanding characteristics of internal gas counting systems which are largely stable to small changes in detector high voltage, amplifier gain, discrimination levels, and environmental temperature. Detector carbon-14 plateaux, with gradients less than 1 per cent per 100 volts, are routinely at least 500 volts long. Both a factor of two change in gain or discriminator threshold and environmental temperature changes from $10^{o}C$ to $40^{o}C$ cause less than 1 per cent change in background or sample count rate.

A further important feature of internal gas counting is the energy discrimination facility which enables monitoring of the carbon-14 spectrum only. While in the Geiger region, all output pulses from a gas counter are uniform in size, independent of the initiating event, in the proportional counters, however, it is possible to monitor only the energy range of interest through rejection of lower or higher energy pulses.

The application of liquid scintillation counting to

C-14 measurement was first reported by Hayes et al. (1955). Synthesised benzene is generally used as the scintillation solvent because it contains 92% carbon and has excellent liquid scintillation properties. Light flashes emitted by the organic solution through activation by beta pulses are detected and highly amplified ($x10^{13}$) by photomultipliers. Noise levels are reduced firstly by refrigeration, which minimises thermionic emission from the photocathode. Secondly, by applying coincidence circuitry whereby two co-axial photomultipliers view a single solution and operate in coincidence, only simultaneous events are transmitted. Single photon phenomena (e.g. fluorescence) are rejected. Liquid scintillation techniques have the great advantage that the total volume of the counting medium is small and the sample is in a condensed phase with a density many times greater than gases; it therefore subtends a much smaller angle to the external background. Massive shielding and the use of anti-coincidence shields are not necessary as the cosmic ray particles (mesons) give large pulses in a liquid scintillator and are easily discarded by pulse height discrimination. The background is mainly determined by the dark current of the phototube, which may be rather high for the energies of carbon-14 dating. Background count rate reduction is achieved through the use of quartz-faced photomultipliers and low potassium counting bottles, which minimise K-40 contribution.

Relative to gas counters, however, liquid scintillation counting, generally, has an inferior figure of merit for radiocarbon ($\leq$ 1000 vs $\geq$ 1000 for internal gas counting). For low level sample counting the figure of merit is directly proportional to the number of samples which can be counted per week to a given statistical accuracy. However, liquid scintillation offers the advantage of automatic sample counting (i.e. counter pumping is unnecessary) and this enables sequential counting of background plus standard during sample counting. In general, large samples are needed to make up sufficient counting volume in liquid scintillation. Thus gas counting is more suited to small sample high precision analysis. Since sample availability in this research is generally limited, the gas counting method is most appropriate.

The selection of an appropriate counting gas requires consideration of several variables. The counting gases currently in widespread use for low level carbon-14 counting are acetylene, carbon dioxide and methane. Acetylene was originally advocated by Suess (1954) and others and has the advantage that the gas contains two carbon atoms per molecule and hence, for a given pressure, twice the carbon content per litre as the other counting gases. However, acetylene cannot be used safely above about 1.5 atmospheres pressure since it liquifies and presents an explosion hazard. Combined with the lengthy chemical procedures required to prepared acetylene,

this technique seems less practicable than its alternatives.

Carbon dioxide as a low level C-14 counting gas was pioneered by de Vries & Barendsen (1953) and Olsson et al. (1962) and is still the most widely used. The apparent simplicity of CO_2 preparation chemistry is, however, deceptive because the plateau characteristics of carbon dioxide are extremely sensitive to electronegative impurities. Fergusson (1955) has reported that an oxygen concentration as much as 1 ppm or a chlorine concentration much in excess of 1 part in 10^7 leads to plateau difficulties. As a result of the extreme purity requirements on the carbon dioxide product the chemical procedures are not simple. In practice it is necessary to make elaborate counter adjustments and data measurements to increase the quality and plateau characteristics of the counting gas. This sensitivity of carbon dioxide operating conditions can, however, be used to advantage in that, by fine voltage control and channels ratio methods, constant gas gain can be accurately reproduced.

Methane, used by Burke and Meinschein (1955), and ethane also make excellent counting gases in terms of high signal-to-noise ratio, long flat plateaux and low operating voltages. CH_4 and C_2H_6 will tolerate 500-1000 ppm of oxygen or water vapour and still give excellent plateaux. In this research carbon dioxide was chosen as counting gas, because it is more direct to use CO_2 as a counting gas than to convert it to methane. More importantly, direct mass spectrometric

analysis of the counting gas to determine isotopic fractionation effects is possible with CO_2 but not with the hydrocarbon gases. Also, the vapour pressure of carbon dioxide is negligble at liquid N_2 temperature ($-196^{o}C$); thus possible fractionation effects and sample handling losses are avoided.

2.2 Sample selection and collection

It must be assumed in carbon-14 studies of tree rings that each ring participates in the carbon cycle for one year only, and thereafter remains a closed system. After correction for slight changes in isotopic ratio which occur during the biochemical reactions in a plant, the carbon-14 activity measured for any tree-ring should be representative of the C-14 activity in the atmosphere at that time. For measurement of annual carbon-14 contents in particular it is essential that samples indicate the average atmospheric C-14 concentration during a time interval of one year or less. In addition, there must not be any exchange of carbon between "death" (i.e. removal from the carbon exchange cycle) and analysis. The direct fixation of atmospheric CO_2 for cell synthesis suggests that plant C-14 content is indeed closely related to atmospheric C-14 levels. However, Baxter and Walton (1970) questioned the use of single tree-rings for their work because of the possibility of carbon exchange between adjacent rings in the outer sapwood area (Broecker and Olson, 1960). In addition, the uptake of soil CO_2 derived from decaying vegetation and from carbonate materials

in the soil may disturb the anticipated correlation. Preliminary studies (Broecker and Walton, 1959; Broecker and Olson, 1960; Baxter and Walton, 1970) have shown that there is a close correlation between nuclear-era C-14 content in atmospheric CO_2 and short-lived biospheric samples such as grain, tree seeds, spirits from grain samples, wines from grapes etc. Thus, root uptake of soil CO_2 appears insignificant for these sample types. Berger (1970) has measured "bomb" C-14 in recent tree rings of pine and oak wood. The results indicate a close correlation between atmospheric C-14 content and tree-ring C-14 levels for both samples. Therefore, any holdover of food supply was not apparent. After a study of several methods for tree-ring chemical pretreatment, Farmer and Baxter (1973) concluded that single tree rings, particularly their inert cellulose fraction, are good indicators of atmospheric C-14 levels and that food holdovers and resin transfer do not play a significant part in determining the C-14 concentration of the wood constituting a given ring.

The samples studied in this research work were single tree rings separated from:-

1) an 18th-century Scots Pine (Pinus Sylvestris) from Inverness-shire (57^{o}N, 5^{o}W) which was planted in 1738 and felled in 1973.

2) Ynyslas Pine (Pinus Sylvestris), approximate age 4700y., collected in February 1974 near Ynyslas (Wales) (longitude $4^{o}10'60"$W, latitude $52^{o}20'92"$N and +1 ft O.D.) and

3) Clarach oak (Quercus robur), approximate age 5,500 y., collected in February 1974 near Clarach (Wales) (latitude 52°20'84"N, longitude 4°10'61"W and 2 ft O.D.).

The Scots Pine was collected by Baxter from a lone-standing site far from the effects of any localised forest atmosphere. It had grown before the times of large industrial input of fossil carbon into the atmosphere. Therefore, it should not indicate a Suess effect on its early rings. As the Scots Pine was perfectly preserved with sharply distinguished and wide tree rings, it was possible to count the rings and establish calendar ages for the tree ring sequence. It is considered unlikely that missing or double growth rings would be observed in a tree of this species growing in this location and climate (Murdoch, 1974).

Ynyslas Pine and Clarach Oak were collected by Heyworth, University College, Wales. Bothwood samples were from submerged forest sites, the preserved remains of forests killed by rising sea level. Samples were subsequently preserved in sand and exposed at low tide after storm activity. These samples, selected because of their wide annual growth rings permit the possibility of investigating the natural short-term carbon-14 constancy further back in time than has ever been previously possible. Dendrochronological dating by Heyworth will in the near future produce calendar ages for these samples. At present, however, only "floating"

chronologies are available.

2.3 Chemical pretreatment and preparation system.

As stated previously, the prime assumption of the dating method is that samples contain only the original carbon atoms present at the time of isolation from the exchange cycle. During the time interval between such removal and analysis, however, samples may become contaminated with foreign carbonaceous materials. The type of contamination a particular sample may undergo depends on its chemical structure and environment in the years following removal from the carbon cycle. The carbon of an inorganic sample (e.g. shell carbonates) may be replaced via ion-exchange by the carbonates of ground waters. Organic samples are less prone to contamination than inorganic samples but contaminating agents commonly found are rootlets, soil components, such as humic acids, carbonates and sand, and soil itself. It is generally desirable to isolate and date the organic fraction. If sample contamination is not eliminated the non-contemporaneous carbon atoms can introduce errors in sample activities which in dating become more significant with increasing sample age. Table 2.1 indicates the size of the errors which result from contamination of old and nuclear era samples by varying amounts of modern and inactive carbon.

Strong alkali and acid washing is usually sufficient to remove humic acids and carbonates (Lerman et al, 1970). Wood is often treated with acid and alkali but some authors believe

TABLE 2.1 ERRORS CAUSED BY SAMPLE CONTAMINATION

1) CONTAMINATION OF OLD SAMPLES BY MODERN CARBON

TRUE AGE OF SAMPLE (YR.)	RADIOCARBON AGE OF SAMPLE (YR.) DEGREE OF CONTAMINAT. WITH MODERN C		
	1%	0.1%	0.01%
5,570	5,490	5,560	5,570
11,140	10,900	11,120	11,140
22,280	21,080	22,160	22,270
44,560	32,260	42,760	44,350

2) CONTAMINATION OF NUCLEAR ERA SAMPLES BY DEAD C

TRUE C-14 CONCENTR. (% DEVIATION FROM (NORMAL LEVEL)	OBSERVED C-14 CONCENTR. (% DEVIATION (FROM NORMAL LEVEL) DEGREE OF CONTAM. WITH DEAD C		
	10%	5%	1%
40.0	26.0	33.0	38.6
60.0	44.0	52.0	58.4
80.0	62.0	71.0	78.2
100.0	80.0	90.0	98.0

that prior extraction with an organic solvent is necessary to remove non-contemporaneous resins (Jansen, 1970). Furthermore, there is a wide range of opinion as to the solvents which should be used in the chemical pretreatment of of wood samples. Some laboratories (Wilson, 1963A; Fairhall and Young, 1970) employ both organic (i.e. acetone, ethyl acetate, petroleum ether etc) and inorganic (e.g. HCl, NaOH etc) solvents. Others (Cain and Suess, 1976) consider either an organic or inorganic pretreatment as sufficient.

In the case of the wood handled in this laboratory, possible contaminants are marine boring organisms, humic acids and resins. All radiocarbon dates are performed on the cellular material of wood, pure white cellulose, since, as mentioned earlier, it is possible that resins and lignin may be transported across adjacent sapwood tree rings.

Resins may be removed from wood by Soxhlet extraction in 40° to 60° C boiling range petroleum ether. However, as such an extraction may add more non-contemporaneous carbon than it extracts, it was abandoned (Wilson, 1961, 1963A, 1963B).

Individual tree rings (10-15 grams) from the sections of wood are separated by chisel, cut into small fragments and treated with boiling 2M potassium hydroxide for 6-8 hours. This process removes humic acids and also degrades and removes most organic resins. The wood is filtered out, washed with acid solution and distilled water, and added to a bleaching solution. This reagent, containing 110 ml of 1M HCl plus 80 grams of

$NaClO_2$ in three litres of distilled water, removes lignin and oxidises components not removed during treatment with alkali. Pure cellulose (6-8 grams) is generally obtained after bleaching for 48 hours at 70° to 80° C. Additional quantities of HCl and $NaClO_2$ are added if bleaching at this stage is incomplete.

Each sample must finally be converted to pure carbon dioxide in two stages involving preparation then purification of the gas. Carbon dioxide is prepared and roughly purified by combustion of the sample and subsequent precipitation then hydrolysis of barium carbonate. All vacuum line procedures require system evacuation to less than 1μHg. This is achieved by two Hg-diffusion pumps backed by rotary pumps. Pressures are monitored on Pirani and Penning gauges. All transfers of carbon dioxide are performed by distillation at liquid nitrogen temperature (-196°C). The purification process, via reversable calcium carbonate formation in a furnace, removes any residual electronegative impurities and regenerates carbon dioxide of the required purity for gas proportional counting. A schematic diagram of laboratory procedure is given in Figure 2.1.

Sample combustion.

Carbon dioxide is obtained by burning the sample in a controlled atmosphere of oxygen in a quartz combustion tube. The combustion apparatus, shown in Figure 2.2, is a modification of the system used by Rafter (1965A), in which

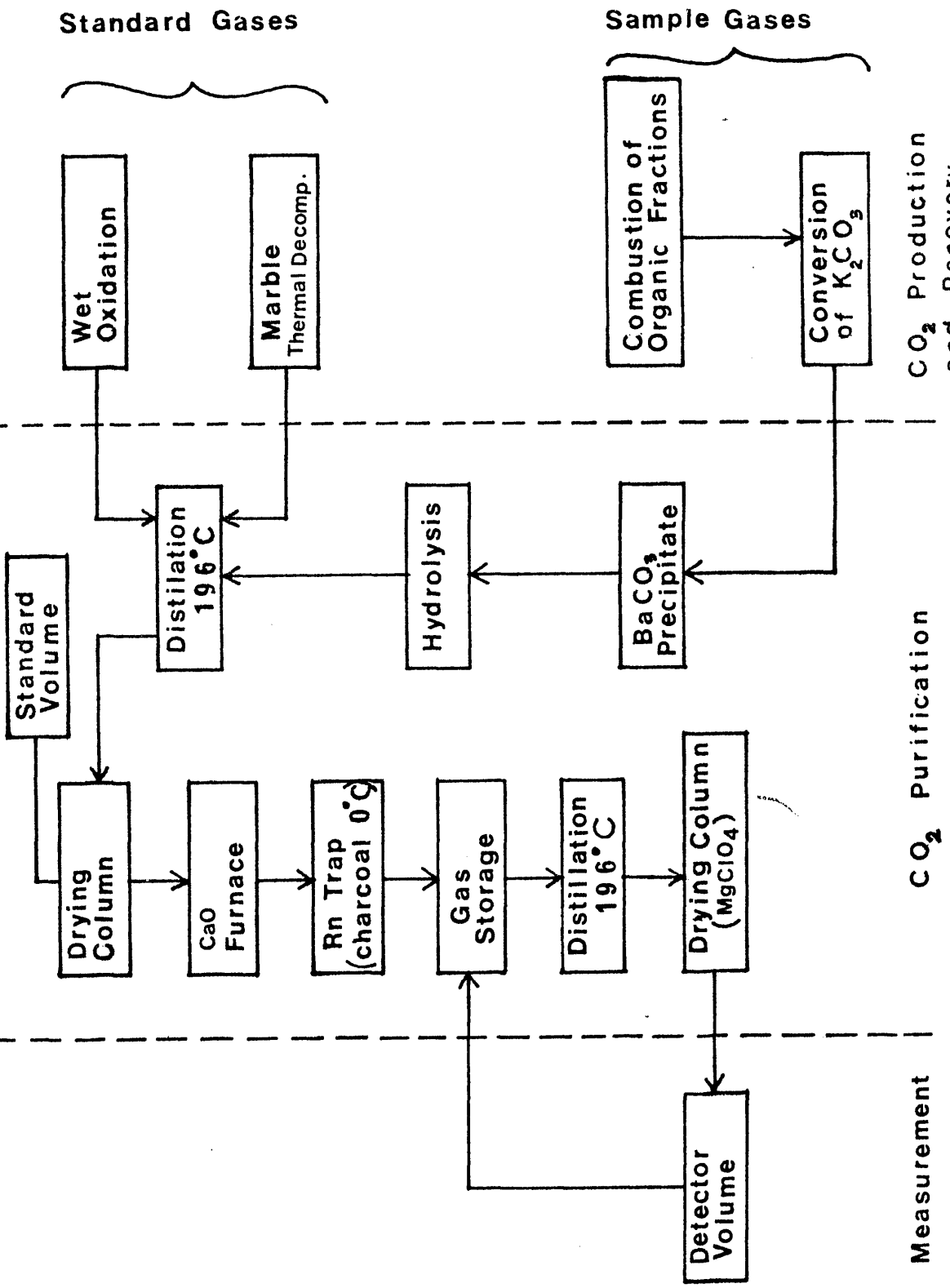

Fig. 2.1 Schematic Diagram of Laboratory Procedure.

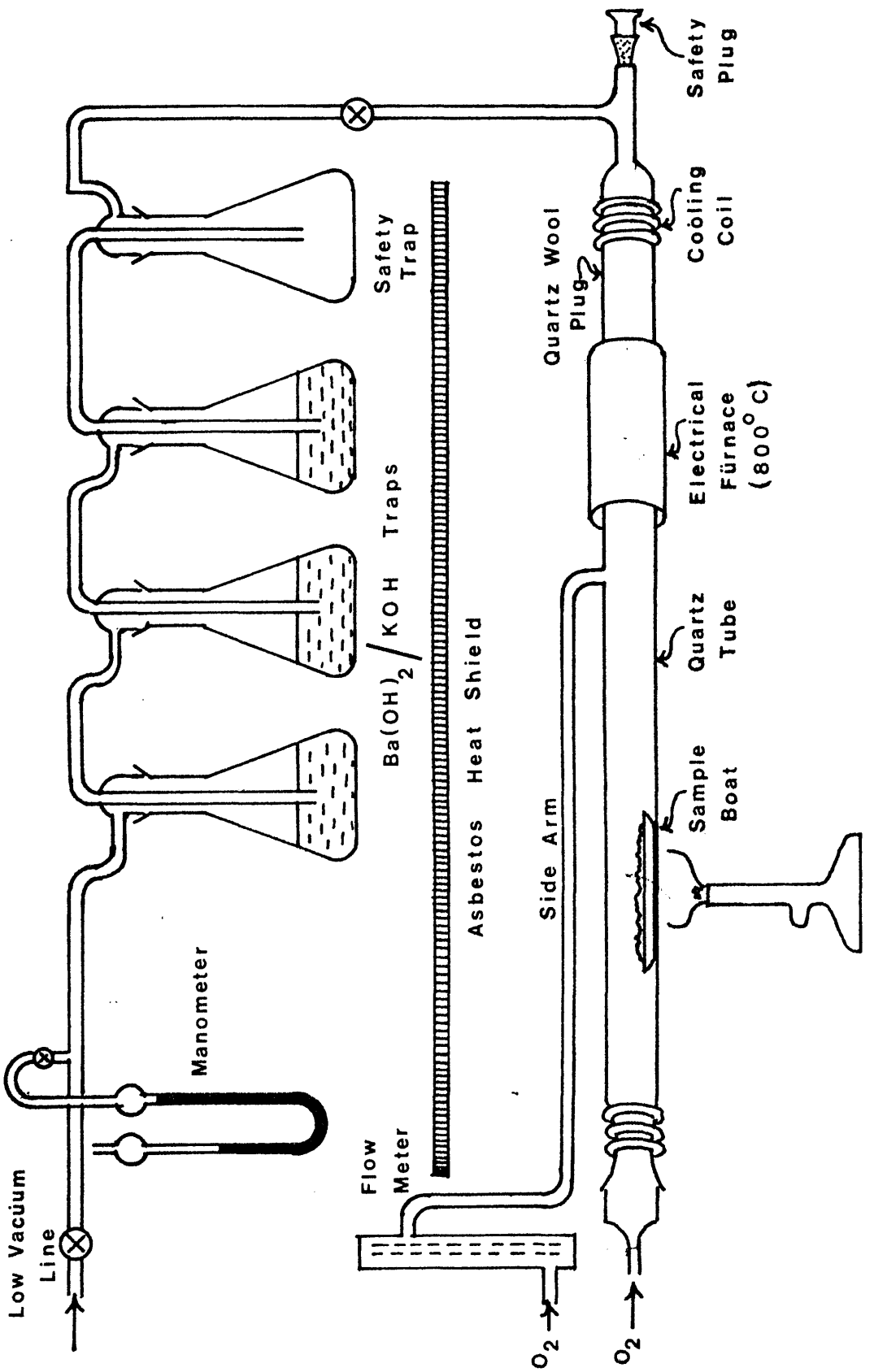

Fig 2.2 Combustion and CO_2 Collection System.

carbon dioxide was cleaned by chemical scrubbing in wash towers and finally collected as "dry ice". This method proved unsatisfactory due to the large quantities of chlorine, nitrogen and occasionally sulphur compounds present in the combustion products. These impurities quickly exhaust conventional wash solutions and contaminate the product CO_2. Furthermore, the chemical combination of Cl_2 with CuO produces a fused mass which caused blockage and rupture of the quartz tube. Therefore, CuO was replaced by a plug of quartz wool. The secondary oxygen flow through the side arm is applied to ensure complete oxidation of the sample carbon. Released carbon dioxide is absorbed in KOH filled traps (Harkness, 1970). Prior to sample combustion, the tube furnace with porcelain boats is roasted in a stream of oxygen for 20 minutes. On cooling, the boats are packed with sample (6-8 grams of cellulose) and replaced in the tube furnace. Three Dreschel bottles are filled with 100ml 4M KOH ($BaCl_2$ solution) while the first empty bottle is so positioned in case of accidental suck-back. The KOH solution is prepared from a bulk 8M KOH solution containing 5g Ba^{2+} per litre. The flow of oxygen through the side arm is kept constant at 150 ml per min. while the flow rate through the main tube is varied to control the rate of combustion. A negative pressure gradient of about 10 cm Hg is maintained throughout the system by pumping at the outlet. The pressure gradient is controlled by a valve and monitored via the mercury manometer. The sample combustion

rate is kept to a minimum to avoid incomplete oxidation and possible isotopic fractionation of carbon. A small degree of fractionation may occur during combustion but this is later corrected for via mass spectrometric measurement of the C-13/C-12 ratio in the final counting gas. Combustion yields are calculated to be > 90 per cent.

Precipitation of $BaCO_3$.

Bariumcarbonate is precipitated by addition of saturated $BaCl_2$ solution to the KOH/K_2CO_3 solution. The precipitation is performed in a closed system to avoid absorption of carbon dioxide from the laboratory atmosphere. Steam from boiling distilled water is passed through the KOH/K_2CO_3 solution to coagulate the precipitate by a combination of heat and agitation. The $BaCl_2$ solution is added via a dropping funnel (Figure 2.3). The carbonate suspension is then filtered, washed free of Cl^- and OH^- ions, dried, weighed (approximately 30-40 grams of $BaCO_3$) and stored in sealed jars.

Hydrolysis of $BaCO_3$.

Carbon dioxide is released from the bariumcarbonate at reduced pressure by addition of 95% orthophosphoric acid. The hydrolysis system, as shown in Figure 2.4, includes a water cooled condenser as a precaution against extensive frothing of the sample in the reaction flask. Two flasks, each surrounded by a dry ice/acetone mixture (-80°C), freeze out moisture from evolved CO_2, which is collected in the third trap maintained at liquid nitrogen temperature (-196°C).

Fig. 2.3 Precipitation of CO_2 as $BaCO_3$

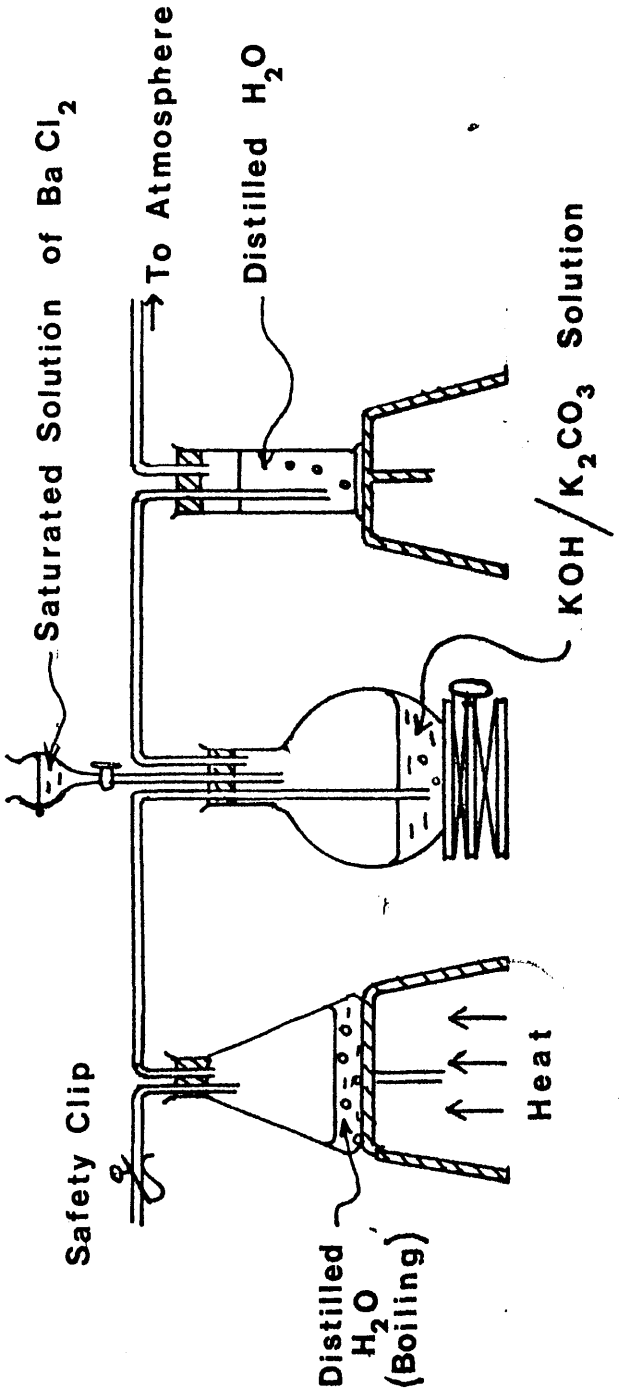

Fig. 2.4 Hydrolysis and Gas Drying System.

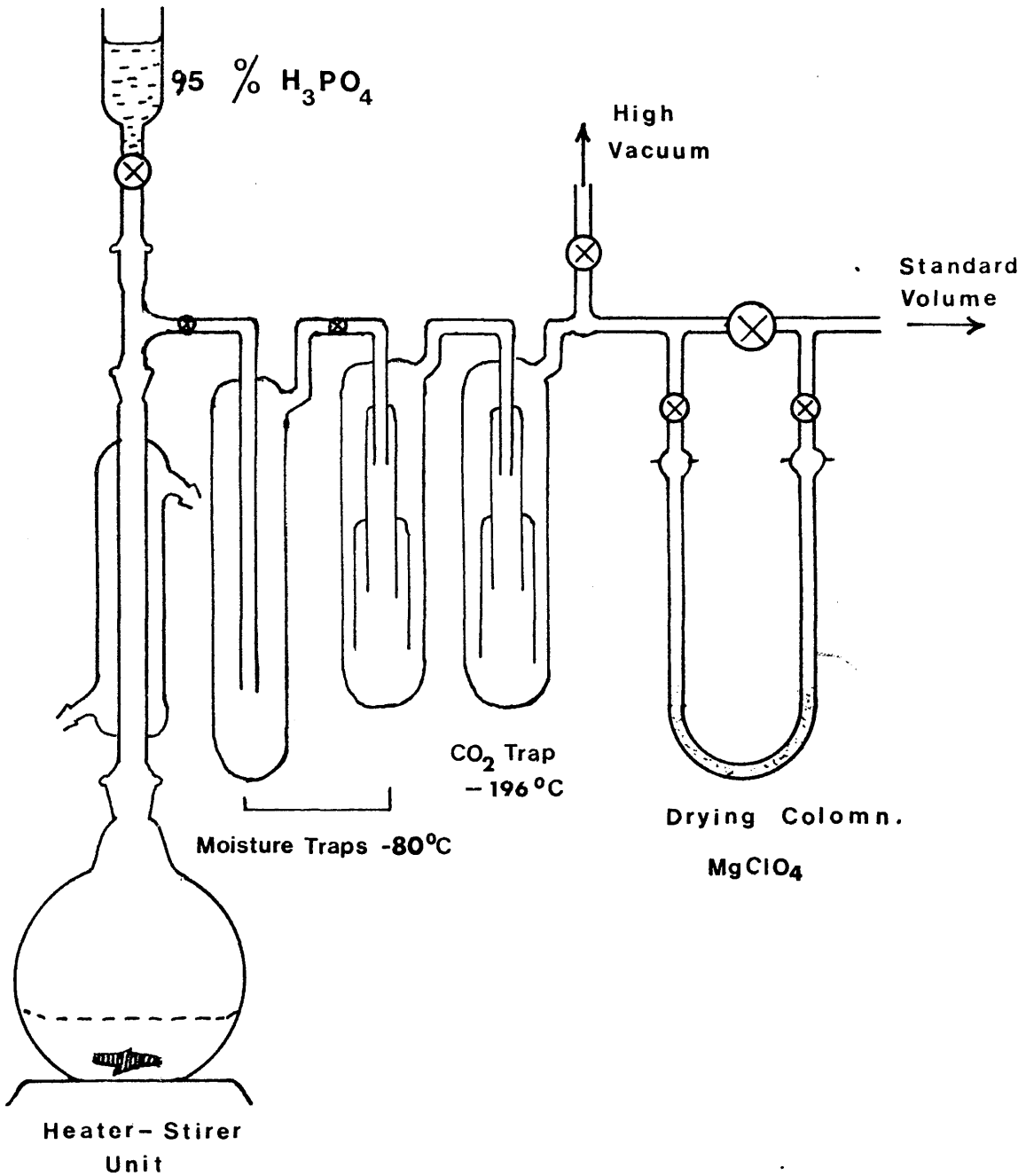

The CO_2 is allowed to sublime through the U-tube of the drying agent ($MgClO_4$ pellets) and into the 5 litre standard bulb, previously evacuated to $< 10^{-3}$ torr. The pressure of CO_2 is measured using a mercury manometer. Room temperature is noted and the hydrolysis yield of carbon dioxide calculated. Yields are typically ~100 per cent.

Purification of carbon dioxide.

Electronegative impurities such as O_2 (1 ppm) and Cl_2 (0.1 ppm) are removed by absorption of the carbon dioxide on calcium oxide at 700–750°C, pumping off impurities at 350°C to 10^{-3} torr and subsequent re-evolution of carbon dioxide at 900°–1000°C:

$$CaO + CO_2 \underset{T<400^{\circ}C}{\overset{T>800^{\circ}C}{\rightleftharpoons}} CaCO_3$$

Figure 2.5 shows the dissociation pressure of $CaCO_3$ as a function of temperature, based on data from Hill and Winter (1956). The impurities remain absorbed on CaO even at 1000°C. After each purification procedure, the CaO is heated to 1050°C; impurities which are labile at this temperature plus any residual traces of CO_2 are removed in preparation for the next sample by pumping to 0.3×10^{-3} torr. Excess moisture present in the CO_2 produced by hydrolysis decreases the rate of re-evolution of CO_2 resulting in the necessary renewal of CaO. Carbon dioxide immediately after the purification procedure contains radon, from impurities in the calcium oxide, (α-emitter, 5.49 MeV, $t_{\frac{1}{2}}$ 3.82 days), a daughter product of

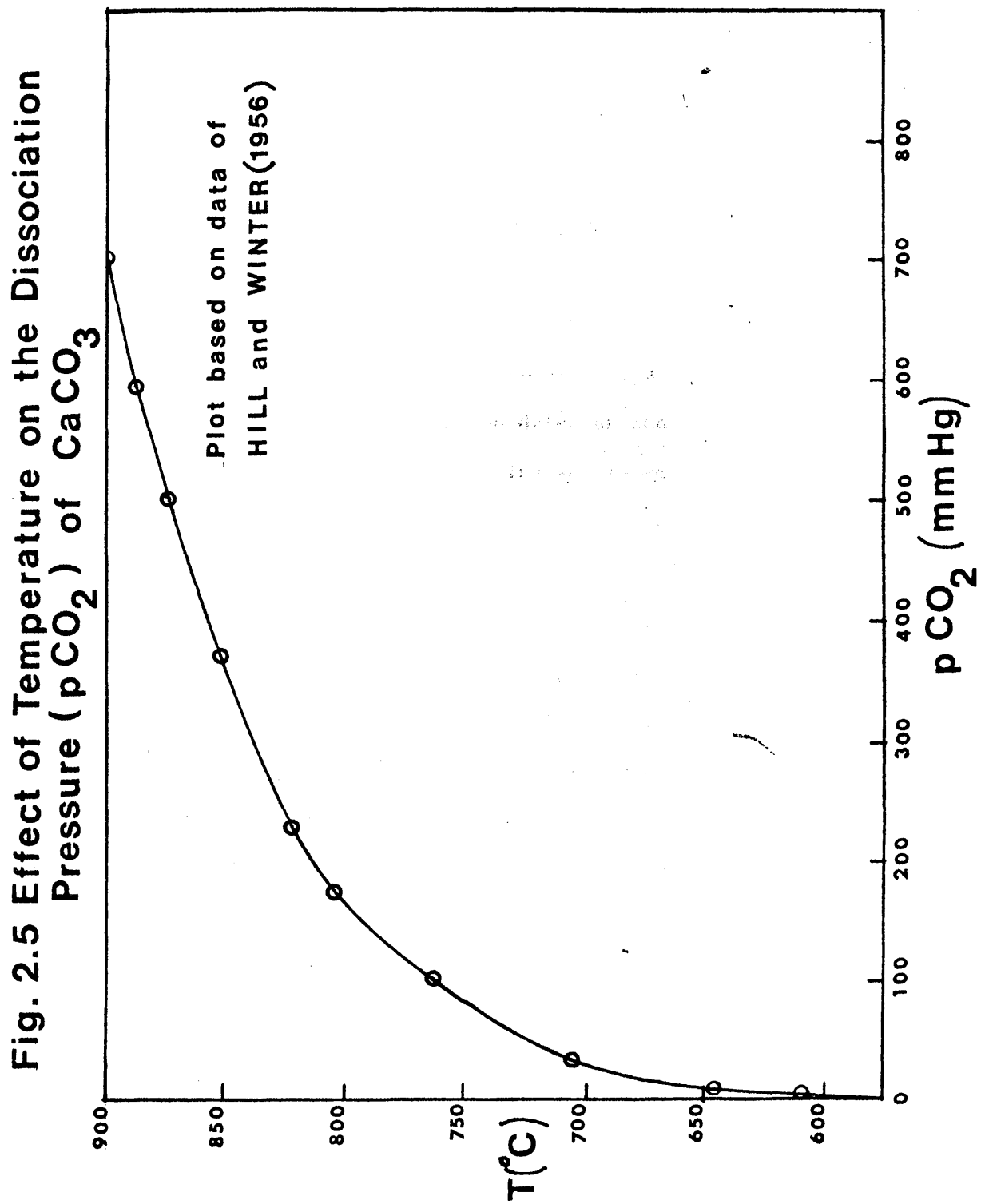

Fig. 2.5 Effect of Temperature on the Dissociation Pressure (pCO_2) of $CaCO_3$

radium. Long (1965) reported almost total removal of Rn^{222} from CO_2 by passage through an activated charcoal trap at -40°C, a procedure lasting two hours. It is possible, however, to remove a high percentage of radon using a similar trap at 0°C. Thereafter, storage of the gas for 2-3 weeks allows any radon and its daughter products to decay. Ten 5 litre glass bulbs are available for gas storage.

2.4 Procedure for CO_2 activity measurement.

The gas filling system is connected to the detector volume by $\frac{1}{4}$ inch diameter oxygen-free, high-conductivity copper tubing terminating in a glass-to-metal seal (Figure 2.6).

Prior to filling, the combined detector and filling system is pumped to 4×10^{-4} torr. The sample gas is condensed from its storage bulb into the filling finger and pumped to 10^{-5} torr at -196°C, before expansion into the counter. Filling pressures up to 2 atmospheres are monitored on a twin manometer unit and the temperature inside the counter shielding recorded with a gas thermometer. Since age determination involves comparison of modern standard and sample activities, the amount of gas introduced into the counter must be accurately known. This is temperature dependent according to the gas laws. In practice, all sample activities are normalised to a filling temperature of 18°C. Thus a linear relationship exists and correction factors are applied e.g. at 23.6°C, the correction factor is 1.020, and at 13°C, the correction factor is 0.983. The correction factor may be

Fig.2.6 Counter Filling System.

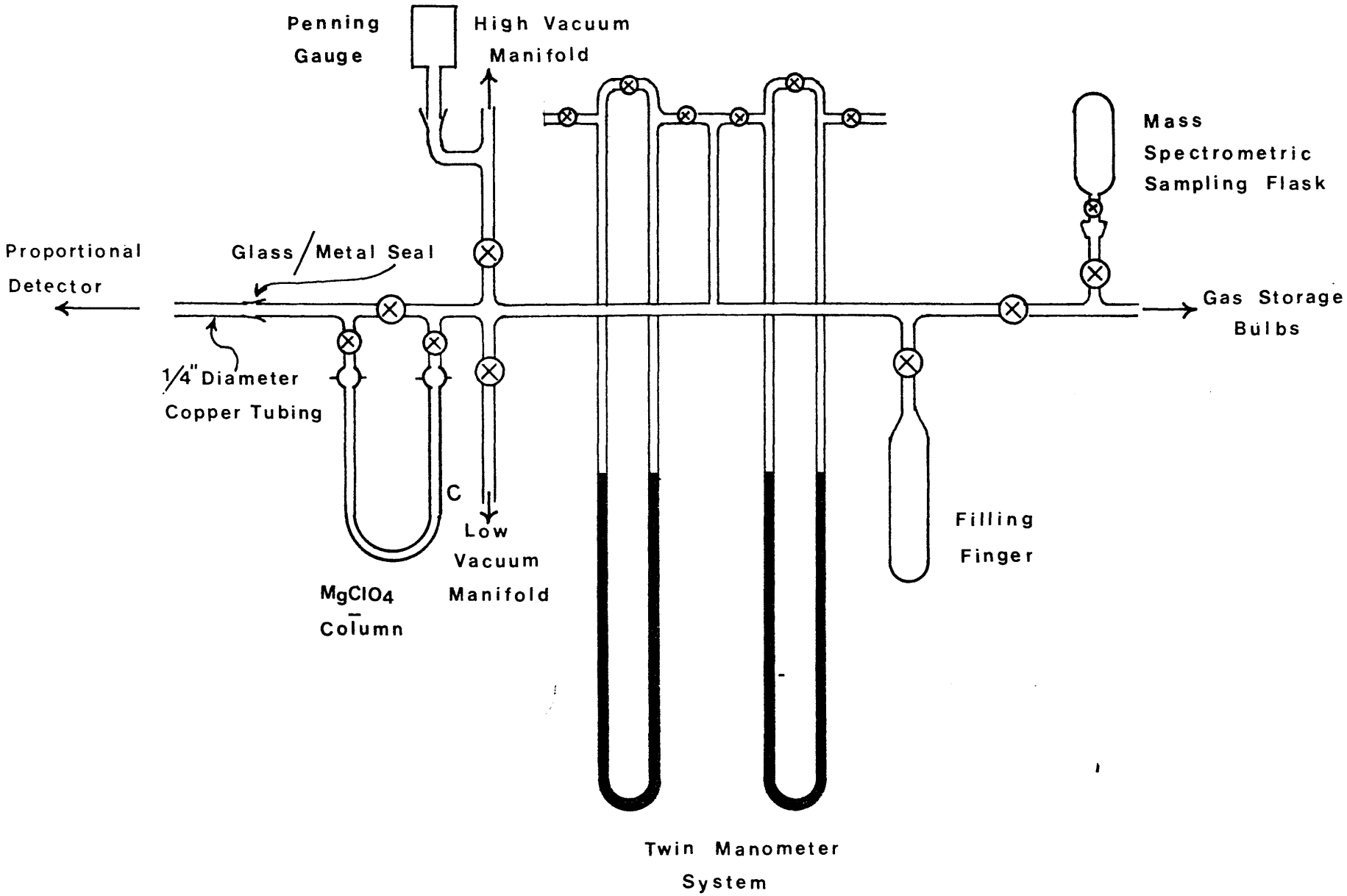

avoided, however, if the carbon dioxide counter pressure is always standardised to a pressure corresponding to 760 mmHg at 15°C, before counting. Thus, each counter volume contains the same weight (1.32 gram) of carbon.

A period of 15 minutes is allowed for the gas temperature to reach equilibrium with its surroundings before the final pressure adjustment is made. After a counting sequence the carbon dioxide is transferred directly to its storage bulb. When carbon-14 measurement is complete, a small sample (25 mls STP) of the carbon dioxide is taken for subsequent isotopic fractionation measurements.

Counting system.

A Johnston Laboratories Inc. Beta-Logic Gas Proportional Counting System is used for carbon-14 measurement.

Detector and guard assembly.

The 2.6 litres sample detector (GC-12) is manufactured from copper (a suitable material because of its relative freedom from radioactive impurities). The anode is 0.001 inch diameter stainless steel wire. The sample detector is surrounded by a meson guard counter (GC-13) and the whole assembly is encased in a 4 inch thick lead shield in which the gamma component of background radiation is largely absorbed. Counting of high-energy mesons which penetrate the lead shielding is minimised by employing sample/guard anticoincidence circuitry i.e. mesons are counted simultaneously in both guard and sample detectors and are automatically cancelled from a

sample count. The guard is operated as a flow Geiger counter using Q-gas (99.0 per cent helium, 0.95 per cent isobutane and 0.00135 per cent butadiene). The flow is adjusted to an outlet pressure of 20 psi. by a pressure regulator, and to a rate of 130 mls per minute controlled by a needle valve and ratemeter. The guard counter contains 12 independent anode wires, each anode separated from its neighbours by an earthed metal fin. Typical guard plateaux are $>$ 300 Volts in length with slopes $<$2.5 per cent per 100 Volts, while working voltages are consistently in the range 1.21 to 1.24 KV. At a gas pressure of one atmosphere, the sample detector working voltage is within the range 3.4 to 3.5 KV. To compare count rates of different gases, it is necessary to operate at a predetermined gas gain (i.e. a constant electron multiplication factor). The presence of extremely small quantities of electronegative impurities significantly decreases the electron multiplication. Adjustment of the operating voltage thus compensates for any variation in gas purity.

Both coincidence and anticoincidence spectra exhibit excellent plateaux characteristics: coincidence plateaux: length $\sim$ 800V, slope $<$ 1.5%/100V; anticoincidence plateaux: length $\sim$ 600V, slope $<$ 1.0%/100V.

A diagram of both the sample detector and guard counter is given in Figure 2.7. Pulses registered in both counters are fed via charge sensitive preamplifier units to an electronic console.

Fig. 2.7 Sample and Guard Counters (cross-sectional view)

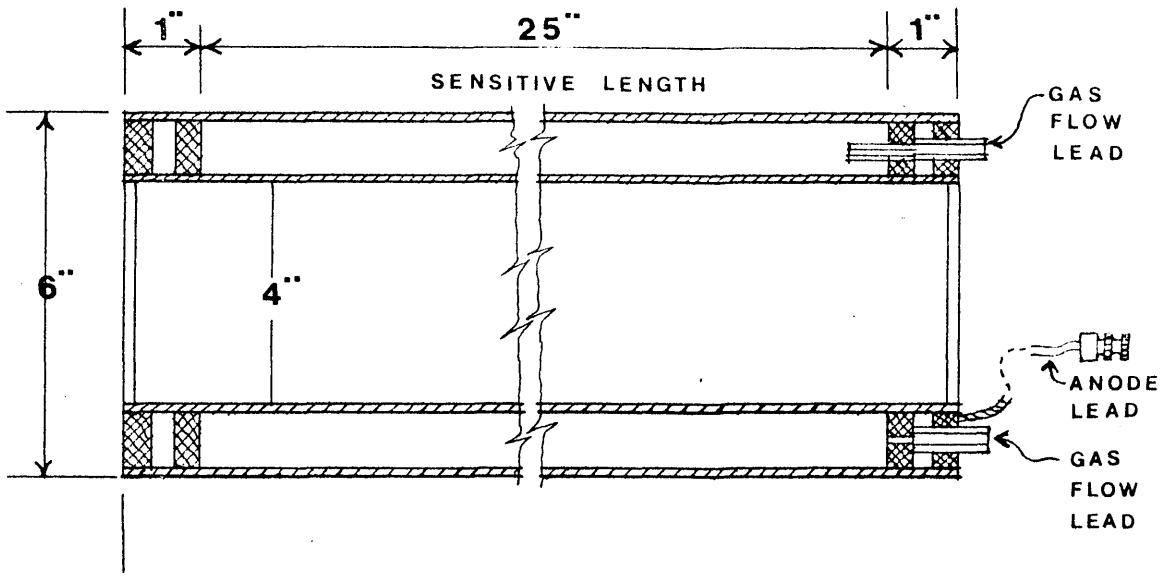

(a) Guard Counter

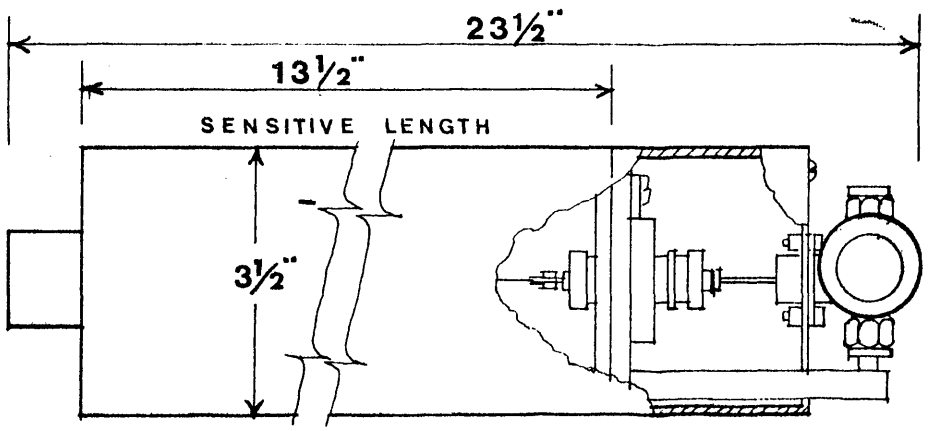

(b) Sample Counter

Electronic console.

Pulses from the sample counter are fed to a preamplifier and subsequently to a series of three amplifier discriminator boards. The discriminators control three energy channels which receive the output pulses. Assuming a gas gain of $2x10^3$, the discriminator settings are adjusted for optimum carbon-14 detection and correspond to the following ranges of pulses leaving the preamplifier:

channel 1	2 mV - 20 mV
channel 2	20 mV - 400 mV
channel 3	> 400 mV

Channels 1 and 2 register carbon-14 pulses while ^{222}Rn is detected in the highest energy channel 3. The pulses from the amplifier/discriminators are thereafter transferred to a diode matrix logic unit for time-coincidence analysis with the guard counter pulses. The diode matrix logic unit utilises information from the guard counter and the three discriminators to provide coincidence and anticoincidence of the three energy channels with the guard. The voltage to both counters is supplied by a fully transistorised dual voltage supply; 500-6100V for the sample counter and 500-4100V for the guard detector. Pulses are shown on four decade scalers, each with a 5-digit register. Sodeco print-out units with scalers coupled to an automatic timer and preset time interval enable long counting times to be split into several smaller periods, typically 30 minutes. Therefore, print-out

analysis represents a valuable check on counter stability over the time of the total count. After the print-out time interval is completed, the registers are automatically reset. The essential features of the counting system are shown in Figure 2.8.

Optimisation of operating conditions.

The operating voltages for each counter fill are obtained by analysis of detector voltage vs. coincidence meson count rate (rather than via the lower anticoincidence count rates). The resultant meson spectrum is a function of gas gain which in turn is sensitive to even low impurity levels in carbon dioxide. Figure 2.9 shows the meson spectra of pure and impure gases. The sharp peaks obtained in channels 1 and 2 in a) are characteristic of a pure gas, while the broader peaks and lower peak-heights in b) are caused by the quenching effect of impurities. For sample counting gases, operating voltages are chosen within the area of steepest gradient of channel 1 and 2 count rates, C_1 and C_2, at the point where the ratio $C_1:C_2$ is 2:3. A range in operating voltage of 3.45 ± 0.05 KV is regarded as acceptable. If, for a given gas sample, the voltage required for a C_1/C_2 ratio of 2/3 lies outside this range, it is repurified.

After the coincidence meson plateau has been plotted and the operating voltage obtained, a 10 minute measurement of coincidence and guard count rates is made before the system is set up for the overnight anticoincidence count of at least

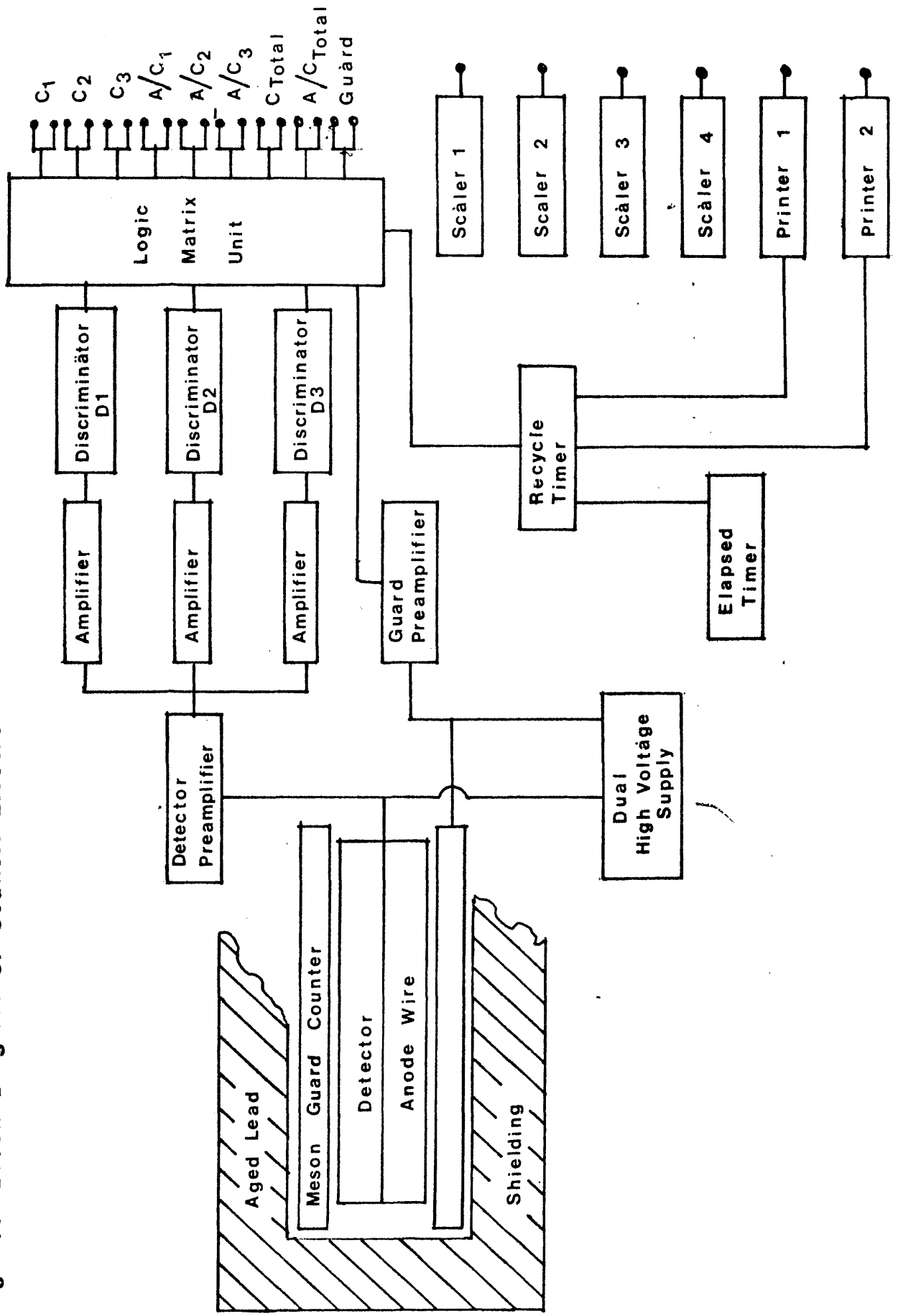

Fig. 2.8 Block Diagram of Counter Electronics

Fig. 2.9 Characteristic Coincidence Spectra.

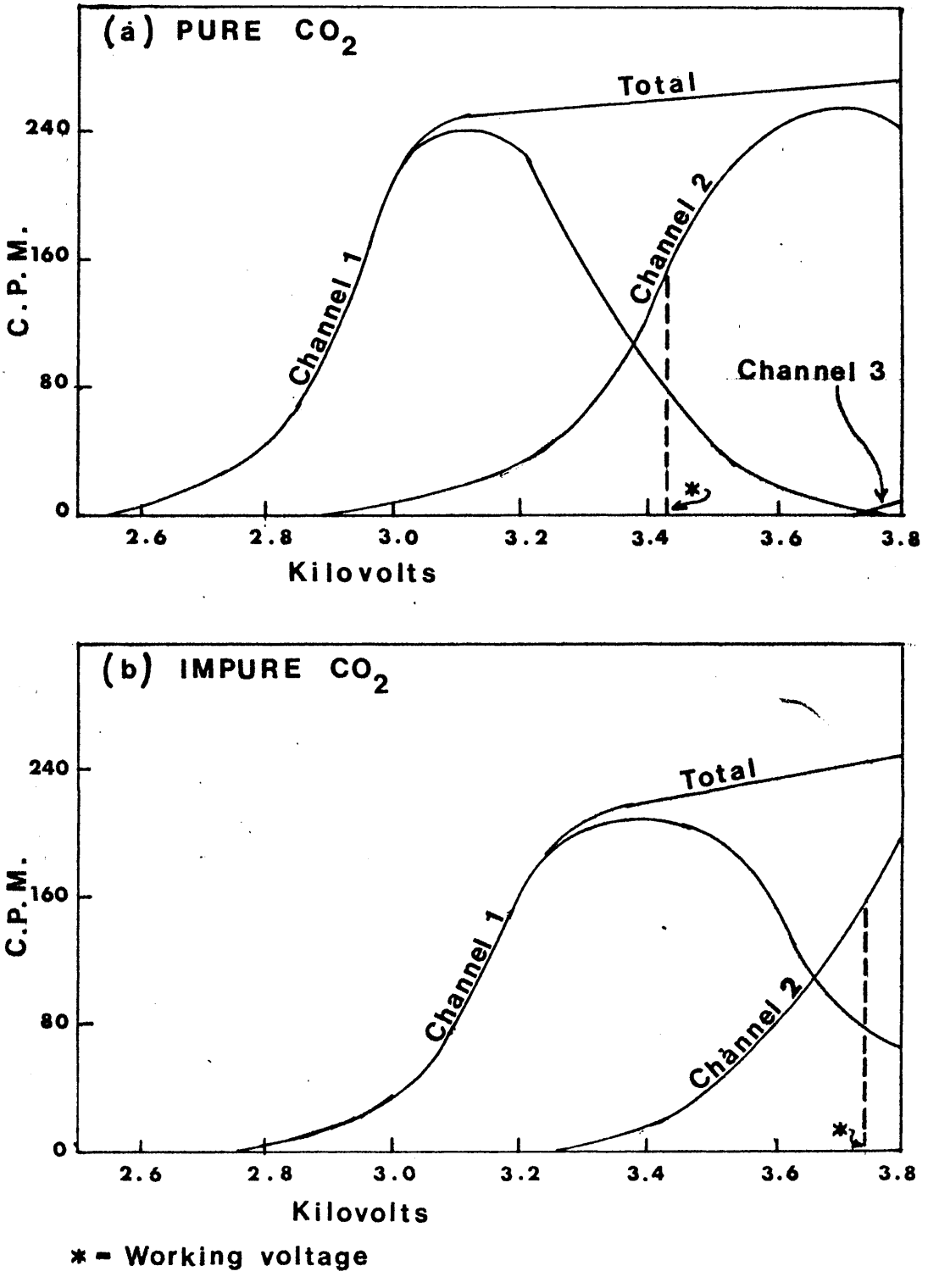

1080 minutes duration. At the end of this period, the coincidence and guard count rates are measured as before to ensure that the operating voltage has not changed significantly. However, the coincidence spectrum for most gases moves, by typically 3.4V, to higher voltages after an overnight count. This effect is assumed to be caused by outgassing from the counter walls. The initial purity of the gas is restored at the next counter fill when the gas is pumped to 10^{-5} torr.

An example from the daily counting log is given in Figure 2.10. At least four overnight counts are performed for every sample gas to accumulate a minimum of 50,000 counts and thereby reduce overall counting uncertainties below 0.5%. Successive count rates differ by $> 2\ (\sigma_1 + \sigma_2)$, where σ_1 and σ_2 are the statistical counting errors (one standard deviation), further counting is performed until there is agreement within the specified error limits. The stability of an overnight count is checked from the print-out tape. A print-out total differing from the mean by $> \pm 2\sigma_{mean}$ is neglected. Barometric pressure, measured continuously on a barograph, is averaged for each counting period.

2.5 Isotopic fractionation of CO_2.

Correction must be made for isotopic fractionation which can occur both in nature and during the chemical procedures employed in the laboratory. Isotopic fractionation occurs in the transfer of carbon between different phases of the environment. Mass spectrometric studies have shown that marine

FIGURE 2.10 TYPICAL EXTRACT FROM COUNTER LAB BOOK

SAMPLE CODE: SP 10 DATE 3/12/74

FILLING PRESSURE: 76.59 CM AT 63°F

VOLTAGE (KV) COUNTS PER 2 MINUTES

	C_1	C_2	C_3	C_T	AC_T
2.60	1	-	-	1	1
2.80	18	-	-	18	5
3.00	150	1	-	151	25
3.20	407	14	-	421	25
3.40	415	90	-	505	34
3.50	204	286	-	490	31

OPERATING VOLTAGE: 3.48 KV GUARD: 1.40 KV

10 MIN.COINC.COUNT	C_1	C_2	C_3	C_T	G
	1035	1501	-	2534	6701

ON : 16.43 3/12
OFF: 11.15 4/12 COUNTING TIME 1110 MINS.

TOTAL COUNT	AC_1	AC_2	AC_3	AC_T
	6200	14603	39	20836
CPM	5.58±0.07	13.15±0.11	0.04±0.05	18.77±0.13

10MIN.COINC.COUNT	C_1	C_2	C_3	C_T	G
	1030	1629	-	2659	6843

ATMOSPHERIC PRESSURE: 1020 MB

---

plants are enriched in C-13 by about 2.0 per cent compared to land plants (Craig, 1953). This is due to preferential uptake of C-12 during photosynthesis. Fractionation in the various stages of laboratory preparation of the counting gas may also occur if the chemical yields are significantly less than 100 per cent. A correction for this effect is necessary before measured C-14 concentrations can be directly compared with a specific standard activity. It is assumed that the fractionation effect for C-14 is twice as large as for C-13 (Craig, 1954).

The C-13/C-12 ratio of each sample of carbon dioxide is obtained via abundance ratio measurements of carbon and oxygen performed by mass spectrometric analysis. The C-13/C-12 and O-18/O-16 ratios are not measured directly but are deduced from the beam intensity ratios 45/44 and 46/(44+45) respectively, where:

mass -44 ions = $^{12}C\ ^{16}O\ ^{16}O$ (98.42 per cent)

mass -45 ions = $^{12}C\ ^{16}O\ ^{17}O$ (0.08 per cent) + $^{13}C\ ^{16}O\ ^{16}O$ (1.1per cent)

mass -46 ions = $^{12}C\ ^{16}O\ ^{18}O$ (0.4 per cent) + $\left.\begin{matrix} ^{12}C\ ^{17}O\ ^{17}O \\ + \ ^{13}C\ ^{16}O\ ^{17}O \end{matrix}\right\}$ ($\simeq$ 0%)

The values in parentheses represent the percentage relative abundances of the isotopic species (McCrea, 1950). Isotopic fractionation analyses are performed using a double collecting, 90° deflection, 6 cm radius, Micromass 602B mass spectrometer (V.G. Micromass Ltd., Winsford, Cheshire). The spectrometer features twin ion collectors which permit direct measurement of

the deviation in sample beam intensity ratios 45/44 and 46/(44+45) from the standard ratios. The enrichment of C-13 in a sample as a result of fractionation is expressed by the symbol δ C-13 defined by the realtionship:

$$\delta C\text{-}13 = \left[\frac{R_{SM}}{R_{ST}} - 1\right] \times 1000\ ^{o}/_{oo}$$

where R_{SM} and R_{ST} are the C-13/C-12 ratios of the unknown sample and standard, respectively.

Therefore, the extent of fractionation is measured in terms of the per milledifference, δ C-13, between the sample and the standard P.D.B. The P.D.B. standard is CO_2 produced from the cretaceous belemnite Belemnitella americana by reaction with 100% H_3PO_4 at 25.2°C (Urey et al., 1951). In practice, a secondary standard, previously intercalibrated with the Belemnitella americana standard, is employed. Dual all-metal inlet systems coupled to a solenoid-operated changeover valve allow rapid comparison of sample and standard ratios. The dimensions of capillary leak and the inlet pressure ($\sim$7 cms Hg) are such that the inlet gas flow is viscous, preventing isotopic fractionation in the sample vessel (Brunnée and Voshage, 1964). Ratios are obtained on a digital output connected to a pen recorder. About 5-6 successive differences between sample and standard C-13/C-12 ratio are obtained on the 45/44 ion beam. Only 4 differences are recorded for the 46/(44+45) ion beam; analysis of these enables a correction to be applied for O-17 contribution via $^{12}C\ ^{16}O\ ^{17}O$ to the mass -45 peak.

The values for sample 45/44 ratio, standard 45/44 ratio and their differences are averaged and expressed as R_1', R_0' and Δ' respectively. An adjustment is made to these values to correct for the slight amount of mixing of sample and standard gases across the changeover valve. Thus the corrected ratios R_1 and R_0 respectively are obtained. Δ, the corrected difference in the mass 45/44 ratio between sample and standard, is calculated from the expression:

$$\Delta = \Delta' \times \frac{R_1 - R_0}{R_1' - R_0'}$$

The measured deviation δC_m-13 of sample from standard is:

$$\delta C_m\text{-}13 = \Delta / R_0 \times 1000 \text{ }^{o}/_{oo}$$

but since $R = ({}^{13}C\ {}^{16}O\ {}^{16}O + {}^{12}C\ {}^{16}O\ {}^{17}O) / {}^{12}C\ {}^{16}O\ {}^{16}O$

a correction factor must be applied for the abundance of ^{17}O. Since enrichments for ^{17}O and ^{18}O differ by a factor of 2 (Craig, 1957), measurement of the 46/(44+45) ion beam ratio enables a correction to be applied to δC_m-13 via δ 0-18, where:

$$\delta 0\text{-}18 = \frac{\Delta''}{R''} \times 1000 \text{ }^{o}/_{oo}$$

Δ'' = the mean of the difference in 46/(44+45) ratios of sample and standard and

R'' = the mean of the 46/(44+45) of standard.

Thus the corrected value of δC_m-13

$$\delta C_{corr}\text{-}13 = 1.065\, \delta C_m\text{-}13 - 0.0325\, \delta 0\text{-}18$$

This value has been calculated relative to the working

standard which was derived from combustion of a sample of human brain during a recent study of C-14 in human tissues (Stenhouse, 1974). Before δC_{SM}-13 - defined with respect to the PDB standard - can be calculated, the δ C-13 value of the working standard relative to PDB must be known. Thus the δC-13 of the brain standard, calibrated relative to PDB is -26.1 per mil, and for an additional tree ring working standard -23.9 per mil. The data for several calibrations of the brain standard are presented in Table 2.2. The Precision of mass spectrometric measurements is limited and dependent on ion statistics. The instrumental stability is of utmost importance and is discussed by referring to the reproducibility of results (Table 2.2). Thus, δC-13 ratios and δO-18 ratios of samples are routinely measured at Glasgow with a precision of $\pm$ 0.05 per mille(1σ).

2.6 Treatment of sample C-14 activity measurements.

The anticoincidence count rates obtained for each sample represent the gross activity of that particular sample and include a significant contribution from background radiation. To reduce the statistical uncertainty on the net activity of a sample it is necessary to measure the background count rate and its variations.

Background count rate measurement.

The major sources of background radiation detected in the sample counter are:

a) cosmic-ray mu-mesons which are not eliminated by anticoincidence shielding

TABLE 2.2 CALIBRATION OF WORKING STANDARD (BRAIN CO_2) FOR ISOTOPIC FRACTIONATION MEASUREMENTS

DATE	$\delta^{13}C_{PDB}$ (BRAIN CO_2) ‰
2/03/76	-26.31
7/06/76	-26.10
9/09/76	-26.14
20/09/76	-26.09
13/11/76	-26.09
26/11/76	-26.00
AVERAGE	-26.12 ($\pm 1\sigma$=0.05)

b) secondary gamma rays produced essentially by interaction of mu - mesons with lead, and

c) radioactive impurities in the counter materials and background filling gas.

The discriminator threshold of 2 mV eliminates counter electronic noise while teflon insulation reduces spurious pulses to a negligble level. During the course of this research non-statistical background counts were observed as a result of contamination by radioactive impurities in the guard gas. Most probably the source of guard gas contamination was radon-222 and its daughter products. Thus, while in the period from 12 September 1973 to 16 October 1974 recorded background count rates were within the range 4.60 to 5.00, after the 3 month period of contamination background count rates increased to a range of 5.30 to 5.80 cpm.

For background measurement, suitable source materials of inactive carbon are:

a) marble chips

b) tank (commercially available) carbon dioxide.

Marble chips ($\sim$90g.) are treated with 2M HCl to remove the outer layer and are subsequently washed in distilled water and dried. Thereafter the chips are added directly to the purification furnace, pumped to 10^{-4} torr at 400^{o}C, heated to 900^{o}C and the carbon dioxide evolved and collected at liquid N_2 temperatures. For the tank (industrial) carbon dioxide it is necessary only to purify the gas.

Thus two separate background carbon dioxide samples are

readily available. Background gases are counted at least once every 14 days but normally once every 10 days. By accumulation of results over a period of months, a series of background vs. atmospheric pressure data is obtained. During this study, barometric pressures ranged from 974 to 1038 mbs. The results are subjected to linear regression analysis by the method of least squares. Details of the procedure, performed via computer are given in Appendix 1. An inverse relationship is obtained by such a treatment whereby the background count rate decreases by 0.01 cpm per mbar. increase in atmospheric pressure. The line applicable to the 12 month period commencing February, 1977 is shown in Figure 2.11 together with the statistical error associated with the linear plot. Such a relationship confirms that the main component of background radiation can be attributed to cosmic rays. A greater physical barrier is presented to the passage of cosmic rays and cosmic ray derived particles by the earth's atmosphere during periods of high rather than low pressure.

Reference standard

For carbon-14 assay, data are generally reported in relation to a standard after appropriate correction for isotope fractionation. Therefore, the reference (standard) material should be universally employed to maintain consistency and reproducibility between laboratories. The standard is oxalic acid, provided by the U.S. National Bureau of Standards to nearly all of the hundred or more laboratories active in this

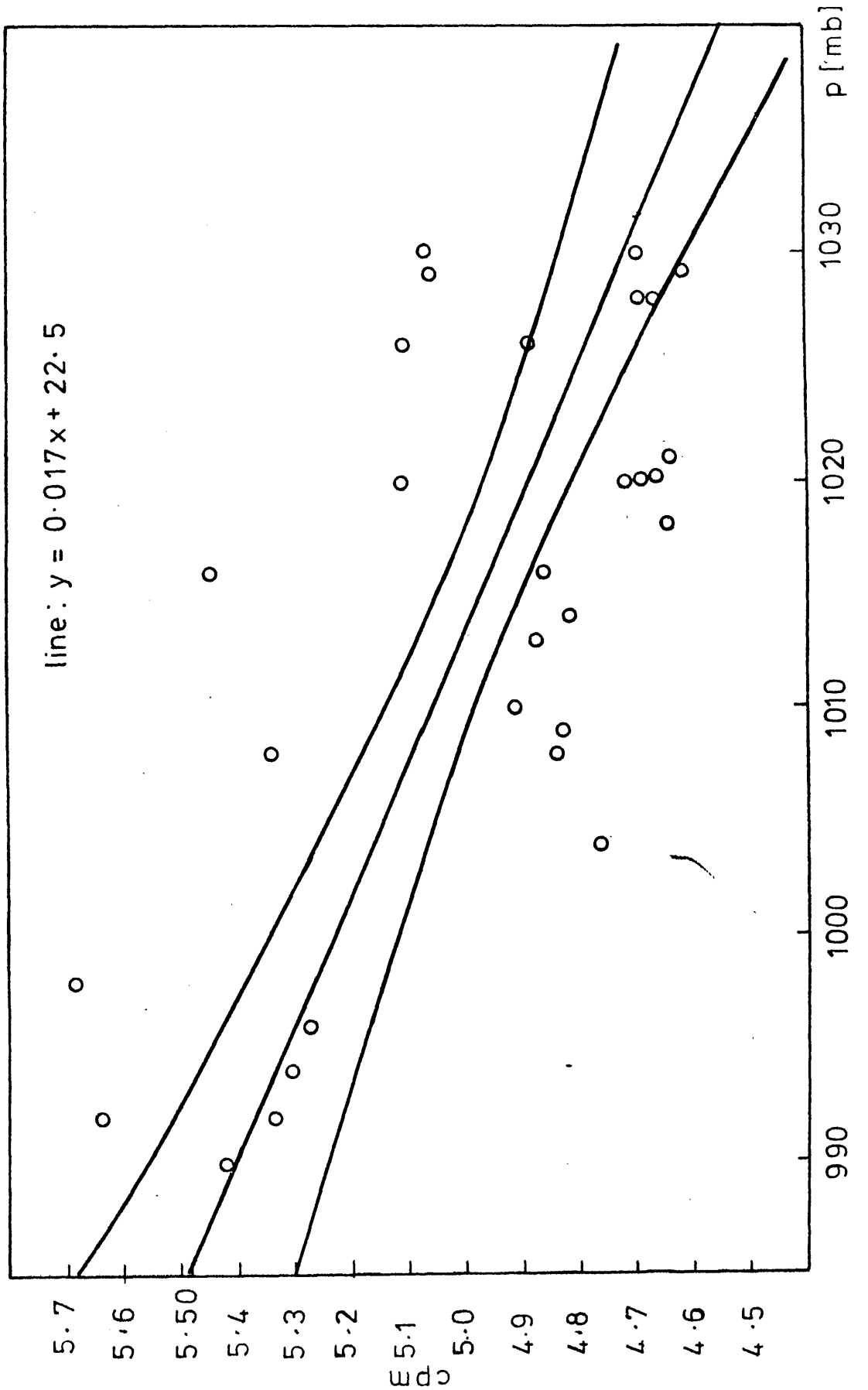

FIG 2.11 BACKGROUND COUNT RATE US. BAROMETRIC PRESSURE

field. As described previously, the standard is related in activity to the natural level in 1890 wood.

Carbon dioxide is prepared from the oxalic acid dehydrate by wet oxidation, performed in the hydrolysis section of the vacuum line. The reaction is allowed adequate time for completion to prevent isotopic fractionation of the carbon dioxide (Grey et al., 1969). A saturated solution of $KMnO_4$ in 0.5 M H_2SO_4, the oxidising reagent, is slowly added to 16 g NBS oxalic acid in distilled water and the following reaction occurs:

$$5(COOH)_2.2H_2O + 6MnO_4^- + 38H^+ \longrightarrow 10CO_2 + 6Mn^{2+} + 26H_2O$$

After addition of excess permanganate (2-3 hours), the solution is stirred for a further 4 hours. Thereafter, the purification of CO_2 is performed in the normal way. As for background samples, the modern standard is counted regularly, on average once every 14 days, to reduce the statistical uncertainty on its activity. In addition, regular standard counting represents a continual check on the stability of performance of the counter. Before the standard can be used in calculation of $\delta C\text{-}14/\Delta$ values, two corrections must be applied to its radiocarbon activity:

a) for isotopic fractionation, since 95 per cent of the standard activity in 1958 normalised to $\delta C\text{-}13 = -19.00$ per mille with respect to P.D.B. standard, corresponds to the activity of 1890 wood (Broecker and Olson, 1961). Therefore all modern standard activities are corrected for fractionation relative to

-19.0 per mil. via the equation:

$$A_o = A' \left[1 - \frac{2(\delta C\text{-}13 + 19)}{1000}\right]$$

where Ao is the final corrected modern activity and δC-13 is the C-13/C-12 ratio in the CO_2 relative to that of the P.D.B. standard and A' is measured C-14 activity of NBS oxalic acid.

b) for radioactive decay, since present day activities of the NBS oxalic acid must be corrected for C-14 decay since the date of calibration, 1958. The decay correction is 0.12 per mil (i.e. $\lambda = \frac{0.693}{5730}$) per year and correction is therefore performed via:

$$A_o = A_t \left[1 + \frac{0.12\ (t\text{-}to)}{1000}\right]$$

where A_o is the decay-corrected 1958 activity and A_t is the measured activity at the time t (yr) after 1958. The resultant activities are combined for periods of statistical agreement and their mean value used in the treatment of sample results. The values of the standard activities measured during the course of this research are shown in Table 2.3

Correction of sample count rates for contamination by Rn-222 plus daughter products.

Occasionally a contribution to the total activity of a sample from radon and associated daughter products is observed, even after two weeks storage. To avoid wastage of counting runs by rejection of such count rates, the relationship between Rn-222 alpha pulses occurring in anticoincidence channel 3 (A/C_3) and the resultant increase in counts observed in A/C_1 + A/C_2 can be determined using samples of predetermined activity

TABLE 2.3 REFERENCE STANDARD

DATE	P (MB)	MODERN,CORR. FOR BACKGR. (CPM)
13/9/73	1026	14.26±0.14
2/10/73	1030	14.45±0.11
4/12/73	1018	14.52±0.11
18/12/73	992	14.87±0.10
8/1/74	995	14.77±0.11
15/1/74	993	14.45±0.11
22/1/74	1004	14.63±0.11
29/1/74	986	14.38±0.11
20/2/74	1020	14.75±0.16
27/2/74	1026	14.41±0.14
13/3/74	1018	14.99±0.14
20/3/74	1012	15.43±0.16
27/3/74	1020	14.43±0.14
	AVERAGE	14.64 ± 0.13

which are subsequently seeded with Rn-222. A residual alpha count rate in $A/C_3 \sim 0.045$ cpm is apparent from numerous measurements. These pulses, which are subtracted from the total A/C_3 count rate are assumed to result from traces of U and Th series nuclides in the counter materials. A similar effect, but to a greater extent, was noted by Fergusson (1955). Thus, if A/C_T represents the total anit-coincidence count rate with Rn-222 present i.e. $A/C_T = A/C_1 + A/C_2 + A/C_3$ where A/C_1, A/C_2 and A/C_3 are the individual channel count rates, then R, the contribution to channels $A/C_1 + A/C_2$ from Rn-222 plus daughter products in A/C_3 i.e. the net beta/alpha ratio is given by:

$$R = \frac{A/C_1 + A/C_2}{A/C_3 - 0.045}$$

R was determined experimentally, under normal CO_2 counting conditions, to be 1.230 ± 0.036. The total correction to be subtracted from A/C_T is therefore:

$$(R + 1)\ (A/C_3 - 0.045) \text{ cpm}$$

i.e. $A_{corr.} = A/C_T - (R + 1)\ (A/C_3 - 0.045)$ cpm.

The error on Acorr., at the 1σ confidence level, is given by:

$$\pm \sigma_{A_{corr.}} = \pm \sqrt{\sigma^2_{A/C_T} + \sigma^2_C}$$

(The error on 0.045 is negligible.)

where $C = (R + 1)\ (A/C_3 - 0.04)$

and $\pm \sigma_C = \pm \sqrt{\left(\frac{\sigma_R}{R + 1}\right)^2 + \left(\frac{\sigma_{A/C_3}}{A/C_3 - 0.045}\right)^2} (R+1)\ (A/C_3 - 0.045)$

Since the error on $(R + 1)$ is negligible compared to $(A/C_3 - 0.045)$, σ_C reduces to $\pm \sigma_C = \pm \sigma_{A/C_3} (R + 1)$

Calculation of results.

Net activities of both sample (A_{SM}) and NBS oxalic acid standard (A_{MD}) are related via the following equation established by Broecker and Olson (1959):

$$\delta^{C-14}_{SM} = \left[\frac{A_{SM}}{0.95 A_{MD}} - 1 \right] \times 1000 \text{ }^{o}/_{oo}$$

The multiplication factor 0.95 adjusts the standard activity to correspond to the C-14/C-12 concentration of 1890 wood. The parameter δ^{C-14}_{SM} is uncorrected for isotopic fractionation of the sample itself; after the necessary correction via δ^{C-13}_{SM} the equation becomes:

$$\Delta \text{ } (^{o}/_{oo}) = \delta^{C-14}_{SM} - (2\delta^{C-13} + 50) \left(1 + \frac{\delta^{C-14}}{1000}\right)$$

(Broeckler and Olson, 1961). Δ represents the per mil difference in C-14 activity between sample and standard, after fractionation effects have been considered. The errors on δC-14 and Δ values expressed below at the $\pm 1\sigma$ confidence level, i.e. one standard deviation, are based on the statistical uncertainty of sample background, and standard count rates, and on the precision of each δ C-13 measurement, via:

$$\sigma(\delta C\text{-}14) = \frac{A_{SM} \times 1000}{0.95 \times A_{MD}} \left[\left(\frac{\sigma_{SM}}{A_{SM}} \right)^2 + \left(\frac{\sigma_{MD}}{A_{MD}} \right)^2 \right]^{\frac{1}{2}}$$

$$\text{and } \sigma(\Delta) = \pm \left[\left(1 - \frac{(2\,\delta C\text{-}13+50)}{1000}\right)^2 \sigma^2 (\delta C\text{-}14) + 4\left(1+\frac{\delta C\text{-}14}{1000}\right)^2 \sigma^2 (\delta C\text{-}13) \right]^{1/2}$$

(Callow et al., 1965).

Age determination.

A sample age, T years, is calculated from the equation:

$$T = 8033 \log_e \left[\frac{1}{1 + (\Delta \times 10^{-3})} \right]$$

where $8033 = t_{\frac{1}{2}}/0.693$

Limits of age are fixed by the error on Δ, as follows:

$$(T + t_1,\ T - t_2) = 8033 \log_e \frac{1}{1 + [\Delta \pm \sigma(\Delta)] \times 10^{-3}}$$

Furthermore, radiocarbon ages are normally quoted in years B.P. (before present) the present being by convention taken as 1950.

Intercalibration of the counting system.

Many interlaboratory calibration samples were measured to check the validty of the carbon dioxide preparation and counting techniques. In general, good agreement within statistical error was obtained (Table 2.4). In the table, Glasgow #2 refers to results obtained totally independently in the second radiocarbon facility at Glasgow University (Campbell, 1977).

2.7 Reproducibility of counting.

Generally, radiocarbon dates are reported in the form $\Delta \pm$ error (or age $\pm$ error). The error term usually expresses the uncertainty associated with the counting procedure only, with any further contribution to overall error from experimental uncertainties being neglected. The results of a

TABLE 2.4 INTERCALIBRATION SAMPLES

SAMPLE	Δ (‰) OR AGE (YR.) ±1 σ	
	THIS LABORATORY	OTHER LABORATORIES
ANY SUGAR IC#1LJ	453.90±6.10 (Δ)	448.20±4.60 (GLASG.# 2)
		489.20±9.99 (E.KILBR.)
WOOD IC#3	-357.30±5.10(Δ)	-410.50±4.50 (GLASG.#2)
		-376.40±4.70 (LA JOLLA)
HITCHOCK IC#4	-19.00±5.20 (Δ)	-31.50±7.00 (GLASG.#2)
		-17.50±8.30 (LA JOLLA)
		-27.20±9.99 (E.KILBR.)
E.K.WOOD# 858	4025±67 (Y.)	3988±32 (GLASG. # 2)
		4278±50 (LA JOLLA)
E.K. WOOD # 393	21,723±532 (Y.)	25,923±372 (GLASG. # 2)
		47,560±545 (LA JOLLA)

SAMPLE	Δ (‰) OR AGE (YR.)±1σ			
	THIS LABORATORY		OTHER LABORATORIES	
E.K. WOOD # 23	3523±64	(Y)	3940±60	(LA JOLLA)
YS-1-RA	-454.52±5.00 (Δ)		-458.40±3.50	(E.KILBR.)
			-453.38±4.77	(GLASG. # 2)
SP-1	192±43	(Y)	196±38	(E.KILBR.)
SP-2	139±48	(Y)	155±34	"
SP-3	180±49	(Y)	163±35	"
SP-4	170±33	(Y)	128±31	"
SP-5	188±33	(Y)	137±32	"
SP-6	170±37	(Y)	106±32	"
SP-7	147±48	(Y)	141±32	"
SP-8	108±43	(Y)	65±34	"
SP-9	144±44	(Y)	133±33	"
SP10	148±38	(Y)	115±34	"

series of replicate analyses have, however, shown that for this laboratory, there is a significant contribution to the overall error due to experimental factors, such as errors in (a) sample selection and preparation (b) pressure and temperature readings and (c) working voltage optimisation. Therefore the total error, including the experimental uncertainties, is expressed as

$$\sigma^2_{\text{TOT.R.}} = \sigma^2_{\text{EXP.R}} + \sigma^2_{\text{COUNT R.}}$$

where $$\sigma_{\text{TOT.R.}} = \left[\frac{\sum(X_i - \bar{X})^2}{n-1}\right]^{\frac{1}{2}}$$

and $$\sigma_{\text{COUNT R.}} = \left[\frac{\sigma^2_{c1} + \sigma^2_{c2} + \ldots + \sigma^2_{cn}}{n}\right]^{\frac{1}{2}}$$

To estimate the contribution from the non-counting experimental error, ten identical samples (each counted four times) were separated from the same sequence of Ynyslas pine (Ys-Ra-1) and finely divided to sawdust. The results are shown in Table 2.5. Thus for the replicate samples it was found that

$$\bar{\Delta}_R \pm 1\sigma_{\text{TOT.R.}}$$

is numerically

$$-45.56 \pm 1.41 \quad (\%)$$

and similarly that

$$\bar{T}_R \pm 1\sigma_{\text{TOT.R.}}$$

is given by 4890 ± 209 (yr)

TABLE 2.5 REPLICATE DATA

CODE	$\delta C-13 \pm 0.05$ (‰)	$\delta C-14 \pm 1\sigma$ (‰)	$\Delta \pm 1\sigma$ (‰)	AGE $\pm 1\sigma$ (Y)
RA- 1	-31.03	-469±9.0	-463±9.0	4992±138
RA- 2	-31.31	-488±9.0	-481±9.0	5273±141
RA- 3	-30.46	-448±11.0	-442±11.0	4684±155
RA- 4	-30.73	-478±9.0	-472±8.8	5133±135
RA- 5	-30.32	-416±9.0	-446±8.6	4742±126
RA- 6	-32.93	-464±9.3	-455±9.0	4879±139
RA- 7	-30.61	-439±9.8	-433±9.7	4554±133
RA- 8	-33.38	-464±9.0	-454±8.6	4869±128
RA- 9	-29.49	-460±8.7	-455±8.7	4874±128
RA-10	-32.98	-465±8.7	-456±8.7	4897±129
		AVERAGE	-455.6±9.11	4890±135

Thereafter $\sigma_{EXP.R.}$ was calculated from

$$1.41^2 = \sigma^2_{EXP} + 0.914^2$$

Thus $\sigma_{EXP.R.}$ equals 1.07 (‰) and 160 (yr) respectively. It should be notes that any inhomogeneity in the replicate samples could give rise to an apparent, but unreal, analytical error. Thus the $\sigma_{EXP.R.}$ values quoted here represent maximum estimates. Since the replicate wood material was finely divided and mixed prior to sampling, it seems likely that these estimates are realistic. Subsequently, total errors for any sample can be calculated according to:

$$\sigma_{TOT.SM} = \left[\left(\frac{\sigma_{EXP.R.}}{\overline{\Delta}_R} \times \Delta_{SM}\right)^2 + \sigma^2_{C.SM}\right]^{\frac{1}{2}}$$

Thus for the 21 tree rings of Scots pine, $\sigma_{EXP.}$ was estimated to be 0.043 ± 0.013 (‰); for the 12 tree rings of Ynyslas pine 1.16 ± 0.05 (‰) and for the 30 tree rings of Clarach oak 1.25 ± 0.06 (‰). These results compare with the following findings, for the same replicate sample (Ys-Ra-1), reported by the other Glasgow University laboratory which is based on the liquid scintillation method:

$$-45.51 \pm 0.58 \quad (‰)$$

i.e. 4857 ± 87 (yr)

with $\sigma_{EXP.R.}$ estimated to be 0.55 (‰) and 79 years respectively (Campbell, pers. comm.). The discrepancy between these two findings in different Glasgow University laboratories perhaps shows that the experimental error cannot be generalised.

Nor can the additional error be attributed entirely to inhomogenuity of the sample since the $\sigma_{EXP.R.}$ values differ between systems. Rather the discrepancy most certainly must be due to differences in sample pretreatment as well as in vacuum line procedures.

The possibility of sample contamination by 'modern' carbon during the various stages of chemical pretreatment and preparation was examined by preparing two counting gases from coal, a material which is radiocarbon-free. The results show no carbon-14 presence in these samples; the differences were $+ 0.03 \pm 0.07$ and $+ 0.04 \pm 0.07$ relative to the background count rate. Thus no significant input of 'modern' radiocarbon contaminant occurs during sample preparation.

CHAPTER 3. Results.

Three listed tables represent all the tree ring data collected over the research period. A $\pm 1\sigma$ error is quoted for δC-13, δC-14, Δ and radiocarbon age results. δC-13, δC-14 and Δ values are expressed in per mille units and radiocarbon ages in conventional C-14 years B.P., based on the Libby half-life of 5568 yr. As already discussed, it was possible only to count and dendrochronologically date the Scots pine tree rings (Table 3.1). Since the Scots pine was cut in 1973 and counted in 1975, the correction due to decay was estimated according to:

$$\Delta_{corr.} = \Delta_{obs.} \times e^{\lambda t}$$

where $\lambda = \frac{\ln 2}{t_{\frac{1}{2}}}$ denotes the radioactive decay constant and t = dendrochronological age + 2 (y).

TABLE 3.1 RADIOCARBON DATA AND CALENDAR AGE FOR SCOTS PINE TREE RINGS

CODE	$\delta C\text{-}13 \pm 0.05$ (‰)	$\delta C\text{-}14 \pm 1\sigma$ (‰)	$\Delta \pm 1\sigma$ (‰)	$\Delta_{corr} \pm 1\sigma$ (‰)	CAL.AGE (Y. AD)
SP22	-25.10	-17.74±7.40	-17.54±7.40	-18.04±7.40	1740
SP21	-25.06	-13.40±3.90	-13.30±3.90	-13.68±3.90	1741
SP20	-25.25	-18.46±5.26	-17.97±5.26	-18.48±5.00	1742
SP19	-22.98	-12.66±7.40	-16.65±7.40	-17.12±7.40	1743
SP18	-25.08	-13.38±5.96	-13.23±5.96	-13.60±7.40	1744
SP17	-23.59	-14.84±5.96	-17.61±5.95	-18.10±6.00	1745
SP16	-25.58	-14.84±5.96	-13.70±5.96	-14.08±6.00	1746
SP15	-25.15	-16.25±4.76	-15.96±4.70	-16.40±4.80	1747
SP14	-22.73	-10.48±4.56	-14.98±4.60	-15.39±4.60	1748

SP13	-20.91	- 6.21±6.80	-14.34±6.70	-14.73±6.70	1749
SP12	-21.95	-11.21±3.88	-17.24±3.86	-17.71±3.40	1750
SP11	-23.23	-14.82±4.75	-18.30±4.74	-18.80±4.70	1751
SP10	-22.43	-11.32±6.10	-16.31±6.10	-16.75±6.00	1752
SP 9	-27.94	-23.43±6.10	-17.70±6.00	-18.18±6.00	1753
SP 8	-22.61	-13.38±5.96	-18.10±5.94	-18.59±6.00	1754
SP 7	-23.81	-17.01±4.60	-19.35±4.60	-19.87±4.60	1755
SP 6	-24.61	-18.40±5.41	-19.17±5.41	-19.68±6.00	1756
SP 5	-23.81	-16.97±4.11	-19.31±4.11	-19.82±4.10	1757
SP 4	-22.71	-17.69±6.10	-22.19±6.10	-12.77±6.10	1758
SP 3	-24.30	-16.29±6.00	-17.66±5.96	-18.12±6.00	1759
SP 2	-23.50	-10.48±5.30	-13.45±5.30	-13.80±5.30	1760

TABLE 3.2. RADIOCARBON DATA FOR YNYSLAS PINE

CODE	δC-13±0.05(‰)	δC-14±1σ(‰)	Δ+1σ(‰)	C-14 AGE ± 1σ (Y.BP)
YS12	-28.56	-462±4.40	-459±4.40	4930±65
YS11	-28.06	-457±5.10	-454±5.10	4863±75
YS10	-27.52	-459±4.40	-456±4.40	4893±65
YS 9	-28.60	-458±5.10	-455±5.10	4871±76
YS 8	-29.28	-508±4.40	-504±4.40	5633±71
YS 7	-30.16	-460±5.10	-455±5.10	4862±75
YS 6	-30.29	-461±6.60	-455±6.50	4827±97
YS 5	-29.70	-456±5.90	-451±5.80	4815±85
YS 4	-27.94	-457±5.10	-454±5.10	4865±75
YS 3	-28.12	-492±5.10	-489±5.10	5395±81
YS 2	-27.33	-458±5.10	-456±5.10	4885±76
YS 1	-27.25	-454±4.40	-451±4.40	4822±65

TABLE 3.3 RADIOCARBON DATA FOR CLARACH OAK

CODE	δC-13±0.05(‰)	δC-14±1σ(‰)	Δ±1σ(‰)	C-14 AGE ± 1σ (Y.BP)
CH43	-25.18	-519±5.0	-519±5.0	5879±90
CH42	-23.18	-484±4.0	-485±4.0	5338±58
CH41	-23.36	-455±4.0	-456±4.0	4895±65
CH40	-25.13	-498±5.0	-498±5.0	5535±87
CH39	-22.02	-456±6.0	-459±6.0	4939±87
CH38	-25.64	-505±4.0	-505±4.0	5644±72
CH37	-25.99	-484±5.0	-483±5.0	5304±80
CH36	-25.67	-495±5.0	-494±5.0	5480±82
CH35	-24.34	-496±4.0	-497±4.0	5513±71

CH34	-24.87	-486±4.0	-487±4.0	5356±69
CH33	-24.30	-473±5.0	-473±5.0	5152±79
CH32	-24.80	-505±4.0	-505±4.0	5657±60
CH31	-21.76	-482±4.0	-485±4.0	5338±69
CH30	-25.62	-477±5.0	-476±5.0	5197±79
CH29	-27.81	-509±7.0	-506±8.0	5668±107
CH28	-27.35	-494±5.0	-492±5.0	5430±81
CH27	-25.13	-499±4.0	-499±4.0	5547±77
CH26	-25.13	-497±5.0	-497±5.0	5523±87
CH25	-25.13	-492±4.0	-492±5.0	5443±76

CH24	-23.64	-521±4.0	-552±4.0	5927±74
CH23	-23.96	-520±5.0	-521±5.0	5910±86
CH22	-24.52	-508±4.3	-509±4.0	5709±72
CH21	-25.13	-493±5.0	-493±5.0	5454±87
CH20	-25.96	-484±4.0	-484±4.0	5293±69
CH19	-23.28	-476±4.0	-478±4.0	5224±68
CH18	-26.98	-514±4.0	-512±4.0	5765±72
CH17	-24.59	-484±4.0	-485±4.0	5337±69
CH16	-27.50	-482±4.0	-479±4.0	5246±68
CH15	-28.01	-518±4.0	-515±4.0	5809±73
CH14	-27.95	-515±4.0	-512±4.0	5762±72

CHAPTER 4. DISCUSSION AND CONCLUSIONS.

In assessing the existence or otherwise of postulated 11-year period oscillations in atmospheric radiocarbon concentrations, an appropriate mathematical model and calculation procedure were obviously required. Since both sunspot numbers and radiocarbon levels are reported to show cyclic variations, a reasonable approach would seem to involve trigonometric functions as follows:

$$W = B_0 + B_1 \cos\left[\frac{2\pi}{T}(t - \delta_w)\right] + \text{error}$$

$$\Delta = A_0 + A_1 t + A_2 \cos\left[\frac{2\pi}{T}(t - \delta_\Delta)\right] + \text{error}$$

where W and Δ represent sunspot number and radiocarbon content respectively, B_0 and A_0 are constants, A_1 a linear gradient indicative of long-term increase, decrease or constancy of C-14 concentration with time (t), A_2 and B_1 are cycle amplitudes, T is the period of the oscillation and δ_Δ and δ_w are phase lags. These equations can be transformed into simplified forms suitable for computing:

$$W_i = B_0 + B_1 \cos\frac{2\pi}{T}\delta_w \cos\frac{2\pi}{T}t_i + B_1 \sin\frac{2\pi}{T}\delta_w \sin\frac{2\pi}{T}t_i + \text{error}$$

$$W_i = B_0 + B_2 \cos\frac{2\pi}{T}t_i + B_3 \sin\frac{2\pi}{T}t_i + \text{error}$$

where $B_2 = B_1 \cos\frac{2\pi}{T}\delta_w$

and $B_3 = B_1 \sin\frac{2\pi}{T}\delta_w$.

Thereafter

$$W_i = B_0 + B_2 Z_i + B_3 V_i + \text{error}$$

where $Z_i = \cos \frac{2\pi}{T} t_i$

$V_i = \sin \frac{2\pi}{T} t_i$

B_0, B_2 and B_3 are calculated by computer (Appendix 2);

amplitudes and phase lags are then quantified via the expressions:

$$B_1 = \sqrt{B_2^2 + B_3^2}$$

and $\tan \frac{2\pi}{T} \delta_w = B_3/B_2$

After the best trigonometric curve fit is obtained by multiple regression analysis, the calculation procedure estimates when peaks occur i.e. determines the phase lag of radiocarbon concentration relative to sunspot number. Thereafter the correlation between these two quantities, for the particular time interval being investigated, is found by linear regression. The period of the sine wave is assumed to be 11 years. The statistical significance of the curve fit is tested according to:

$$F = \frac{R^2/k}{(1-R^2)/(n-k-1)}$$

where F is a distribution (the values of which are listed in Statistical Tables by Murdoch and Barnes, 1974),. R is the correlation coefficient, n the number of data points and k the number of degrees of freedom. This mathematical model and calculation procedure was applied to all the available data sets of sunspot numbers and radiocarbon levels which showed significant scatter outside the experimental limits on a best

fitting straight line plot of C-14 versus time.

The radiocarbon data for Scots pine, Ynyslas pine and Clarach oak are shown in Figures 4.1, 4.2 and 4.3. Data points are shown with their associated $\pm 1\sigma_{TOT.}$ error bars. Through the radiocarbon data points the best fitting straight lines are drawn. These show long term decreases of radiocarbon levels for both Scots pine and Clarach oak, by -0.017% per year and -0.056% per year respectively; a long term increase by +0.009% per year is observed for Ynyslas pine. The lower section of Figure 4.1 presents sunspot number oscillations within the Scots pine wood growth interval (1740-1760 A.D.) showing a cycle of 11 years, statistically significant at >0.1% level (i.e. there is > 99.9% probability of this cyclic trend being real). Since, however, no calendar age can as yet be assigned either to Ynyslas pine (Figure 4.2) or to Clarach oak (Figure 4.3), it is not possible to correlate C-14 and sunspot numbers for these samples. For Scots pine (Figure 4.1) and for Clarach oak (Figure 4.3) the curve fits are statistically significant at 2.5% and 1% levels respectively, showing an optimum period for Scots pine C-14 values of 15 years and for Clarach oak, 13 years, with cycle amplitudes (peak to trough) of 0.40% and 2.45% respectively. Since the radiocarbon cycle period for Scots pine differs from that of the sunspot cycle for the investigated time interval, it is not meaningful to calculate a phase lag relationship or a correlation between radiocarbon and sunspot number. In

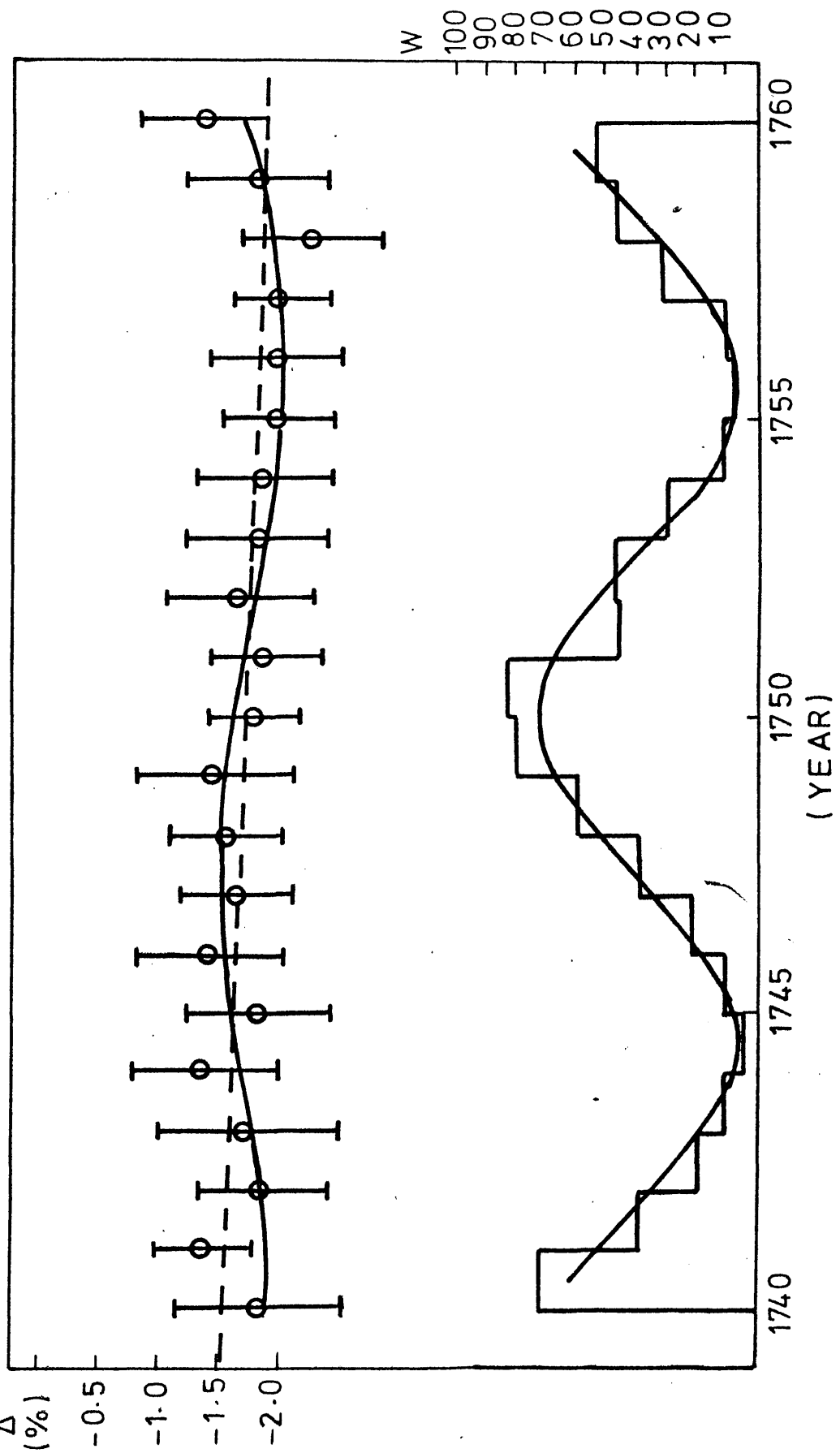

FIG. 4.1 GLASGOW RADIOCARBON DATA FOR SCOTS PINE.

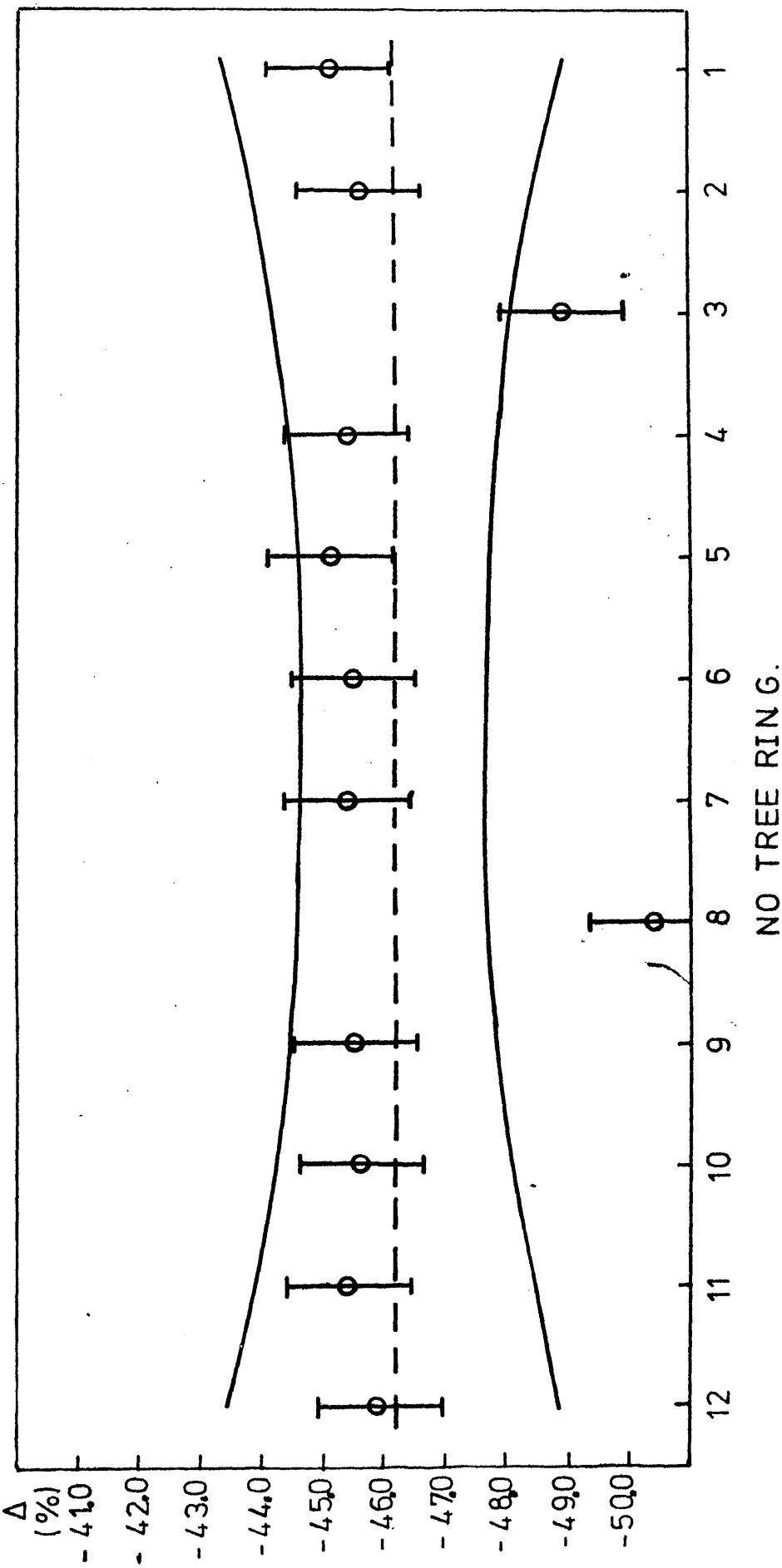

FIG. 4.2 GLASGOW RADIOCARBON DATA FOR YNYSLAS PINE.

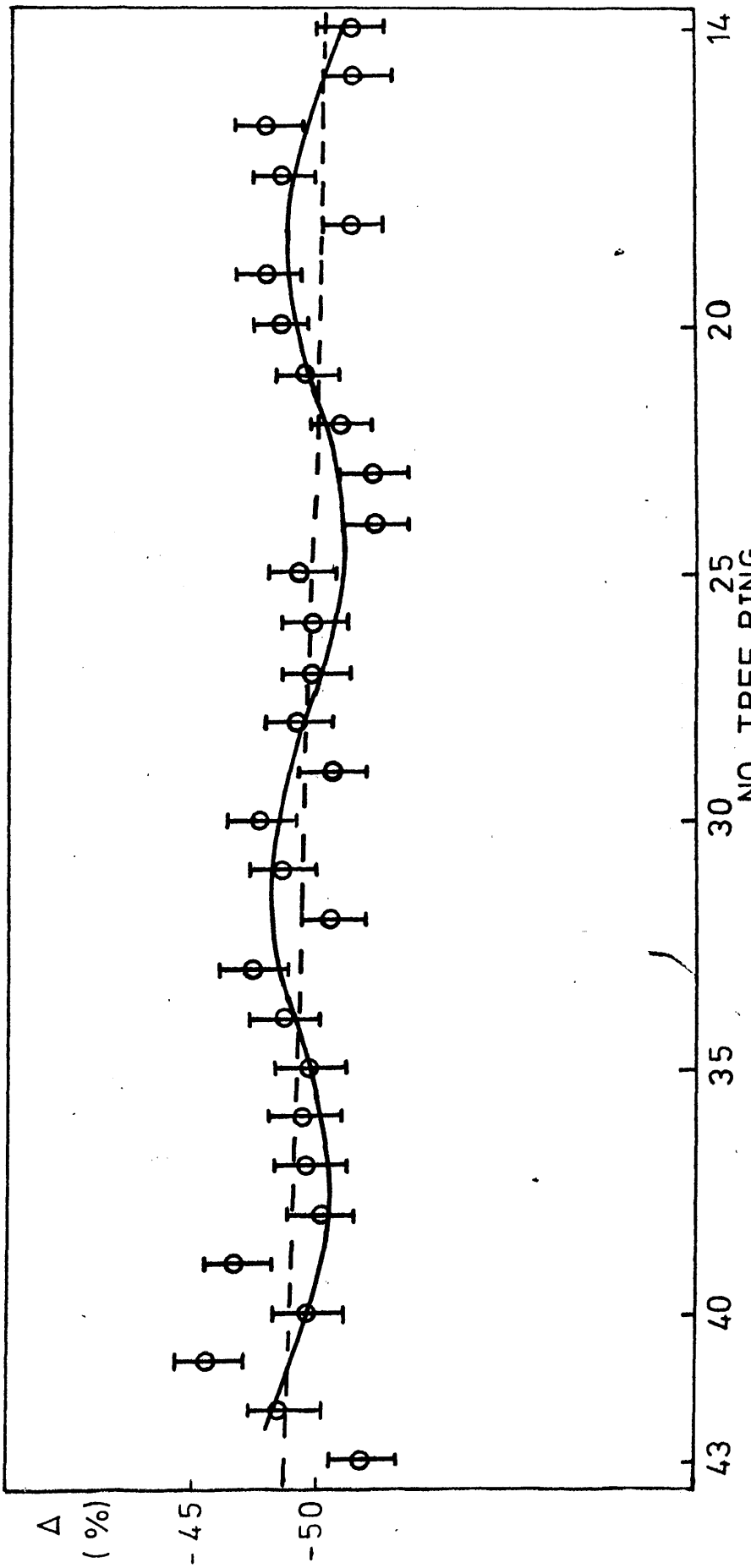

FIG.4.3 GLASGOW RADIOCARBON DATA FOR CLARACH OAK.

addition the cycle amplitudes in both Scots pine and Clarach oak do not exceed the $2\sigma_{TOT.}$ error terms quoted for each measurement, namely $1.10 \pm 0.4\%$ and $2.50 \pm 0.2\%$, respectively. For Ynyslas pine, however, no statistically significant sine curve was obtained, although curves of various frequencies were tested (the frequency being $\omega = \frac{2\pi}{T}$, where $\pi = 3.14$ and T = 8, ... 22). Thus for this sample the best fitting straight line only was drawn. The 95% confidence interval for the Ynyslas data points is also shown in Figure 4.2. All data points lie within the 95% confidence interval with the exception of two anomalous points (8 and 3), probably reflecting normal counting statistical deviations plus possibly some additional error contribution to the measurement procedure. Considering the radiocarbon data deviations from the best straight line fits for each of the three investigated samples, and, in addition, reviewing the periods and amplitudes of the data oscillations obtained for two samples - Scots pine and Clarach oak - no significant sunspot-related year to year fluctuations in atmospheric radiocarbon concentrations are immediately evident.

It is also of interest to collect and review the relevant data obtained by other workers and to treat their findings by this statistical method. These results are shown in Figures 4.4 (after Lavrukhina et al., 1973), 4.5 (after Alekseev et al., 1974), 4.6 and 4.7 (after Kocharov et al., 1974), 4.8 (after Stuiver, 1976), 4.9 (after Farmer and Baxter, 1973), 4.10 (after

Baxter, 1969) and 4.11 (after Damon et al., 1973).

Figures 4.4 and 4.5 show the Russian data obtained for the same Sequoia wood tree rings dating from 1904 to 1916 (Figure 4.4) and from 1890 to 1904 A.D. (Figure 4.5). All data points are plotted with their associated $\pm 1\sigma_{COUNT.}$ error bars. The best fitting straight lines drawn through the results have gradients of -0.040 % per year (this gradient being estimated by drawing such a line that the same number of data points lie above and below the line) and +0.025% per year, respectively. For this same period, Grey (1969) estimated a long-term decrease of radiocarbon content by 0.030% per year. The curve fit to the data of Lavrukhina et al. is highly significant (> 0.1%) showing radiocarbon oscillations of 11 years period and cycle amplitude 2.2%. For the data of Alekseev et al. (1974) the curve fit is statistically significant at the 2.5% level, with a radiocarbon cycle of 11 years and an amplitude of 0.94% For both time intervals (1890-1904 and 1904-1916 A.D.) sunspot numbers show statistically significant (> 0.1%) cycles of 11 years. Since both radiocarbon and sunspot number cycles are of the same period, it is possible firstly to calculate the phase lag between radiocarbon and sunspot number and, secondly, for that particular phase lag, to estimate the correlation between radiocarbon and sunspot number. For the Lavrukhina et al. data this correlation is found to be +0.87 with phase lag 1.7 year, corresponding to a > 99.9% probability of a positive correlation. Similarly for the data

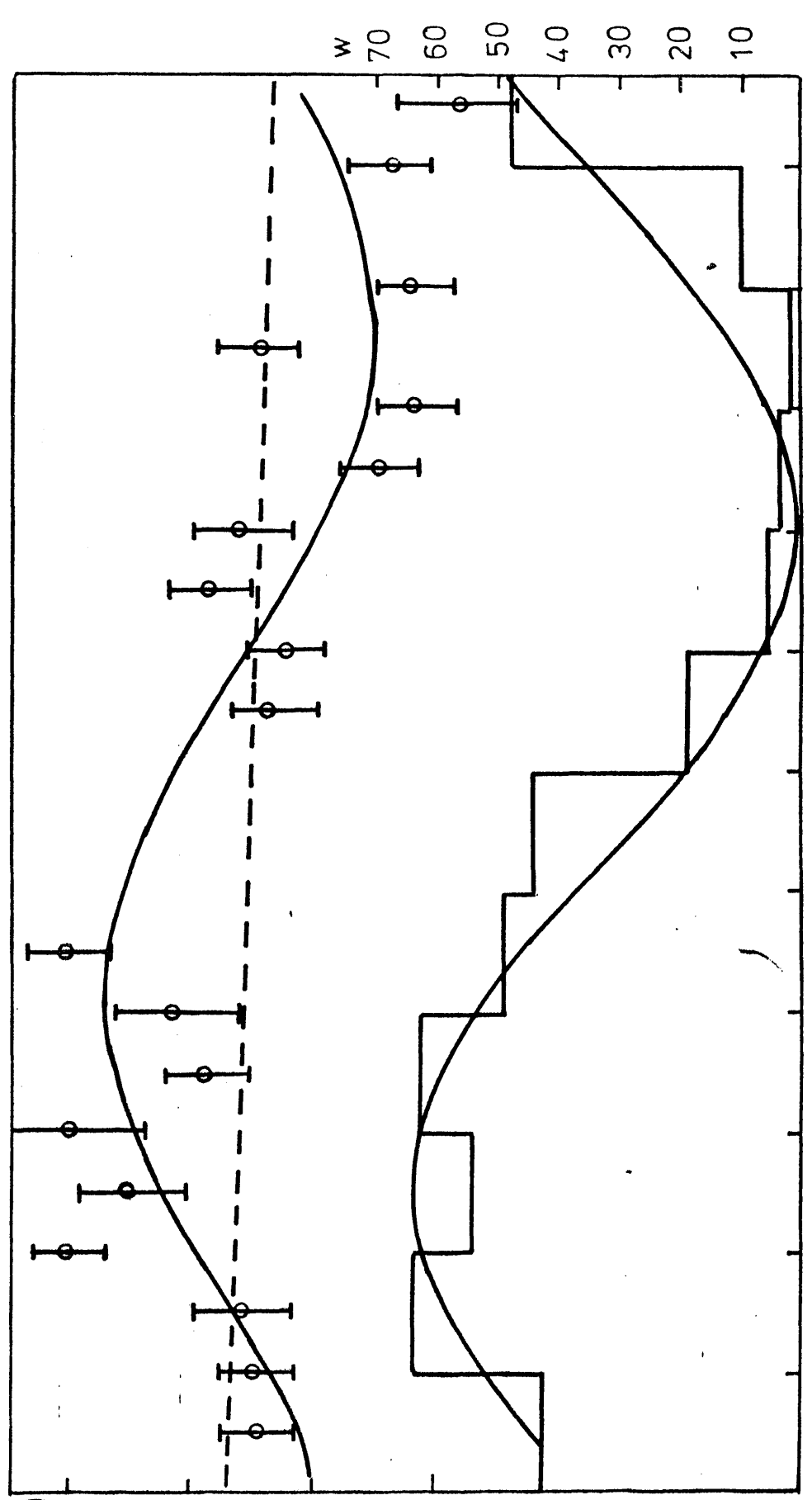

FIG. 4.4 RADIOCARBON IN TREE RINGS (LAVRUKHINA ETAL, 1973)

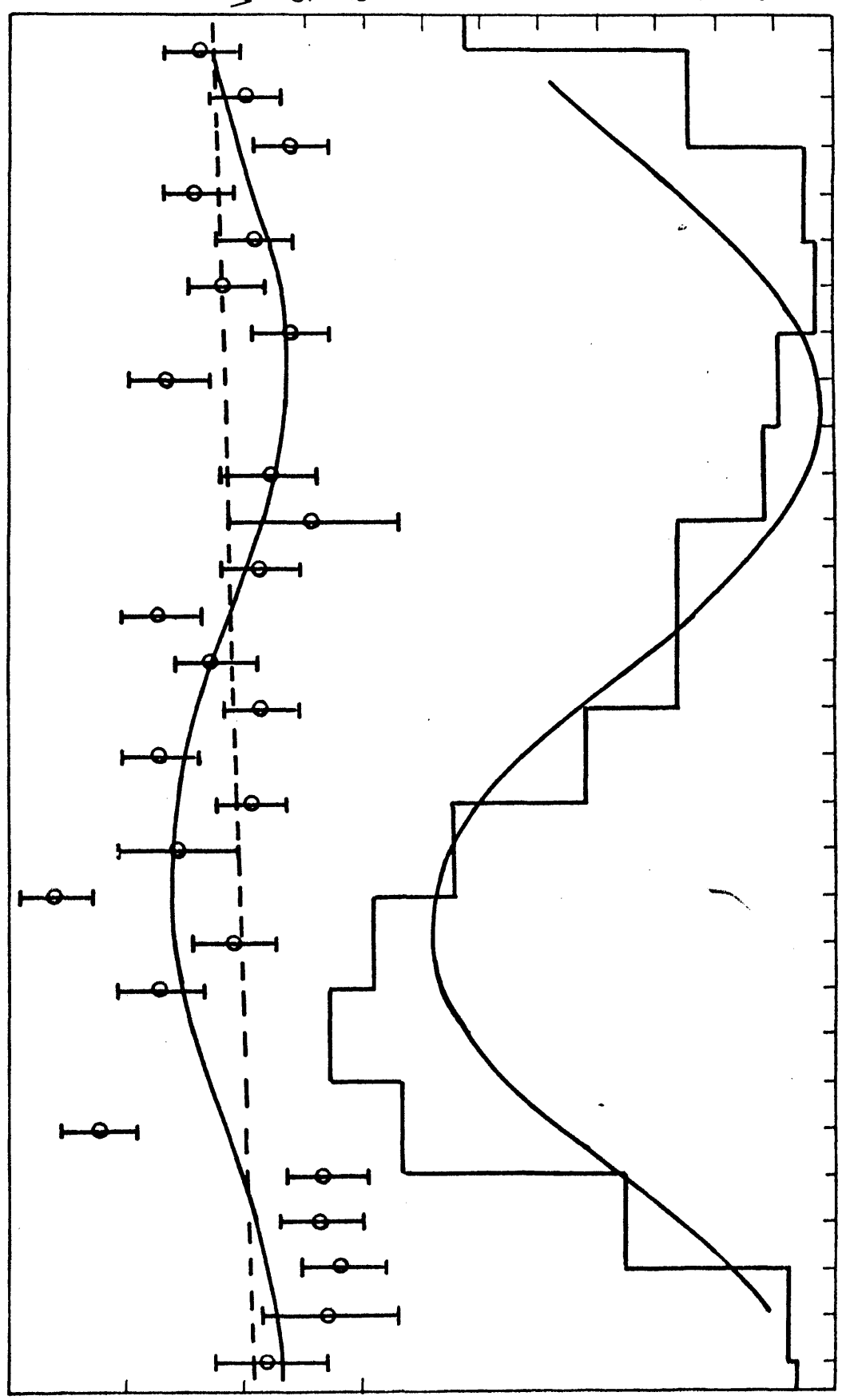

FIG. 4.5 RADIOCARBON IN TREE RINGS (ALEKSEEV ETAL, 1974)

of Alekseev et al. a correlation coefficient of +0.57 with phase lag 1.5 year was calculated, this result being statistically significant at the 1% level. Figures 4.6 and 4.7 (after Kocharov et al., 1974) present radiocarbon results for pine tree rings for the time intervals 1593 to 1615 and 1688 to 1712 A.D. respectively. Data were not corrected for isotopic fractionation and each point is shown with its associated $\pm 1\sigma_{COUNT.}$ error bars only. For the time interval 1593 to 1615 A.D. no detailed sunspot number data are available but estimates by Schove (1955) of the intensity and timing of sunspot maxima and minima are incorporated into Figure 4.6. The curve fit to sunspot data for the 1688-1712 time interval, however, shows a cycle of 11 years, statistically significant at the 5% level (Figure 4.7). The linear gradients in temporal C-14 levels for these cases are -0.017% and +0.019% per year. For the time interval A.D. 1593-1615 the curve fit is statistically significant at the 5% level with a period of 15 years and an amplitude of 1.1% (Figure 4.6). For the time interval 1688-1712 A.D., however, no statistically significant trigonometric curve fit is obtained and only the best straight line fit is plotted along with its 95% confidence interval curves (Figure 4.7).

Figures 4.8 (after Stuiver, 1976) and 4.9 (after Farmer and Baxter, 1973) show the data obtained for the same time interval, 1829 to 1865 A.D. In the first case American Douglas fir tree rings were investigated, in the second an English oak. Both trees were grown at the same altitude (near

FIG. 4.6 RADIOCARBON IN TREE RINGS (KOCHAROV ETAL, 1974)

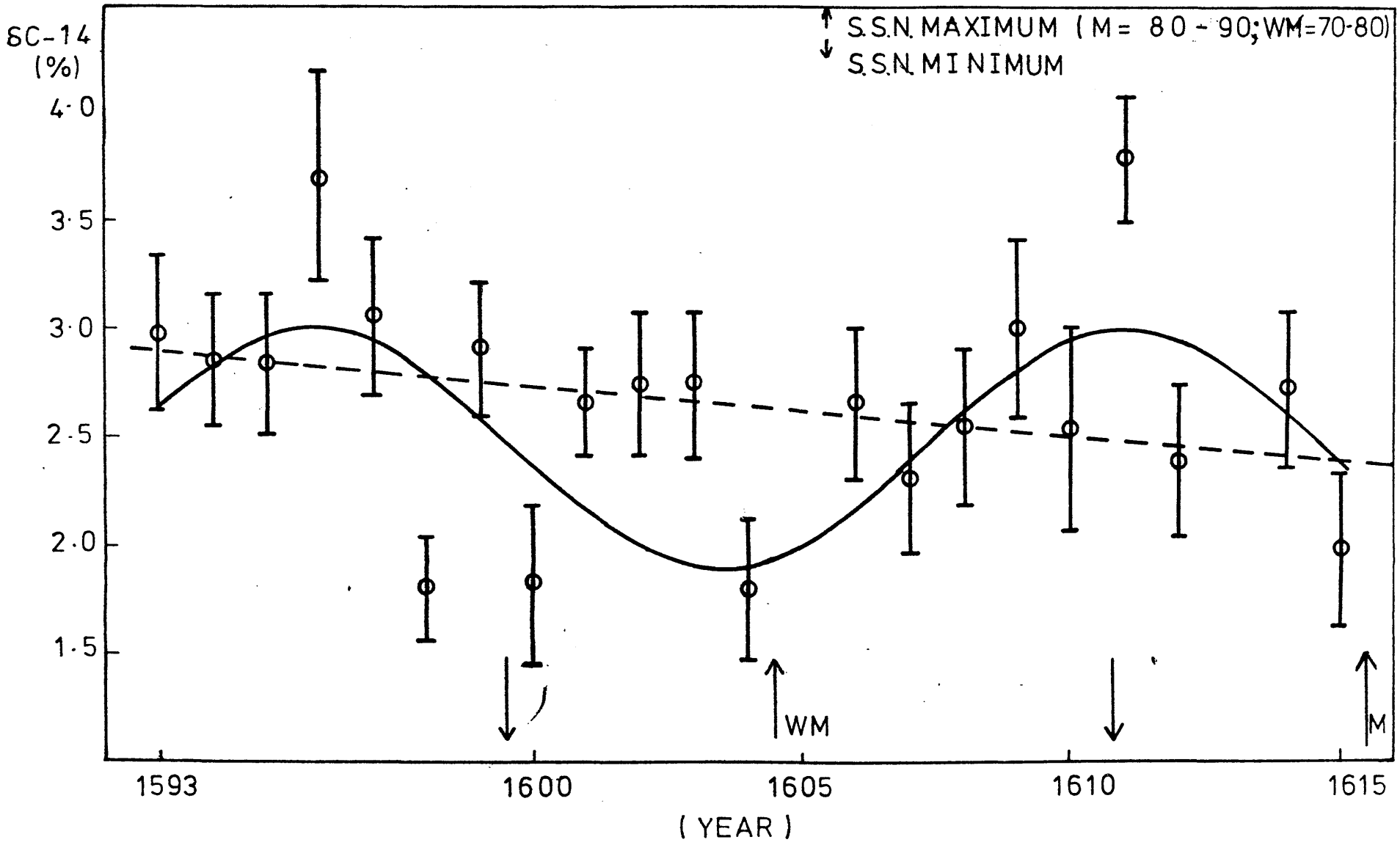

FIG. 4.7 RADIOCARBON IN TREE RINGS (KOCHAROV ETAL, 1974)

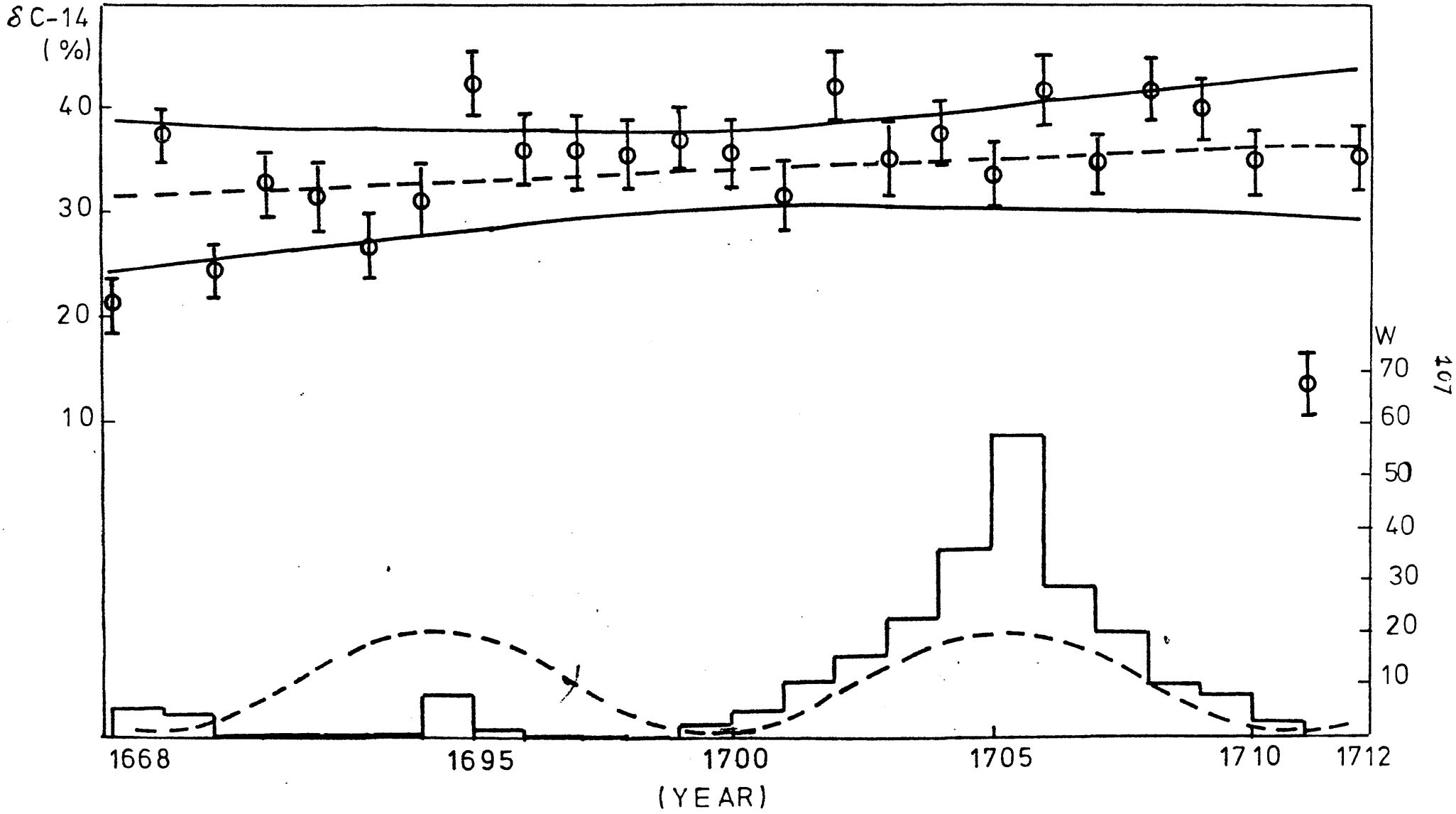

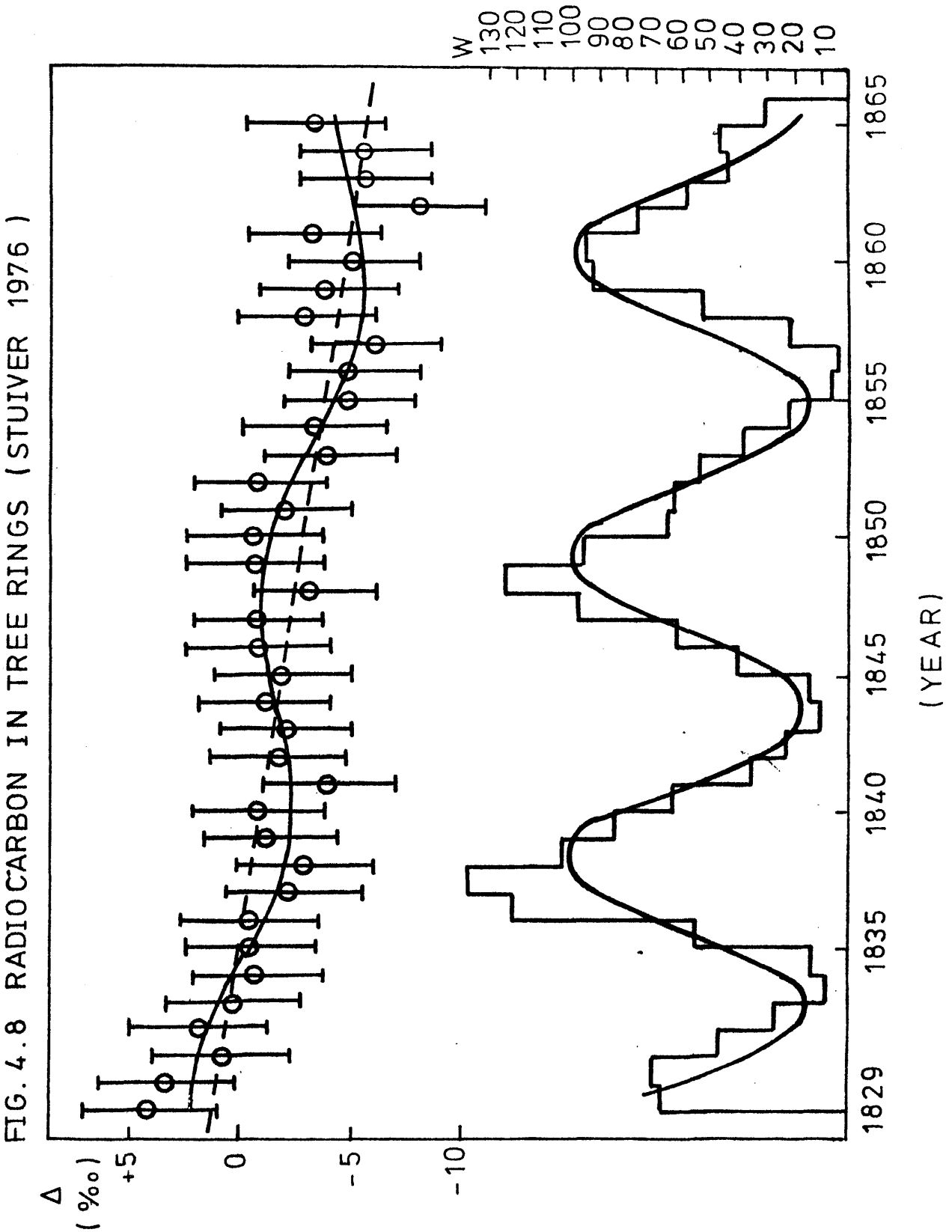

FIG. 4.8 RADIOCARBON IN TREE RINGS (STUIVER 1976)

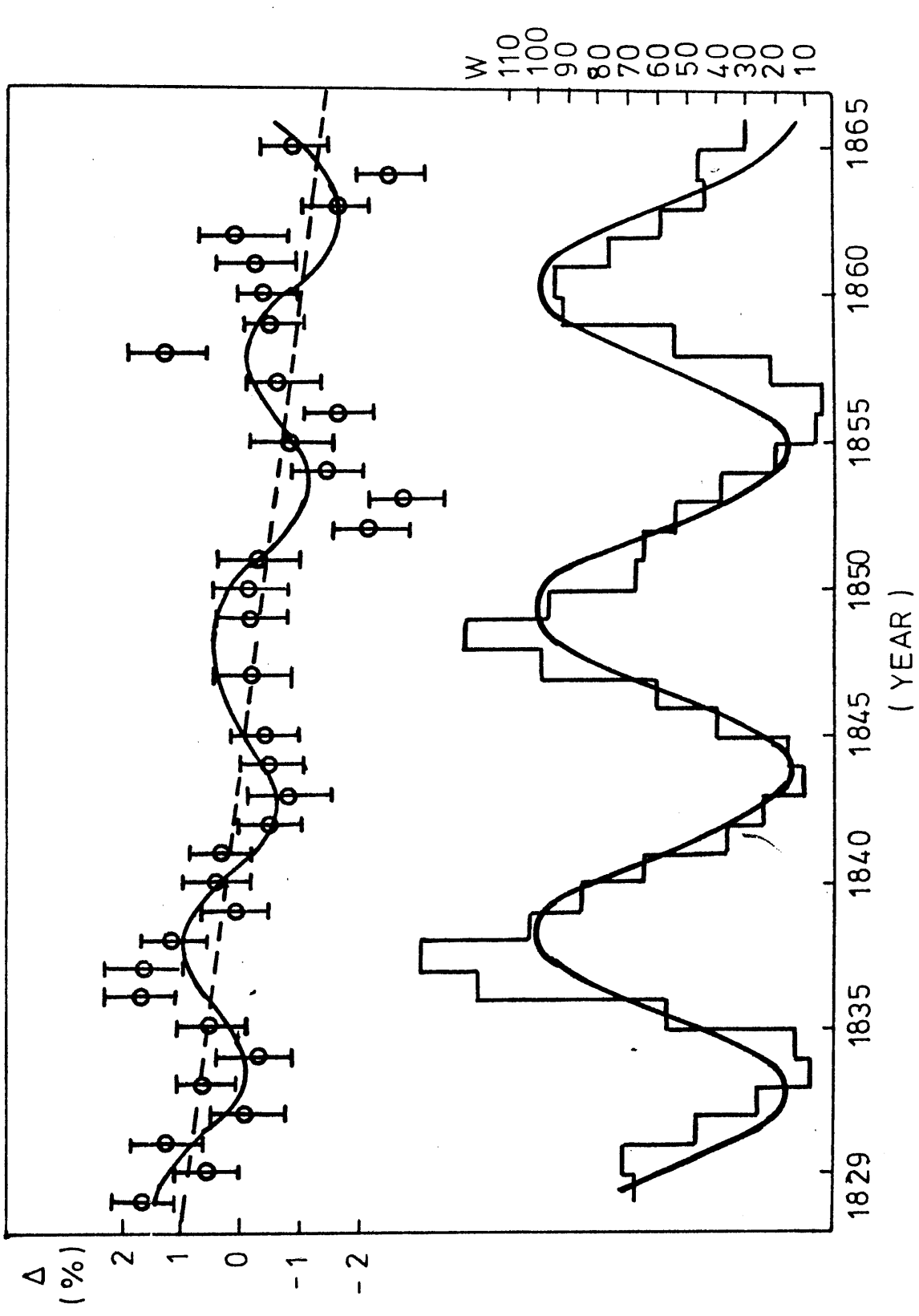

FIG. 4.9 RADIOCARBON IN TREE RINGS (FARMER AND BAXTER, 1973)

sea level) and at nearly the same latitude, 48°N and 52°N respectively. Thus latitudinal effects should be excluded. However, the long term decrease for Douglas fir was found to be -0.019% per year and for English oak -0.06% per year. In both cases the curve fits were highly statistically significant (> 0.1%) showing the period and amplitude of radiocarbon oscillations for Douglas fir to be 19 years and 0.3% and for English oak to be 9 years and 1.3%. A first impression might attribute the discrepancy between data points for these two studies to differences in chemical pretreatment and analytical methods between the two laboratories. For example, for 1853A.D. samples, Farmer and Baxter quote a Δ value of $-2.7 \pm 0.56\%$ while Stuiver reports two values $-0.52 \pm 0.24\%$ and $-0.33 \pm 0.16\%$. The latter were, however, obtained by applying the identical chemical pretreatment of the wood as employed by Farmer and Baxter. Similarly, for 1836, Δ values are reported to be $+1.72 \pm 0.54\%$ for English oak and for Douglas fir -0.15 ± 0.18 or $+ 0.05 \pm 0.17\%$, respectively. According to Stuiver (1976), therefore, the differences in chemical pretreatment can produce Δ differences of 0.19 and 0.2 per cent only, and are not statistically significant. It remains an open question therefore whether the discrepancies could reflect non-latitudinal local effects such as forest, marine or longitudinal fluctuations. It is interesting in this respect also that the Russian data already discussed for the early 20th century (Lavrukhina et al., 1973, Alekseev et al., 1974) do not indicate the highly depressed C-14 levels measured universally

and attribted to the Suess effect.

Figures 4.10 and 4.11 only partly involve the same time interval. In the former (Baxter, 1969) the time interval investigated was 1925-1953 adn in the latter (Damon et al., 1973), 1940-1954 A.D. The linear trend in the former shows a long term radiocarbon decrease of -0.010% per year while in the latter a long term increase of + 0.028% per year is implied. The curve fit to the results of Baxter is statistically significant at the 1.0% level, showing a cycle period of 10 years and an amplitude of 2.1‰. For the radiocarbon data presented in Figure 4.11 (after Damon et al., 1973) no statistically significant trigonometric curve fit was obtained. Thus, the best fitting straight line through the data points and its associated 95% confidence interval curves are presented (Figure 4.11). For both cases the sunspot number oscillations show highly significant ($>0.1\%$) cylces of 11 years. All data considered here are summarised and presented in Table 4.1.

The results obtained here from Scots pine, Ynyslas pine and Clarach oak tree rings, as well as those obtained by other workers, do not allow unique and unambiguous identification of 11-year C-14 cycles correlated with sunspot number and with amplitudes exceeding the errors associated with C-14 measurement. The criteria for such a solar-related cyclic oscillation in atmospheric radiocarbon are nearest fulfilled by the data of Lavrukhina et al. (1973). Here, the probability of a radiocarbon cycle with an 11-year period and of a positive correlation

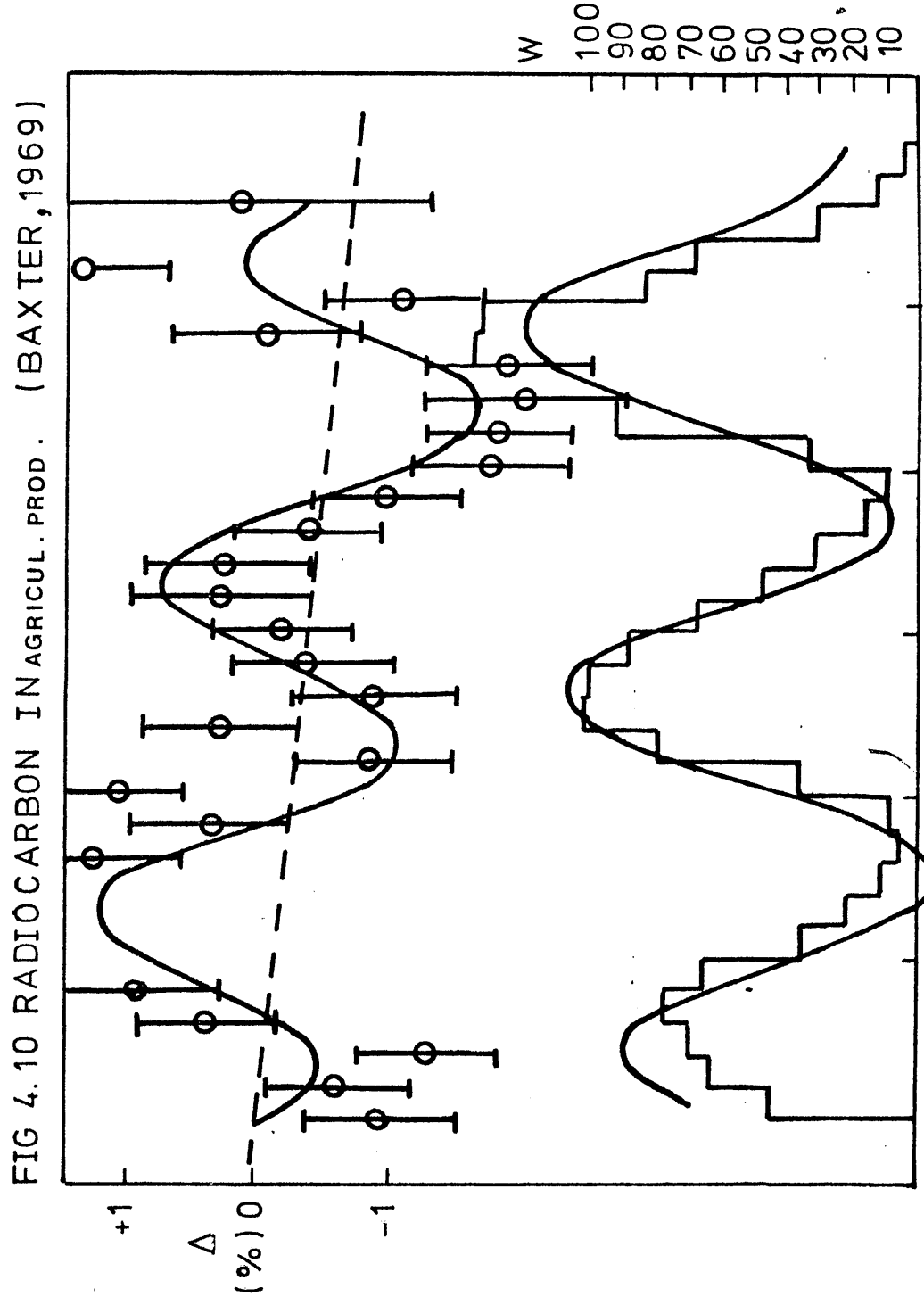

FIG 4.10 RADIOCARBON IN AGRICUL. PROD. (BAXTER, 1969)

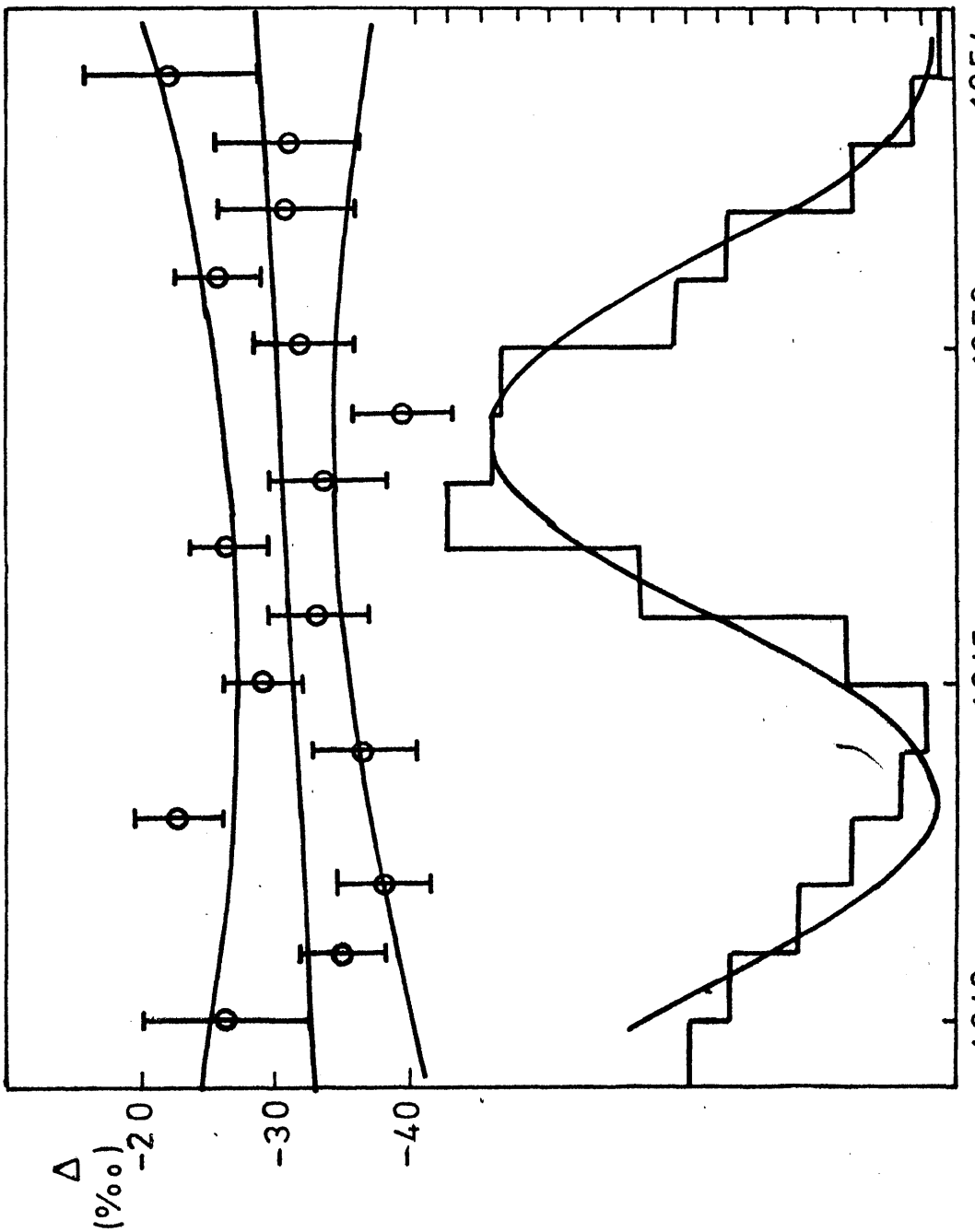

FIG. 4.11 RADIOCARBON IN TREE RINGS (DAMON ETAL, 1973)

TABLE 4.1 PHYSICAL DATA FOR RADIOCARBON IN TREE RINGS

CODE	LINEAR TREND (%/Y.)	STAT.SIGN. CURVE FIT (%)	PERIOD (Y)	AMPLIT. (%)	PHASE LAG(Y)	CORR.COEFF. WITH SSN	STAT.SIGN. OF SSN CORR. (%)
FIG.4.1	-0.017	2.5	15	0.40	-	-	-
FIG.4.2	+0.009	-	-		-	-	-
FIG.4.3	-0.056	1.0	13	2.45	-	-	-
FIG.4.4	-0.040	0.1	11	2.20	1.70	0.85	0.1
FIG.4.5	+0.025	2.5	11	0.94	1.50	0.57	1.0
FIG.4.6	-0.017	5.0	15	1.10	-	-	-
FIG.4.7	-0.019	-	-	-	-	-	-
FIG.4.8	-0.019	0.1	19	0.30	-	-	-
FIG.4.9	-0.060	0.1	9	1.30	-	-	-
FIG.4.10	-0.010	1.0	10	2.10	-	-	-
FIG.4.11	+0.028	-	-	-	-	-	-

between C-14 content and sunspot number of the time interval A.D. 1904-1916, exceeds 99.9%. However, the magnitude of this cycle amplitude is still an open question, since experimental errors associated with these data have not been determined. In addition, by reviewing the results listed in Table 4.1 it is evident that all radiocarbon data, with the exception of three samples, show some kind of statistically significant cyclic behaviour, with variable periods of 9, 10, 11, 13, 15 and 19 years. Whether these oscillations represent true cycles or whether they are accidental results of random fluctuations is the key question. Dergachev et al. (1976) have summarised all the available data from the last 300 years (1688-1951 A.D.); their compilation including the results of Cowan et al. (1965), Stuiver (1969), Lerman et al. (1970), Baxter and Walton (1971), Baxter and Farmer (1973), and Kocharov et al. (1974). In order to exclude such effects as local variations, different methods of measurement and calibration, use of different standards and human error, since all these cause errors which exceed the errors quoted by the various authors [for example, for the year 1695 A.D. a Δ C-14 value of $1.81 \pm 0.2\%$ (Stuiver, 1969) and a δC-14 value of $4.25 \pm 0.3\%$ (Kocharov et al., 1974) were reported], Dergachev et al. applied the method of the generalised line receipt:

$$\bar{X} = \frac{\sum_i p_i X_i}{p_i}$$

where $p_i = \frac{1}{\sigma_i^2}$, σ_i being the standard error of the

measurement. Thereafter the autocorrelation functions and autospectra of the generalised line for both radiocarbon data and sunspot numbers were calculated. According to this calculation, 11 years is shown to be the fundamental period for sunspot numbers but 80 years is the basic period for radiocarbon oscillations. However, within the C-14 autospectrum minima of C-14 content were evident with a period of ~8 years and with amplitudes 2.5-3 times smaller than the amplitude of the 80-year cycle. The nature of the ~8-year cycle might be explained by various complex processes involved within the system atmosphere-ocean-bioshphere.

It seems therefore that definitive assessment of short-term cyclic behaviour of C-14 requires future radiocarbon analyses of very high precision ($\tilde{\sigma}_{TOT} \leq 0.2\%$). With the quality of analytical data presently available it is difficult to distinguish unambiguously the experimental scatter of data from any real C-14 fluctuations. Furthermore, studies of the phase of the cycles suggest that, if the periodicity has a solar origin, its phase appear to be determined by another mechanism. Nevertheless it is possible to make further comment. As indicated in Table 4.1 eight of eleven relevant studies include data to which a trigonometric curve can be fitted with high statistical significance. By definition of the statistical significance parameter, these curves are unlikely to be produced by random data alone. If, however, the C-14 data-scatter observed in these studies has been produced by non-quantified analytical

errors, its distribution would almost certainly be random. Thus, from this approach, it can be inferred that the accumulated results thus far do support periodic fluctuations of atmospheric radiocarbon, but with variable amplitudes, periods and solar correlations. In other words, cycles of period from 9 to 19 years can be identified, with amplitudes of 0.30 to 2.45%. It is likely that the limitations of the C-14 data, of the statistical model applied here and of nature itself would introduce a moderate degree of flexibility to the criteria employed in this study, so that perhaps the 9-year period in the data of Farmer and Baxter (1973), the 10-year period in the data of Baxter (1969) and the 13-year period in the Clarach oak results could each be considered to lie within the allowable range of correlation with the 11-year solar cycle. If so, 5 solar-related cycles could be identified [two inversely correlated with the solar cycle (Baxter, 1969; Farmer and Baxter, 1973), two positively correlated with the sunspot cycle (Lavrukhina et al., 1973; Alekseev et al., 1974) and the fifth impossible to assess since no solar activity data are available]. In addition, two 15-year cycles, one 19-year cycle and 3 cycle-less periods could be identified. The conclusion would then be that the short-term distribution of C-14 is highly complex, with variations both in time and space and with perturbing mechanisms which can, but need not necessarily, be triggered by solar phenomena. It should in addition be emphasised that, in all these studies, C-14 data from short-lived biological materials

have been employed. Thus the vast majority of annual wood growth occurs within a two to three month period in spring/early summer of each year. The C-14 data are therefore not yearly averaged figures but are heavily weighted to the very months when stratospheric inputs of radionuclides to the troposphere are known to have maximum effects [e.g. the "Spring peaks" of fission products (Fairhall and Young, 1970)]. It seems therefore that according to this preliminary evidence it is reasonable at least to suggest that cyclic C-14 fluctuations could be produced by short-term stratospheric inputs to the troposphere during the growth periods of biospheric materials. Whether such C-14 effects would be significant or even observed at all would be critically dependent on the timing and location of biospheric growth relative to those of the C-14-rich stratospheric input. Thus cycles of decreasing amplitude would be observed as a function of distance from the input. Samples of slow (or late) growth would reflect no cyclic behaviour, nor would materials growing far removed from the stratospheric incursion. On the other hand, the magnitude of "spring peaks" themselves would be a function of solar activity so that, during periods of solar calm, no cyclic behaviour would be induced. Indeed, Reiter (1973) has shown that the influx of stratospheric air to the 3 km level increases on the second or third day after an H_α and/or X-ray flare as reflected in almost doubled tropospheric levels of the stratospheric radionuclides Be-7 and P-32 (Figure 4.12). In the Figure, tropospheric activities of

FIGURE **4.12**

Mean ^{7}Be & ^{32}P in Tropospheric Air as Function of Solar Flux [Reiter, J.G.R., 78, 6167, 1973]

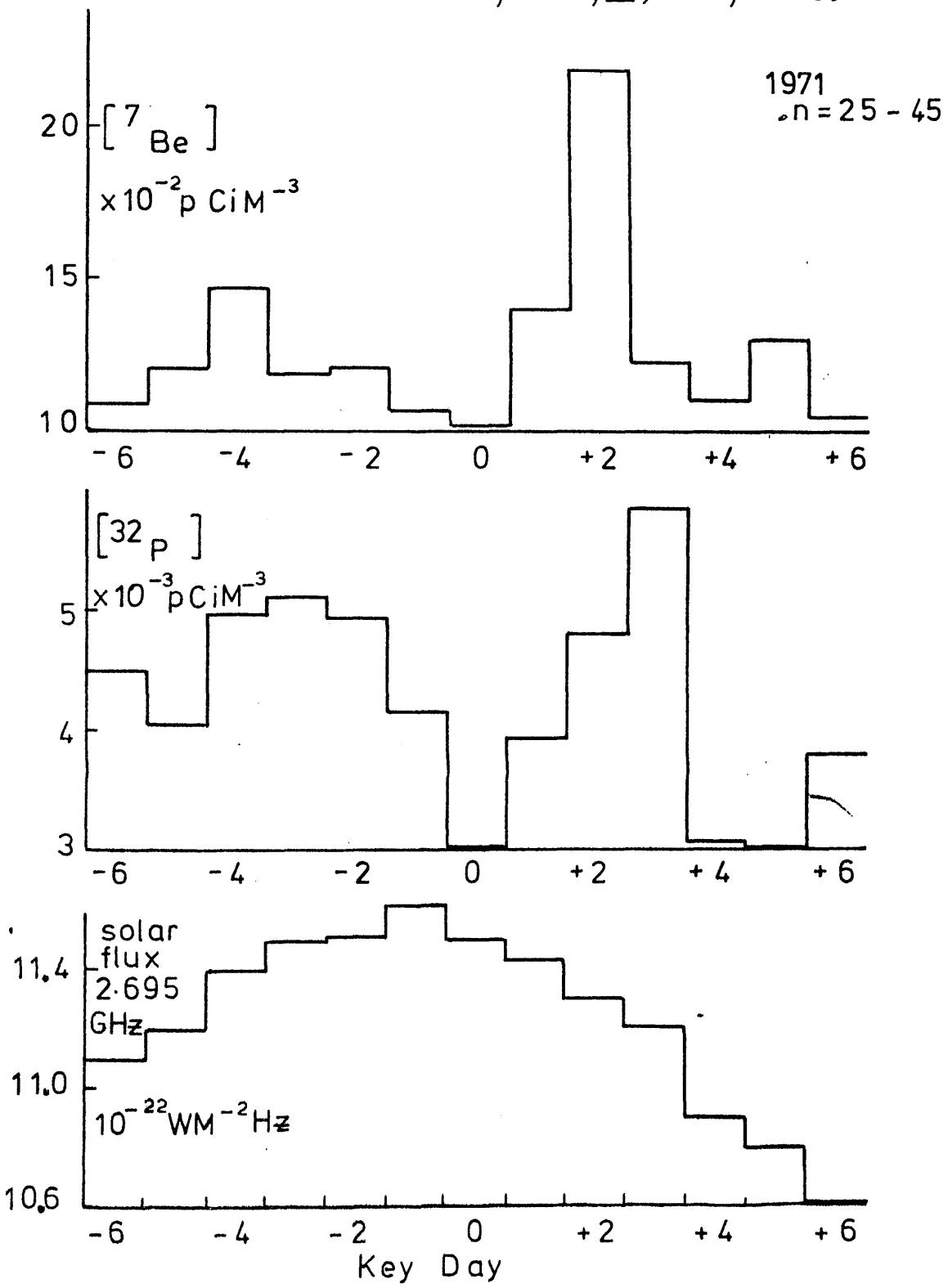

Be-7 and P-32 are plotted in units of pico Ci per M^3, n represents the number of days, the solar flux was measured at the frequency of 2.695 Giga (10^9) Hz, while the intensity of the solar flux is expressed in 10^{-22} Weber Hz per M^2. The one day difference between the maxima of Be-7 and P-32 in Figure 4.12 is probably due to the half-life difference of these two radionuclides. Therfore, according to Reiter "the use of this statistically evident solar-terrestrial relationship would be in order in the practical forecasting of influxes of stratospheric air into the biosphere."

Reiter's data are perhaps the most relevant available for discussion of short-term C-14 levels. It is, because of the combined effects of the artificial 'bomb' and 'Suess effects', impossible to measure natural C-14 levels on a day-to-day basis. Be-7 and P-32, however, are produced in the stratosphere in a similar manner to C-14 so that it is reasonable to postulate that tropospheric levels of C-14 should reflect the highly solar-dependent behaviour of its cosmogenic "sister" nuclides. It is perhaps possible also to make an approximate assessment of the magnitude of daily C-14 variations. Both Be-7 and P-32 show maxima which represent approximate doubling of tropospheric long-term average activities. If we assume that for only one day of an assumed one hundred day rapid wood growth season, tropospheric levels of C-14 show a transient 100% increase over the long-term average concentration as a result of localised stratospheric input, then the resultant C-14 content of the

whole annual ring would be

$$\frac{99(0) + 1(100)}{100} = +1\% \ (\Delta)$$

Thus such effects, as extrapolated from Reiter's results, could indeed give rise to the observed variations in C-14. If the variations are of such a localised nature, it is to be predicted that the observed range of amplitudes, periods and correlations would be found.

In addition, variations in the length and onset of the growing season in the U.K. are well-known to correlate with solar activity (King, 1973) so that biospheric materials, by systematically sampling varying proportions of the "spring peaks" of stratospheric-derived C-14, might readily accumulate a cyclic C-14 trend over the solar cycle. It is therefore apparent that localised effects could produce a wide variety of apparently conflicting data both temporally and geographically.

In support of these proposals, it is becoming evident that important aspects of lower atmospheric behaviour are indeed associated with solar phenomena ranging from such events as solar flares, 27-day solar rotations and 11-year, 22-year and ~80-year solar cycles. Solar-terrestrial relationships within the zones of the lower stratosphere and the upper troposphere, involving processes such as formation and deepening of troughs, changing of tropospheric circulation patterns and cooling within the tropopause level have been studied by Shapiro (1959), Roberts (1960), Shapiro and Ward (1962), Roberts (1962), Twitchell (1963) and Schuurmans (1969). Some of the lower

atmospheric phenomena also occur several days after the associated geomagnetic activity (Roberts and Olson, 1973; Stolov and Shapiro, 1974). For example, the vorticity area index for troughs increases by 40% five days after magnetic disturbance. The response of the troposphere to the 11-year sunspot cycle therefore may be an integration of the effects caused by short-lived phenomena such as solar flares or geomagnetic storms, which are much more frequent at sunspot maxima than minima. Furthermore, recently Eddy (1976) has shown that radiative output of the sun could be almost entirely independent of the phase of the 11-year sunspot cycle, which may be only the carrier frequency. There is, therefore, a need for further study towards development of a definitive atmospheric model to quantify such apparent effects as coupling between the solar wind and the magnetosphere, the constancy of the solar constant and stratosphere/troposphere exchange enhancement by solar activity increases.

The above discussion is based on the assumption that the scatter in C-14 data is non-random, hence non-experimental and therefore indicative of real C-14 fluctuations. Regardless of the veracity of this assumption there are significant implications for radiocarbon dating which will be mentioned in conclusion. For, regardless of the origin of scatter, the results show clearly that, for a single short-lived sample which might be submitted for radiocarbon dating, there can be a considerable uncertainty in the age-measurement. It is therefore important

to attribute to any such radiocarbon data an associated error not based on the counting error alone but on the averaged scatter observed in sets of analyses of such samples. Thus, from this research, appropriate 1σ error terms would be ± 43, ± 214 and ± 427 years for samples of radiocarbon ages 1000, 5000 and 10,000 years respectively. It is highly suspect therefore to attribute high precision to dates on cereals etc on the assumption that these involve less uncertainty than wood which generally has significant time-lag between growth and final use. Thus the results presented here strongly support the view that radiocarbon dates be accorded increased error terms, in line with previous statements by Baxter (1974) and Clark (1975).

PART TWO

RADIOCARBON IN RECENT SEDIMENTS

CHAPTER 1. INTRODUCTION.

1.1 Sediment composition and origin.

Marine sediments are composed essentially of materials of a) detrital, b) biogenic and c) authigenic origins. Detrital materials originate mainly through erosion of continents and are primarily in the form of alumino-silicate minerals dropped by wind or transported by rivers into the oceans. The larger, heavier, particles settle out in coastal regions so that deep ocean sediments are composed essentially of particles in the $< 2\mu$ size fraction. Thus in the deep ocean, most detrital material comes from a dilute colloidal suspension (0.05 mg l^{-1} to 1.0 mg l^{-1}) with a resultant low rate of coagulation. This results in a slow rate of deposition and, therefore, in a wide areal distribution of detrital material (around 0.3 g detrital cm^{-2} 10^{-3} yrs).

The majority of detrital materials are clays, formed by the weathering of silicate rocks and minerals on land. In addition, detrital materials have a small contribution from unweathered rock fragments/mineral grains which are transported by wind, water, ice, organic agencies or volcanic activity.

The second major fraction of sediments is the biogenic component, comprising the remains of marine organisms, mainly calcite ($CaCO_3$) and opal (SiO_2). Species such as Coccoliths (plants) and Forams (animals) contribute to calcite, while Diatoms (plants) and Radiolarians (animals) deposit as opal.

The distributions of $CaCO_3$ and SiO_2 are not uniform but are dependent on solubility and productivity variations.

The final important component of natural sediments is the authigenic fraction which consists of minerals formed by spontaneous crystallisation either on the ocean floor within the sediment column or precipated direct from solution. Authigenic minerals are rare relative to detrital and biogenic matter. Relatively abundant authigenic minerals are barite, zeolites, iron oxides and Mn-nodules.

Thus deep ocean sedimentation rates, typically in the mm 10^{-3} mm y^{-1} range, reflect the relatively slow deposition of materials derived originally from the continents (neglecting very small contributions from sea floor volcanism and cosmic dust). As expected natural inshore sediments have much higher sedimentation rates, typically in the 0.1 to 1 mm y^{-1} range, reflecting the increased detrital, biogenic and authigenic contributions found in areas close to the source region of element input. Thus inshore sediments are generally of larger detrital particle size and flux and have enhanced inputs of organic rich and authigenic materials. Since they often underly nutrient rich and highly productive waters the biogenic contribution is also increased relative to pelagic sediments. In addition, inshore sediments are markedly susceptible to anthropogenic effects so that in industrial areas the accumulation rate is significantly increased by inputs of particulates from this source. For

example, modification of erosion patterns by forestry or farming activities or by dam formation on inflowing rivers can modify detrital inputs. Sewage or dredge spoil disposals, petroleum spills and industrial effluent releases can each cause major changes in sediment deposition. Leaching of fertilisers can enhance biogenic input, while similar release of toxic species, both organic and inorganic, can reduce or even eliminate biological activity. The high organic load associated with industrial and domestic wastes can easily reduce dissolved oxygen levels in the sediment and overlying waters so that anoxic conditions and rapid organic accumulation can occur.

Thus human activities can modify sedimentation process to a major degree so that the anthropogenic contribution essentially overwhelms the natural system. It is therefore of major importance that, in such areas, the impact of human inputs be assessed.

1.2 Stratigraphical markers and relative age determination

Deep ocean/lake core sediments often contain unique stratigraphical markers (horizons) which can be recorded over large regions of the ocean/lake floor. After absolute dating of a core containing such a marker, the level in all other cores where that stratigraphical marker has been found can be assigned the same age. By determination of the ages of several such horizons, the rate of deposition of sediment can be calculated.

There are three common kinds of stratigraphical

horizons preserved in consolidated ocean/lake sediments which can be employed in relative age determinations.

Paleomagnetic markers.

Minerals, which are naturally magnetic, when allowed to deposit freely through the water column, arrange themselves along the magnetic axis in exactly the same way as would a compass needle. Thus magnetic crystals in sediments become aligned with the geomagnetic vector, recording the intensity, direction, declination and dip of the magnetic field at the point of deposition. (The clockwise angle from the geographical North Pole assumed by a magnet is called the magnetic declination, while the angle with the horizontal is called the magnetic inclination or dip.) Similarly, in rocks and minerals the characteristics of the earth's magnetic field at the time of rock crystallisation can be established by measuring the thermoremanent magnetic vector. This magnetisation of Fe-bearing mineral crystals along the geomagnetic axis occurs at the time the basaltic rock crystallised.

During the past 4 million years, the magnetic poles have reversed 9 times. At each transition, the magnetic field decreases to about one quarter of its usual intensity and thereafter increases again with poles reversed (Cox, 1969). Thus, all rocks with ages less than 0.7 million years are normal in polarity, while most rocks between 0.7 and 2.5 million years old have reversed polarity. The same

temporal sequence of magnetic polarity is recorded in deep ocean/lake cores.

Therefore it is possible to assign ages to deep ocean cores based on the continental rock measurements previously made and on parallel radiometric dating of these rocks by methods such as K/Ar and Rb/Sr techniques. Furthermore, the magnetic susceptibility, an easily measurable parameter, is taken as a general indication of variations in the level of mineral inwash within and between sediments. Initial magnetic susceptibility is a function of the detrital titanomagnetic component in sediments.

Floral and faunal markers.

The gradual development of agricultural activity since prehistoric times has been observed in the stratigraphical record by assay of cereal and weed pollen in bogs and lake sediments (Firbas, 1949; Overbeck, 1950; Nilsson, 1964; Schmitz, 1968; Starka, 1970; Averdieck et al., 1972; Bortleson & Lee , 1972). In addition, the results of paleomagnetic research on deep cores have revealed a close correlation between reversals and faunal extinctions and pollen zonation (Harisson & Funnell, 1964; Opdyke et al., 1966; O'Sullivan et al., 1973).

These correlations may be explained by acceleration in mutation rates caused by increases in cosmic radiation reaching the earth's surface during reversals when the earth's magnetic field shielding against cosmic rays is reduced. On

the other hand, the climatic changes during the past have led to marked changes in faunal distributions.

Plantago lanceolata and Pteridium have often been exploited in pollen analyses as indicators of forest clearance, soil disturbance and agricultural activity. Changes in grass are difficult to explain since a number of biomes produce high grass pollen values - fringing reed swamps and Molinia - dominated bog or fen swards as well as pasture or waste grounds. Thompson (1975) has found that in the top 200 cm of lake sediments, high susceptibility and grass pollen values correspond to low total carbon contents.

Since fossils which could be used for stratigraphical classification did not appear before the beginning of the Cambrian, rocks from the earlier periods cannot be dated by this method.

Climatic markers.

This third approach to relative dating is less reliable because paleoclimatic changes have been repetitive at intervals of roughly the same duration. However, climatic changes are recorded in deep ocean/lake cores by changes in $CaCO_3$ concentrations, O-18/O-16 ratio variations in $CaCO_3$ from foram shells, faunal and coarse fraction changes, the distribution of evaporites and red-beds.

The paleoclimatic data are limited, scattered and not necessarily latitudinally dependent. Ancient glacial deposits

agree well with paleomagnetic prediction of polar regions. Thus, widespread Permian glacial deposits are found in South Africa, India, Australia and eastern South America, and Ordovician glacial deposits in the Sahara. In North America, Ordovician sequences consist of thick limestones and beds characteristic of low latitudes in confirmation of the lower Paleozoic separation of North America and Gondavanaland.

1.3 Methods of absolute age determination.

The absolute age of sediments is determined by measuring the radioactivity of nuclides which were trapped in or absorbed onto the sediments at the time of deposition. For a radioisotope to be of value in dating sediments, it is essential that the half-life be of the same order as the expected age. Therefore, the calculation of absolute ages can be correct only if the geochemical characteristics of the radionuclides are clearly defined. In addition, much caution must be applied in assessing the significance of a single radiometric result. It is only when several or many ages are measured that they can be regarded as definitive.

There are several methods of absolute dating. One involves radiocarbon dating as previously discussed; a second involves thorium-230 (Th-230) and protactinium-231 (Pa-231), two radioactive isotopes produced by the decay of uranium dissolved within the ocean; a third common method involves radioactive potassium-40 (K-40), which decays to a gas, argon-40 (Ar-40).

The age of sediments can be calculated from the rate of disappearance after burial of thorium-230 received from uranium-238 dissolved in the ocean (Figure 1.1). Thorium-230 has a half-life of 75,000 years, convenient for dating in the range of a few hundred thousand years (~400,000y).

Accurate dating by the thorium-230 method is, however, possible only under special circumstances - both the rate at which the sediment particles settle onto a given area of the ocean floor and the rate at which the Th-230 atoms are incorporated into this falling sediment must remain constant with time.

Like thorium-230, protactinium-231 is insoluble and is removed from ocean water to sediments soon after it is produced (by the decay of uranium-235) (Figurel.1). Thus, the decay of this excess Pa-231 as a function of time, or depths in sediments, provides a dating system analogous to the Th-230 excess method. Protactinium-231 (half-life 34,000y) allows mean sedimentation rates to be established over the past 150,000 years.

To date beyond 400,000 years the potassium-40/argon-40 method is employed. Thus, potassium-40 (half-life 1.31×10^9y) in volcanic rocks undergoes radioactive decay and produces argon, which remains trapped in the crystal lattice of the rock. Knowing the content of Ar-40 and K-40, it is possible to calculate the length of time elapsed since the rock crystallised.

Figure 1.1 The decay series of U-238, Th-232 and U-235

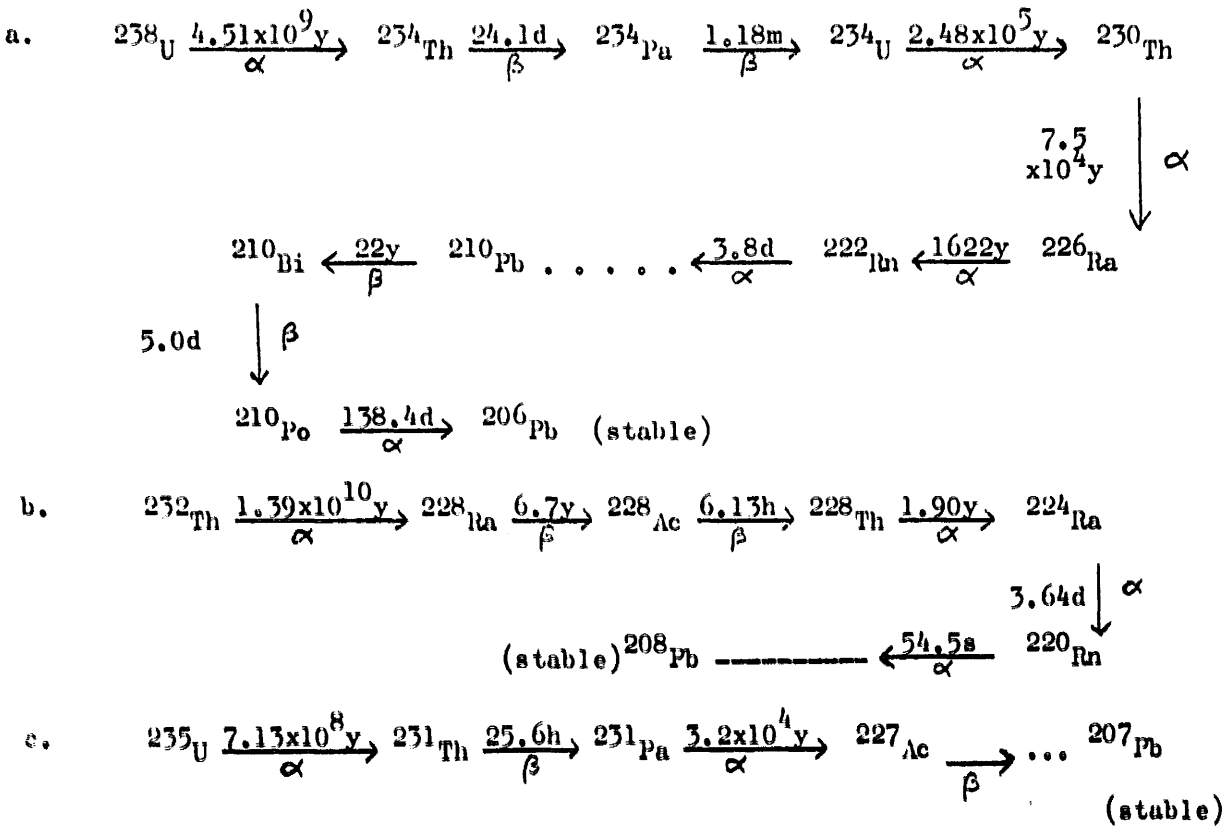

To apply this method directly to deep ocean core sediments requires the presence of a layer of volcanic ash. Unfortunately, volcanic ashes in deep ocean sediments are very rare and the potassium/argon method has therefore only limited direct application. The major relevance of the method to sedimentology has been its use in establishing the chronology of magnetic reversals in continental rocks and hence, by implication, in the sediment record.

In the last decade, interest has grown in determination of rates of sedimentation in recent coastal marine and lake sediments, especially in areas of heavy industrialisation. For this purpose, lead-210 (Pb-210) dating of sedimentary deposits appears ideal for the last 100 to 150 year period (Koide et al., 1972).

Lead-210 (half-life 22.26y) is also a member of the U-238 natural radioactive decay series (Figure 1.1). When gaseous Rn-222 escapes from surface rocks into the atmosphere, it decays (half-life 3.8 days) via a series of short-lived daughters to Pb-210. Lead-210 is thereafter removed from the atmosphere by rainout and gravitational settling and is thus introduced into the hydrosphere. Subsequently, the insoluble Pb-210 is adsorbed onto suspended material in the water column and is deposited into the sediments, where, assuming a chemically closed system, it decays as a function of time or depth.

It is necessary, however, to distinguish the excess

("unsupported") Pb-210 introduced in this way from "supported" Pb-210 actually produced in the sediment by decay of Ra-226 contained in the sediment minerals. If the input of Pb-210 is assumed constant and providing there is no mixing or migration of Ra or Pb within the sediment column, the concentration of unsupported lead-210 decreases exponentially with depth in the core.

Thus, the age of the sediment at any depth and the average sedimentation rate can be established from its unsupported Pb-210 activity relative to that at the surface and from the known decay rate defined by its radioactive half-life.

In this context, caesium-137 is another environmentally important radionuclide. This species has received considerable attention because of a) its occurrence in fall out and as a by-product of applied nuclear technology, b) its long half-life (~30y), c) its energetic beta-gamma emission, and d) its tendency to accumulate in human tissues, notably in bone. Large scale environmental surveys of radiocaesium have documented its overland sedimentary flow (Ritchie et al., 1971; Plato and Goldman, 1972); its uptake, accumulation and alimination in aquatic ecosystems (Pendleton and Hanson, 1958); its localisation in sediments (Lomenick and Gardiner, 1965) and its behaviour in various substrate systems (Tamura and Jacobs, 1960).

In Britain there is a major source of both Cs-137 and

Cs-134 (half-life 2y), the reactor-produced isotopes released during fuel reprocessing at Windscale in Northumberland. The output from Windscale into coastal waters moves in a net northwards direction resulting in a radio-caesium plume which can be detected along the Scottish coast at least as far as Cape Wrath (McKinley et al., 1976; Swan et al., 1976).

Radio-caesium isotopes have long residence times in sea water, have convenient half-lives for geochemical studies, are easily determined and are therefore highly suitable for dating recent rapidly depositing sediments.

Caesium-137 is on its own also useful as a means of dating fresh water sediments, since the profile of activity versus depth should show a peak related to the maximum atmospheric fallout of bomb-produced Cs-137 in the 1963/64 layer. In marine sediments from western U.K. coastal waters the onset of caesium release from Windscale around 1959 dominated the fallout contribution and shows a continual increase in sediments deposited since then. Thus sedimentation rates over the last 20 years can be calculated via the Cs-137 method.

An additional application involves the ratio Cs-134/Cs-137, which has a half-life around 2 years and can therefore be used to assess vertical mixing in the surface sediments. The presence of caesium isotopes in the upper layers of a sediment core proves beyond doubt that the surface layers have been retrieved in the coring process, thus removing a major uncertainty in most sediment studies.

1.4 Carbon-14 as a tracer of urban pollution.

The combustion of fossil fuels in cities, and in industrial areas in general, releases large quantities of carbon dioxide into the local atmosphere. Because of their extreme age, such fuels no longer contain carbon-14 and the radiocarbon activity of atmospheric carbon dioxide is therefore locally depleted. The degree of depletion provides a useful measure of carbon dioxide pollution at any sampling site. In addition, industrial activities commonly release fossil carbon into the hydrosphere as solid or liquid wastes. Thus, fossil carbon represents an effective tracer species for following effluent transport through the various environmental reservoirs. This tracer application is a general approach which may be valuable in any situation where organic pollution presents major problems.

Baxter and Harkness (1975) have shown that up to 20 per cent of the carbon dioxide present in the Glasgow region atmosphere is derived from local industrial and residential emissions. These authors have found also that surface sediments in the Clyde dumping area at Garroch Head are considerably depleted in radiocarbon relative to the raw sludge input. Thus C-14/C-12 ratios in the surface layers of the sediments are lower than would be expected in the absence of pollution. Indeed, the radiocarbon age of surface sediments was calculated to be around 3000 years with

an "artificial" sedimentation rate of 7.5 mmy^{-1}. At depths greater than 40 centimetres, natural sedimentation rates of 0.3 to 0.6 mmy^{-1} were reported.

Recent sediment cores from the western Baltic sea have been analysed for heavy metal and carbon isotope contents by Erlenkeuser et al. (1973). These workers found a sedimentation rate, based on radiocarbon dates, of 1.4 mmy^{-1}. The "recent age" of the sediment was about 850 years. Within the upper 20 cm of sediment heavy metals became increasingly enriched towards the surface, while simultaneously the carbon-14 content decreased by about 14 per cent. Thus both the enrichment in heavy metals and decrease in radiocarbon concentration during the last 130 ± 30 years correspond to industrial growth as reflected in European fossil fuel consumption within the same period of time. For the upper 20 cm no sedimentation rate could be calculated from the C-14 dates. The 850 year surface radiocarbon age, however, represents the "zero age" of the sediment age scale. A surface age of zero years could be expected only for samples which derive their carbon exclusively from atmospheric carbon dioxide. In other environments, a higher zero-age may result, i.e. central European fresh water carbonates have zero-age values of up to 1500 years (Münnich, 1968). The surface age simply reflects the admixture of radiocarbon-free fossil carbon and thus provides a basis for assessment of pollution effects.

1.5 The Clyde Sea and Loch Lomond areas.

The Clyde Sea area includes within it a system of seven sea lochs originating from a glacial scouring during the Pleistocene. This area, total surface area 2,500 km^2, extends to the north of a line joining Girvan to the Mull of Kintyre (Figure 1.2). The physical dimensions of the Clyde Sea area are shown in Table 1.1.

Deep core sediments from the area appear to be glacial, postglacial and recent. Besides these, there are sandy muds, sand and gravel deposit layers in the littoral and sub-littoral areas (Deegan et al., 1973). In deep waters also manganese nodules (authigenic formation) have been extracted, a finding which indicates comparatively slow sedimentation rates, particularly along the Kintyre coast and to the south of Arran (Calvert and Price, 1970; Deegan et al., 1973). Indeed Moore (1931) estimated a mean natural sedimentation rate of around 0.5 cmy^{-1} in the Loch Striven area, varying throughout the year as a function of diatom population. Industrial inputs, for example sludge dumping, may significantly alter the sediment regime.

The circulation pattern of Clyde estuary waters indicates a partly mixed system with residence times of water in the Firth of less than or around nine months (Mill, 1892; Craig, 1959). The tidal range of the Clyde is comparatively small and thus tidal currents are weak. Fresh water input to the system is small and inadequate for total dispersal of

Fig. 1.2 The Clyde Sea Area

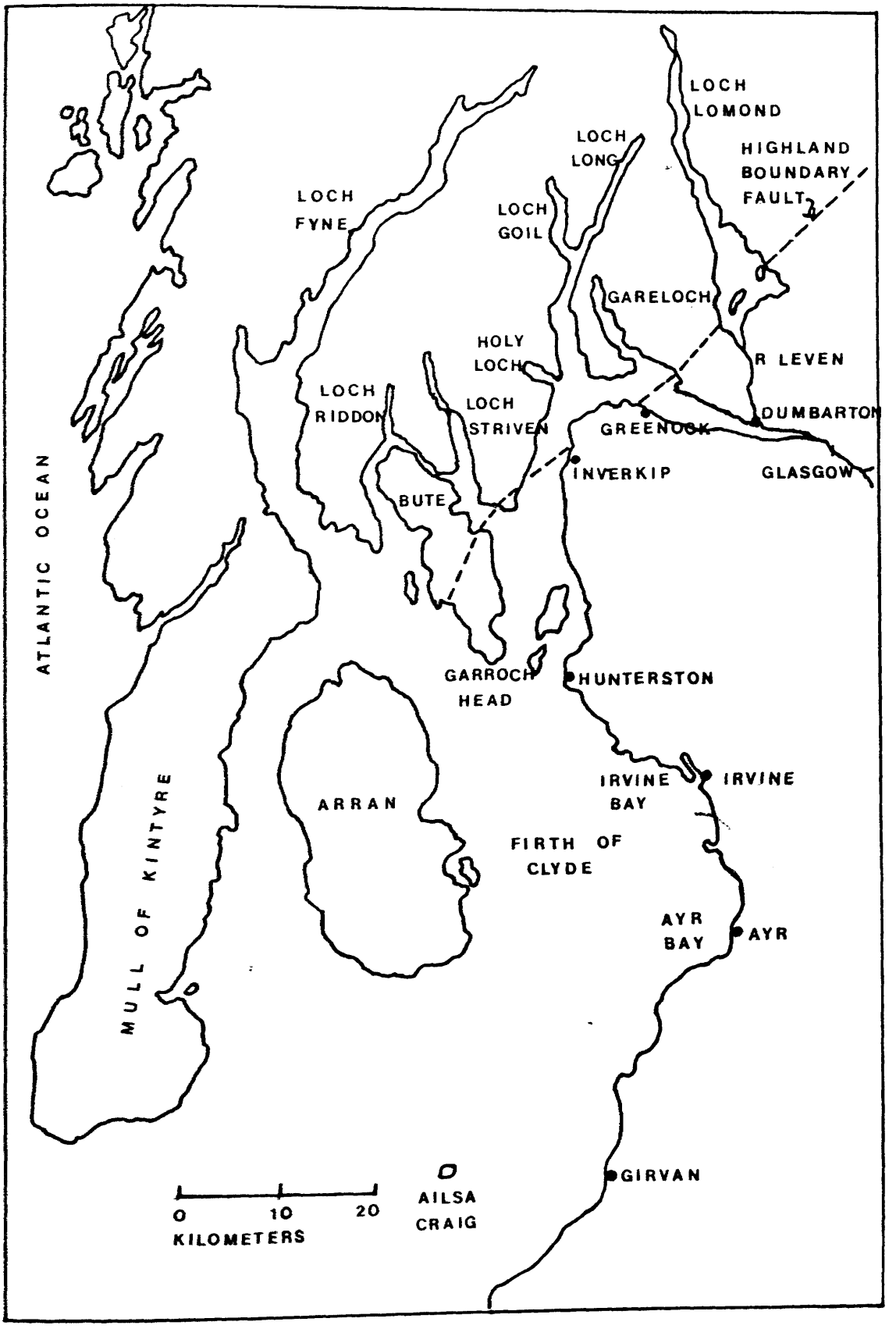

TABLE 1.1 PHYSICAL DIMENSIONS OF THE CLYDE SEA AREA

SECTION	COASTLINE (KM)	AREA (KM^2)	VOLUME (KM^3)
TOTAL CLYDE SEA AREA		2,500.0	165.00
ESTUARY	170.0	69.0	0.90
INNER FIRTH		185.0	7.80
GARE LOCH	33.0	20.5	0.21
LOCH LONG	57.0	36.2	1.30
LOCH GOIL		9.0	0.31
HOLY LOCH	11.0	4.9	0.07
LOCH STRIVEN	33.0	15.0	0.50
LOCH RIDDON	67.0	44.5	1.27
KYLES OF BUTE			
LOCH FYNE	183.0	210.0	13.3

(CLYDE RIVER PURIFICATION BOARD , 1976)

effluents so that within the estuary anaerobic conditions develop. The estuary receives fresh water input from the rivers Kelvin, Carts and Leven. The latter is the outlet for the Loch Lomond catchment area. Rainfall over the catchment area is small compared to the volume of the Clyde sea area. Data for total freshwater input to the estuary are given in Table 1.2.

Pollution in the area derives from many sources. Domestic sewage and industrial effluents from urban areas, dumping of sludge and sewage off Garroch Head and the discharge of nitrogenous effluents from industrial plants are important factors. In addition, oil pollution is a major problem in the Clyde sea area since the sea lochs offer deep water terminals for oil transportation. Thus about 60 significant oil spillages are reported each year. The major pollution effect is therefore of organic materials. In addition, concentrations of pollutants in rainfall and Irish Sea water entering the area are considerable (Cambray et al., 1975). The data of some major pollutant inputs are shown in Tables 1.3 and 1.4.

Many of the sea lochs of the Clyde sea area are fiord-like, being long, narrow, steep sided and deep. Loch Goil and Gare Loch are protected by characteristically fiord-like entrance sills. Thus, surface borne materials such as sewage, plastics and oil are retained and accumulate within these lochs. Many have long retention times

TABLE 1.2 FRESH WATER FLOW IN THE NORTHERN SECTION OF THE CLYDE SEA AREA

SECTION	FRESH WATER FLOW ($M^3 SEC^{-1}$)			
	5% EXCEEDENCE	50% EXCEEDENCE	95% EXCEEDENCE	MEAN
ESTUARY	335.0	80.0	28.0	113.0
INNER FIRTH	17.0	2.4	0.4	
GARE LOCH	5.7	0.5	0.1	1.9
LOCH LONG	23.7	2.3	0.3	12.2
LOCH GOIL	17.8	1.7	0.3	7.8
HOLY LOCH	31.3	6.8	1.4	11.2
LOCH STRIVEN	12.5	1.2	0.2	3.7
LOCH RIDDON	23.6	2.3	0.3	7.2
KYLES OF BUTE				
LOCH FYNE	129.0	12.3	1.9	38.4
RIVER CLYDE	140.0	23.0	8.0	
RIVER KELVIN	26.3	5.0	1.4	
RIVER CARTS	28.0	8.5	2.7	
RIVER LEVEN	92.0	37.3	14.6	

(CLYDE RIVER PURIFICATION BOARD, 1976)

TABLE 1.3 SEWAGE INPUT TO THE CLYDE SEA AREA

SECTION	ESTIMATED INPUT ($M^3 DAY^{-1}$)
UPPER ESTUARY	10^6
LOWER ESTUARY	0.045×10^6
FIRTH	0.059×10^6

(NATIONAL ENVIRONMENT RESEARCH COUNCIL, 1974)

TABLE 1.4 SOME MAJOR METAL POLLUTANT INPUTS TO THE CLYDE SEA AREA

METAL	INPUT FROM RIVER CLYDE (TONNES Y^{-1})	SEWAGE SLUDGE DEPOSITS (TONNES Y^{-1})	INPUT FROM FRESH WATER IRISH SEA (TONNES Y^{-1})	INPUT BY RUN-OFF (TONNES Y^{-1})	RAIN WATER (TONNES Y^{-1})
Cu	10.0	25.0	43.0	10.0	50.0
Zn	45.0	60.0	270.0	50.0	250.0
Cd	0.4	0.25	4.0	0.6	1.7
Pb	20.0	25.0	8.0	35.0	60.0

(NATIONAL ENVIRONMENT RESEARCH COUNCIL, 1974)

(~4 to 12 months). The capacity of most of these lochs to receive organic wastes without serious oxygen depletion is significantly limited and, in most, anoxic conditions develop in deep waters and sediments. For example, anoxic conditions have been observed in the deep waters of Loch Goil in late summer, with a rapid increase in dissolved oxygen concentration in early winter (Figure 1.3). These observations indicate a summer stratification of the loch, with little vertical mixing during "winter overturn".

Loch Lomondis situated in the middle of Lennox, a wide area which includes the whole of Dumbarton and much of west Stirlingshire (Figure 1.2). Loch Lomondtrends nearly north-south and in straight line is about 34 km in length. Following the sinuous axis of maximum depth, however, the length is nearly 37 km. The upper northern portion for a distance of 19 or 21 km from the head of the loch is narrow, mostly less than 2 km across, but to the south of Ross Point the loch opens out and a maximum breadth of 8 km at about 5 km above the exit of the river Leven at Balloch. In superficial area Loch Lomond is the largest of all the Scottish freshwater lochs, being estimated to cover 70.4 square km. The area draining into the loch is about 691.5 km^2 or ten times the area of the loch. The most considerable input river to the loch is the Endrick in the south-east region; on the west side it receives the waters of Uglas, the Luss and other smaller rivulets. The volume of water contained in

Fig.1.3. Variation of Dissolved Oxygen in the Bottom Water of Loch Goil During 1974.

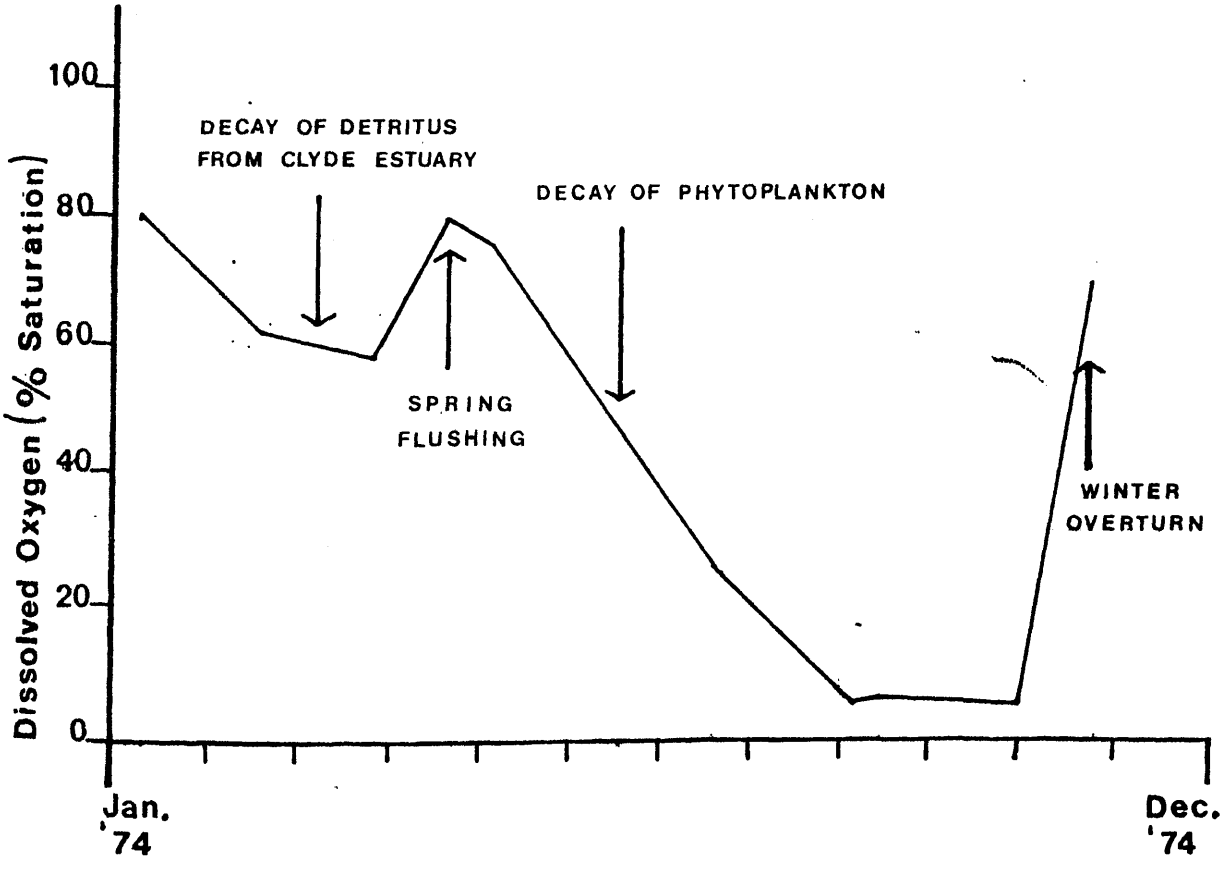

(Clyde River Purification Board, 1974.)

the loch is estimated at 9.28×10^{10} cubic feet or over 2×10^{9} m^3. In this respect Loch Lomond ranks second among the Scottish lakes being exceeded only by Loch Ness, the capacity of which is about three times greater. The maximum depth recorded is 190 m, the mean depth being around 37 m consistent with the fact that more than two-thirds of the lake-floor is covered by less than 30.5 m of water.

With regard to the formation of Loch Lomond, it is known by observation of glacial scratches on rock surfaces that the dominant direction of ice movement during the last glaciation of the area was from north to south. With retreat of the ice, Loch Lomondemerged as it is at the present, discharging via the river Leven into the Clyde estuary and, in fact, providing a freshwater input about equal in magnitude to that of the river Clyde itself. The freshwater input and discharge through the river Leven have a long-term average value of 38.873 m^3 per sec (Clyde River Purification Board, 1975).

There were large fluctuations in sea level in late glacial times so that at a period when the sea level stood low, water overflowing from the loch cut a deep valley in the position of the Vale of Leven. When sea level rose again, a direct connection with the Firth of Clyde may have been established. The final cold stage of the last ice age, known as the Loch Lomond Readvance, was completedabout 10,000

years ago and the land, freed from its burden of ice, rose gradually. Shortly before 6000 B.C. sea levels began to rise again. The evidence for this rise in sea level is provided by deposits of carse clays in many parts of Scotland. The rise in sea level probably reached a maximum after 4000 B.C. and recession began about 3500 B.C. Further adjustment in sea level finally led to the loch as it is today with a rise in sea level of about 30 feet required for it to become tidal again (Sissons, 1967).

The list of present uses of Loch Lomond and its surroundings includes agriculture, forestry and recreation. The loch itself is a major source of fresh water and hydro-electric power. Other important uses include sand and gravel extraction.

Aim of research.

The aim of this research project is to perform C-14 analyses on sediment cores from the sea lochs of the Clyde sea area and to interpret the data with regard to carbonaceous pollution of the area.

In addition, it is of interest to compare the C-14 results with those obtained by Pb-210 and Cs-137 dating methods for the same cores. In this way industrial impact on the sedimentary system can be evaluated.

A second and allied aim is to date a long sediment core (up to 6 metres in length) from Loch Lomond and to compare C-14 data with stratigraphical markers such as paleomagnetic

(susceptibility, intensity, declination) and pollen horizons. In this way, the historical development of climate and agriculture in the area can be established. In addition, a critical assessment of each technique can be made.

CHAPTER 2. EXPERIMENTAL METHODS.

2.1 Sample selection and collection.

Two sea lochs in the Clyde system, Loch Goil and Gare Loch, were chosen for sample collection because of their specific pattern of pollution. The former is near the major oil terminal at Finart and is therefore susceptible to sporadic fossil carbon pollution. It is known to develop anoxic conditions. The latter is the sea loch nearest to the Clydeside industrial complex and to the anoxic estuary.

Sediment cores were collected using a gravity corer (Figure 2.1) operated by the staff of the Clyde River Purification Board.

The gravity corer is lowered to within 5 m of the sediment surface before it is allowed to free-fall. The sediment is retained inside the plastic core liner by means of a metal core catcher. A one way valve allows expulsion of water from the core barrel during the collection of sediments and prevents disturbance of sediment while the corer is hauled to the surface.

The first two sediment cores from Loch Goil were obtained on 8 April, 1975 (latitude 56° 08' 20" N, longitude 04° 53' 21" W and water depth 82 m). A third sediment core from the same Loch Goil site was collected on 10 August, 1976. The first two cores from Loch Goil were 60 cm long, the third 100 cm. The diameter of plastic core liner was 6 cm.

A sediment core from Gare Loch was collected by gravity corer on 7 November, 1975 (latitude 56° 02' 42" N, longitude 04° 49' 36" W and water depth 48 m). The length of the core was 60 cm.

Fig. 2.1 Schematic Diagram of Gravity Corer.

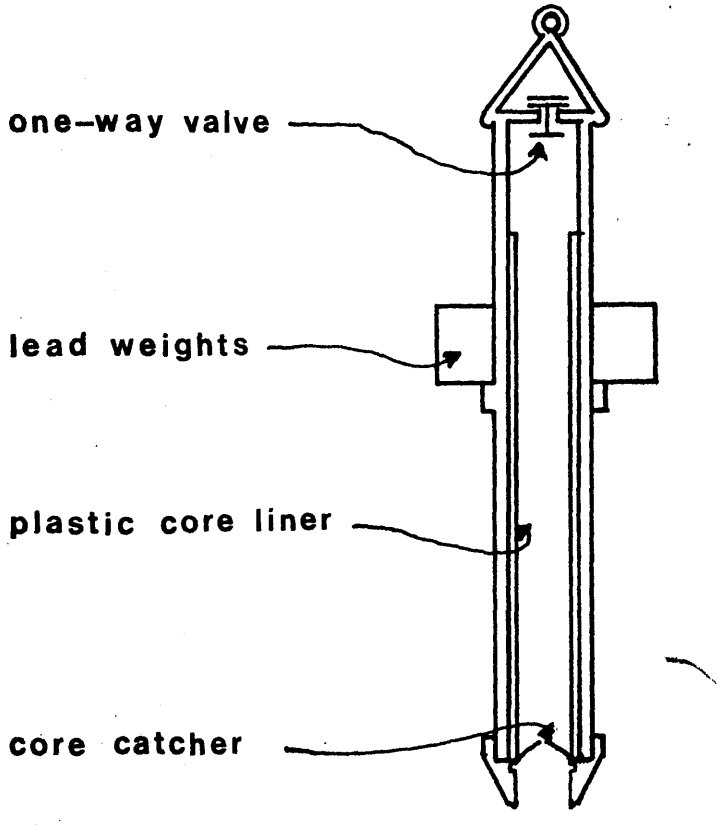

Loch Goil sediments were predominantly composed of soft muds, while Gare Loch sediments were more consolidated. All cores were deep frozen immediately on collection, in a combined freezer/transporter unit, to minimise the possibility of sediment mixing during transport. Thereafter, sediment cores were cut into 4 inch segments, which were individually weighed (wet/dry), powdered and subjected to chemical pretreatment and carbon dioxide preparation.

A 6 metre long sediment core was taken by a pneumatically driven Mackereth corer (Figure 2.2) from Loch Lomond (latitude 56° 05' 49" N, longitude 04° 35' 45" W). The core was collected by Dr R. Thompson, Department of Geophysics, University of Edinburgh. The sample sediments were withdrawn by extruding the sediment from the coring tube by means of a free piston driven hydraulically up the coring tube. The sample collector was designed to minimise disturbance of the mud-water interface while sampling. This Loch Lomond sediment core, LLRD1, was preliminarily studied by Thompson in 1976 and by Dickson and Stewart, Botany Department, University of Glasgow, in 1977, for paleomagnetic and pollen relative dating methods respectively.

The sampling depths for radiocarbon dating were based on the major changes in magnetic declination as follows: A (95 to 105 cm); B (118 to 132 cm); C (138 to 162 cm); D (163 to 177 cm); E (218 to 232 cm); F (260 to 280 cm); G (313 to 337 cm); H (342 to 358 cm); I (442 to 458 cm) and M (506 to 534 cm); while the sampling depths at L (177 to 199 cm), K (285 to 313 cm) and T (410 to 430 cm) were chosen to confirm the major trends of sediment deposition.

Fig.2.2 Cross Section of the Complete MacKereth Corer (1958)

A- Stainless Steel Tube (20ft X 3ins)
B- "Duralumin" Coring Tube
C- Brass Plug
D- Narrow Brass Tube
E- Compressed Air (in flow)
F- "Duralumin" Plug
G- Anchor Chamber
P- H_2O Pumping Out
M- Chain
S- Air Escape
Y- Downward Pull

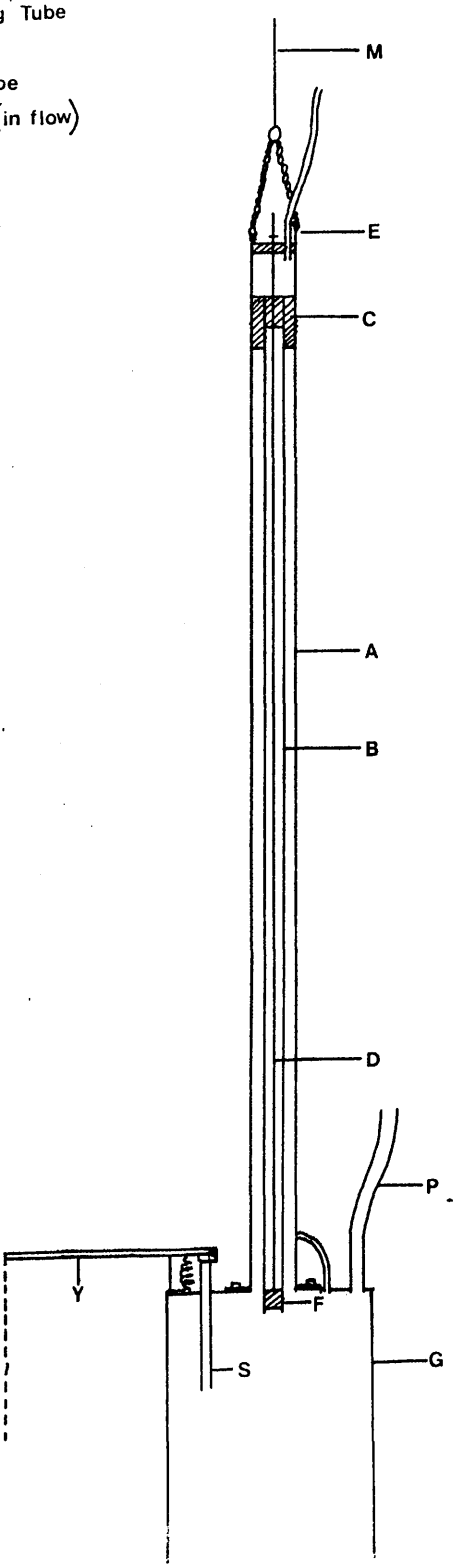

2.2 Chemical pretreatment.

All sediment samples, $\sim$10 cm length, are first heated for 90 minutes in 0.5 M HCL to remove any inorganic carbonates. Thereafter, samples are washed several times in distilled water to remove residual traces of HCL. The final sediment/water mixture is left for an hour to allow the divided sediment to settle prior to decanting off the supernatant liquid. Each sediment sample is then dried in an oven at 100^0 C to constant weight. The caked sediment is then ground and combusted.

Because of the low organic carbon content of sediments relative to cellulose, several differences from the previously described combustion technique are necessary. Firstly, the sample volume is considerably greater, so that sediments are not contained in combustion boats but simply packed in the quartz tube itself. Secondly, the sediment requires roasting in a high O_2 flux with little fine control of reaction conditions. All stages subsequent to the combustion process are identical to those discuss in Chapter 1-2.

In addition, for each sample, the wet/dry weights, the dry weight after inorganic carbon removal, the weight after sediment combustion and finally the $BaCO_3$ weight are recorded. From such data it is possible to calculate the percentage H_2O, inorganic and organic carbon contents and thus to monitor the efficiency of combustion and precipitation of $BaCO_3$ for each sample experiment.

2.3 Auxiliary studies.

Sediment sample cores were also distributed for Pb-210 and Cs-137 assays. Thus Pb-210 was measured by alpha-spectrometry of

its Po-210 grand-daughter and Cs-137 by direct gamma-spectrometry. X-rays of the sediment cores were obtained using a modified medical X-ray system.

As mentioned already, detailed paleomagnetic and pollen measurements were performed on the Loch Lomond core. Furthermore, a small quantity (up to 1 g) of each sediment aliquot was microanalysed for C, H, N, Al, Fe, Cr and Pb contents.

2.4 Replicate analysis.

For sediments no replicate analyses were performed. Sediments being open and complex chemical systems are prone to various localised changes in composition and, as a result, it is dubious whether a homogeneous sediment replicate sample could be collected. However, since in the study of sediments, larger scale differences are generally being investigated, it is believed that errors introduced due to non-counting experimental procedures will not influence the results to a significant extent relative to the C-14 concentration differences under study. This is in contrast to the tree ring analysis described previously where experimental error exceeds, or is equivalent in magnitude to, the C-14 variations being investigated. In this sediment project therefore results are treated in the conventional C-14 manner, that is with reference to statistical counting errors only. It should be understood, however, that these errors are minimum estimates of the total precision.

CHAPTER 3. Results.

The following tables contain all the sediment data collected over the research period. In circumstances where a δC-13 measurement is not available, due for example to escape of sample CO_2 during storage, a mean value for the core was assumed and is shown in parenthesis. A $\pm 1\sigma$ error is quoted for δC-13, δC-14, Δ and radiocarbon age results. δC-14 and Δ values are presented in per mille units and C-14 ages in conventional radiocarbon years B.P. ($t_{\frac{1}{2}}$ 5570 $\pm$ 30g.). Three sediment cores GLG-2, LGG-3 and $LRDD_1$ were microanalysed. For the other cores the carbon contents were calculated from experimental $BaCO_3$ yields and the observed dry weights. All micro-analytical data have an associated 0.3% error. For each sediment segment water volume was calculated according to the equation:

$$V_{H_2O} = \frac{Gw.w.-Gd.w.}{\delta_{H_2O}} \quad (cm^3)$$

where Gw.w. denotes the weight of the wet sediment, Gd.w. the weight of dry sediment and δ_{H_2O} the water density at 4^oC ($\delta^{4^oC}_{H_2O} = 1g/cm^3$). Thereafter the porosity of each sediment sample was calculated via:

$$p = \frac{V_{H_2O}}{V\ total} \qquad [\theta]$$

where V total denotes the total volume of wet sediment. The bulk density (g/cm^3) is defined as the wet sediment weight divided by the total sediment volume and the sediment density (g/cm^3) as the dry weight of sediment divided by its volume.

TABLE 3.1 MICROANALYTICAL DATA FOR GARE LOCH CORE GLG-2

DEPTH (CM)	C (%)	N (%)	H (%)
9	5.61	0.26	1.07
10	5.51	0.25	1.19
15	5.25	0.25	1.08
20	5.15	0.20	1.15
25	5.39	0.25	1.02
30	5.14	0.26	1.09
32	5.20	0.25	0.99

TABLE 3.2 PHYSICAL DATA FOR GARE LOCH CORE GLG-2

DEPTH (CM)	WET WT. (G)	DRY WT. (G)	POROSITY (%)	BULK DENSITY (G/CM^3)	SED. DENSITY (G/CM^3)
0-10	358.0	139.0	0.77	1.27	2.17
10-20	380.0	180.0	0.71	1.34	2.17
20-30	393.0	185.0	0.73	1.39	2.47
30-40	386.0	188.0	0.70	1.36	2.21
40-50	388.0	189.0	0.70	1.37	2.25
50-60	326.0	175.0	0.53	1.15	1.33
60-70	334.0	182.0	0.53	1.18	1.39

TABLE 3.3 RADIOCARBON DATA FOR GARE LOCH CORE GLG-2

DEPTH (CM)	δC-14±1σ (‰)	δC-13±1σ (‰)	Δ±1σ (‰)	AGE ±1σ (y. B.P.)
0-10	-392.1±7.30	-28.55±0.05	-388.00±7.30	3942±96
10-20	-530.0±5.80	-28.62±0.05	-526.50±5.80	6007±99
20-30	-528.0±5.80	-31.07±0.05	-522.0±5.80	5931±98
30-40	-457.0±7.30	-29.19±0.05	-452.08±7.20	4834±107
40-50	-449.0±7.30	-29.31±0.05	-444.00±7.20	4715±105
50-60	-439.0±4.40	-28.75±0.05	-435.00±4.40	4588±63
60-70	-462.0±6.60	-29.09±0.05	-457.30±6.50	4911±97

TABLE 3.4 PHYSICAL DATA FOR LOCH GOIL CORE LGG-1

DEPTH (CM)	WET WT. (G)	DRY WT. (G)	C CONTENT (%)	POROSITY (ϕ)	BULK DENSITY (G/CM^3)	SED. DENSITY (G/CM^3)
0-10	327.0	60.0	4.40	0.94	1.16	3.75
10-20	340.0	76.0	4.60	0.93	1.20	4.00
20-30	351.0	101.0	2.50	0.88	1.24	3.06
30-40	352.0	111.0	2.80	0.85	1.24	2.64
40-50	356.0	122.0	2.60	0.83	1.26	2.50
50-60	367.0	126.0	3.34	0.85	1.30	3.00

TABLE 3.5 PHYSICAL DATA FOR LOCH GOIL CORE LGG-2

DEPTH (CM)	WET WT. (G)	DRY WT. (G)	C CONTENT (%)	POROSITY (ϕ)	BULK DENSITY N G/CM^3)	SED. DENSITY (G/CM^3)
0-10	342.0	77.0	4.15	0.94	1.21	4.28
10-20	350.0	87.0	4.10	0.93	1.24	4.35
20-30	361.0	109.0	3.80	0.89	1.28	3.52
30-40	371.0	118.0	4.01	0.89	1.31	3.93
40-50	378.0	127.0	2.80	0.89	1.35	3.97
50-60	381.0	139.0	3.40	0.86	1.35	3.39

TABLE 3.6 PHYSICAL DATA FOR LOCH GOIL CORE LGG-3

DEPTH (CM)	WET WT. (G)	DRY WT. (G)	POROSITY (ϕ)	BULK DENSITY (G/CM^3)	SED. DENSITY (G/CM^3)
0-10	329.0	86.0	0.86	1.16	2.15
10-20	347.0	116.0	0.82	1.29	2.23
20-30	355.0	130.0	0.80	1.25	2.24
30-40	367.0	157.0	0.74	1.30	2.15
40-50	381.0	161.0	0.78	1.35	2.56
50-60	368.0	246.0	0.43	1.30	1.53
60-70	370.0	158.0	0.75	1.31	2.24
70-80	378.0	159.0	0.77	1.34	2.48
80-90	258.0	102.0	0.55	0.91	0.80
90-100	237.0	96.0	0.50	0.84	0.68

TABLE 3.7 MICROANALYTICAL DATA FOR LOCH GOIL CORE LGG-3

DEPTH (CM)	C (%)	N (%)	H (%)	AL (%)	Fe (%)	Cr (%)	Pb (%)
0-20	4.05	1.88	2.54	3.83	4.30	0.04	0.70
20-30	3.19	1.31	1.61	5.50	6.07	0.04	0.04
30-40	3.72	3.43	0.98	5.45	6.07	0.04	0.03
40-50	1.68	1.93	0.72	4.34	4.04	0.03	0.03
50-60	6.13	0.80	1.68	4.70	5.47	0.04	0.04
60-70	2.20	0.78	1.45	5.42	6.12	0.04	0.04
70-80	2.96	0.97	1.33	4.10	3.67	0.03	0.06
80-90	2.40	0.88	1.30	4.93	6.32	0.04	0.04
90-100	3.18	0.50	1.30	5.13	6.90	0.04	0.04

TABLE 3.8 RADIOCARBON DATA FOR LOCH GOIL CORE LGG-1

DEPTH(CM)	$\delta C-14 \pm 16$ (‰)	$\delta C-13 \pm 26$ (‰)	$\Delta \pm 16$ (‰)	AGE(YR.B.P.)
0-10	-332.0±9.5	-26.73±0.1	-330.0±9.4	3212±114
10-20	-383.4±5.9	-27.74±0.1	-380.0±5.8	3841± 76
20-30	-314.5±7.3	-27.11±0.1	-311.6±7.3	3001± 86
30-40	-427.6±5.10	-26.73±0.1	-425.6±5.1	4455± 72
40-50	-266.6±5.9	-26.49±0.1	-264.4±5.9	2467± 64
50-60	-488.6±5.9	-25.58±0.1	-488.0±5.8	5378± 92

TABLE 3.9 RADIOCARBON DATA FOR LOCH GOIL CORE LGG-2

DEPTH(CM)	$\delta C \pm 1\sigma$ (‰)	$\delta C\text{-}13 \pm 1\sigma$ (‰)	$\Delta \pm 1\sigma$ (‰)	AGE (Y.B.P.)
0-10	-340.0±6.6	-27.13±0.1	-337.8±6.6	3311±80
10-20	-345.6±5.2	-28.14±0.1	-341.5±5.2	3357±63
20-30	-234.7±6.6	-27.61±0.1	-230.7±6.6	2107±69
30-40	-276.4±6.6	-27.13±0.1	-273.6±6.6	2569±73
40-50	-272.4±5.2	-26.89±0.1	-269.6±5.2	2525±57

TABLE 3.10 RADIOCARBON DATA FOR LOCH GOIL CORE LGG-3

DEPTH (CM)	δC-14 ±16(‰)	δC-13 ±26(‰)	Δ ±16(‰)	C-14 AGE(YBP)
0-10	-262.2±5.9	-29.70±0.1	-255.3±5.8	2368±63
10-20	-252.0±5.2	-29.22±0.1	-245.8±5.1	2266±55
20-30	-210.7±5.2	-29.52±0.1	-203.6±5.2	1829±52
30-40	-202.0±5.9	-31.50±0.1	-191.6±5.8	1709±58
40-50	-133.1±6.6	-28.36±0.1	-127.3±6.6	1094±61
50-60	-249.2±5.2	-30.66±0.1	-241.0±5.4	2212±54
60-70	-212.9±5.2	-27.79±0.1	-208.5±5.2	1899±53
70-80	-248.4±5.2	-27.40±0.1	-244.8±5.2	2256±55
80-90	-140.4±5.2	-22.83±0.1	-144.1±5.2	1250±49
90-10	-208.0±6.6	-26.37±0.1	-205.6±6.6	1850±67

TABLE 3.11 MICROANALYTICAL DATA FOR LOCH LOMOND CORE LLRD1

DEPTH (CM)	C (%)	N (%)	H (%)
90	2.40	-	1.50
150	3.80	-	2.50
200	2.83	-	1.95
250	1.56	-	1.89
300	2.80	-	2.10
350	3.25	-	1.10
400	5.15	-	1.40
450	4.48	0.54	2.13
500	1.38	-	1.46
550	0.95	-	1.23
595	1.55	-	1.25

TABLE 3.12 RADIOCARBON DATA FOR LOCH LOMOND CORE LLRD1

DEPTH (CM)	δC-14±1δ(‰)	δC-13±0.05(‰)	Δ±1δ(‰)	AGE±1δ(Y.BP)
100	- 81±5.9	-27.14	- 77±5.9	643±52
125	-210±6.6	(-29.95±2.6)	-202±7.7	1815±78
150	-196±5.2	-33.00	-183±5.1	1627±51
170	- 31±6.7	-26.26	- 28±6.7	231±55
188	-157±6.0	(-29.95+2.6)	-149±7.3	1294±69
225	-211±5.9	-28.96	-205±5.9	1838±59
270	-200±5.9	-28.83	-194±5.9	1730±59
299	-293±5.9	(-29.95±2.6)	-286±5.9	2712±78
325	-365±4.4	-31.33	-357±4.4	3542±55
350	-418±4.4	-34.23	-408±4.4	4205±59
420	-548±5.8	-30.50	-543±5.8	6293±102
450	-703±5.8	-29.26	-701±5.8	9694±156
520	-627±5.8	(-29.95±2.7)	-622±5.8	7832±131

CHAPTER 4. DISCUSSION AND CONCLUSIONS.

4.1 Clyde sediments.

It is evident from the C-14 results that in the Clyde area a large excess of fossil carbon from fuels and industrial waste materials has been deposited locally, thus diluting natural C-14 concentrations and producing abnormally old ages in near surface sediments. This depression of surface ages enables approximate assessment of carbonaceous pollution in the area. The radiocarbon age vs. depth profile of cores GLG-2, LGG-1, LGG-2 and LGG-3 are shown in Figures 4.1 and 4.2. The data of Figures 4.1 and 4.2 are based on results listed in Tables 3.3, 3.8, 3.9 and 3.10. All results are corrected for isotopic fractionation. The data points are accompanied by their 2σ error bars (horizontal) for C-14 age, while vertical bars represent the depth increment analysed. For the Gare Loch core GLG-2 (Figure 4.1) an inversion point is observed at 35cm depth. Below the inversion point the radiocarbon age vs. depth profile is almost uniform indicating natural C-14 levels with no significant decay over the depth interval. In other words, the time-scale of sedimentation in this depth increment is considerably shorter than the C-14 half-life so that classical C-14 dating cannot precisely quantify the natural sedimentation rate. Thus the approximate within error constancy of the C-14 data as a function of depth below 35cm enables only a minimum assessment of the natural sediment accumulation rate. A minimum value of 0.4 mm y^{-1} is obtained

Fig. 4.1 Radiocarbon-Age Vs Depth in Core GLG-2

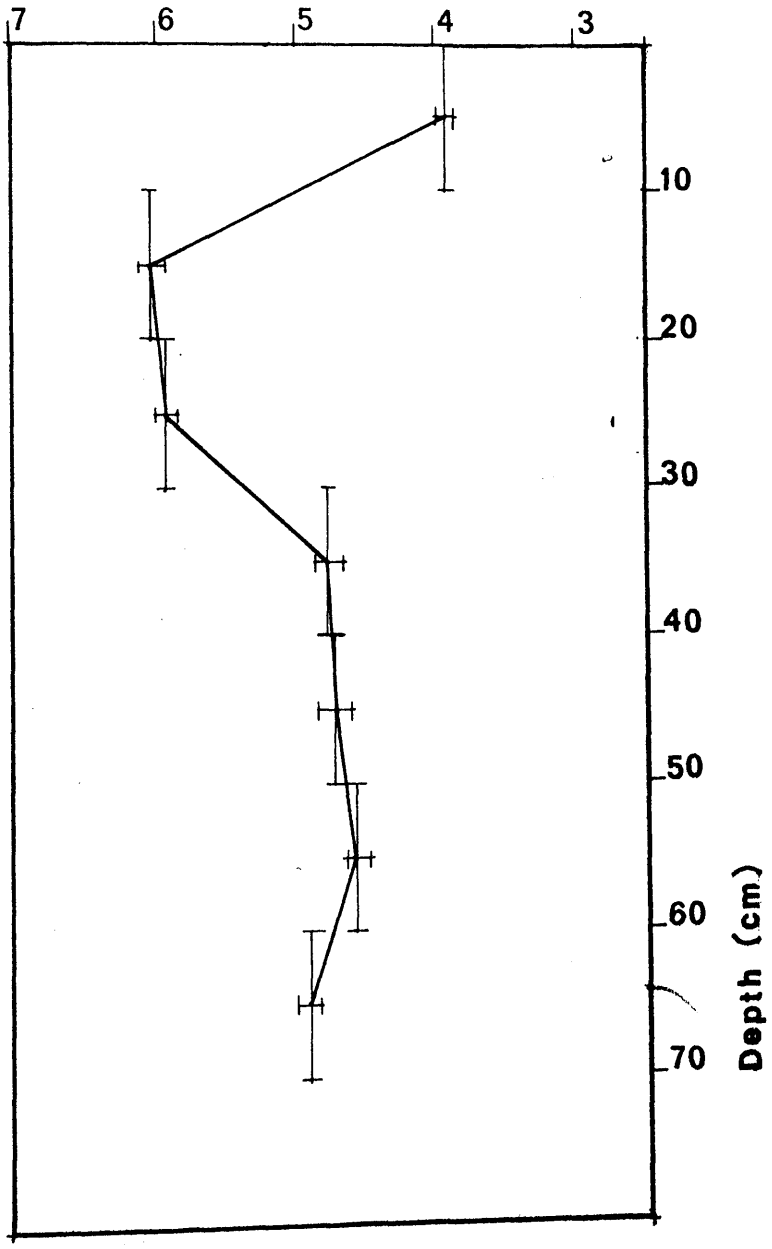

Fig. 4.2 Loch Goil Cores LGG 1, LGG 2, LGG 3.

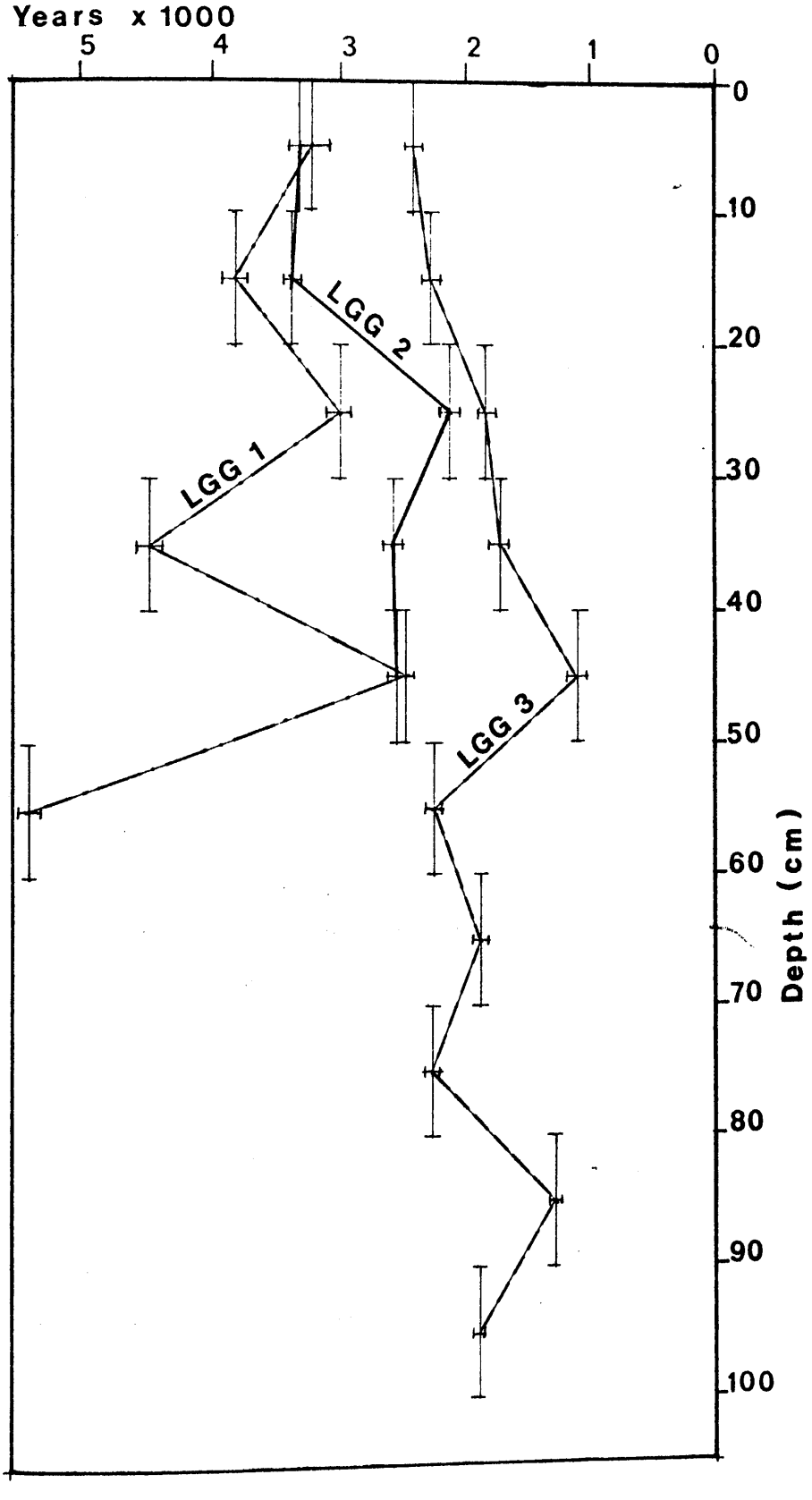

from the line of least gradient which still approaches the deagonal limits of the $\pm 2\sigma$ error bars. Any line of smaller gradient than 0.4 mm y^{-1} would represent an anomalously low sedimentation rate and would introduce a significant decay effect not indicated by the data. Above 35 cm sediment depth, however, a deviation from this relatively constant trend is apparent with radiocarbon ages increasing towards the surface. At depth 15 cm a second transition is observed in Gare Loch core GLG-2. Thus the topmost point shows a younger age indicating, probably, the local admixture of modern carbon. For the Loch Goil sediment cores LGG-1 and LGG-3, however, no inversion point is observed (Figure 4.2). On the contrary, all Loch Goil sediment cores appear to be affected by variable sediment composition as evidenced by differing C-14 ages between cores and considerable scatter with depth. Such variations imply highly localised variations in fossil carbon content. A similar phenomenon may of course occur in Gare Loch but, since only one core has been analysed, this cannot be quantified. It is apparent that any interpretation of Loch Goil sediment data must remain highly tentative prior to further analyses particularly on longer cores. Loch Goil sediment core LGG-2, however, does show a less variable C-14 age vs. depth profile somewhat similar to that found in core GLG-2. Here the inversion starts at a shallower depth -25 cm, possibly indicating a recent sedimentation rate lower than that of Gare Loch. Below 25 cm a constant trend is again observed with

nearly uniform radiocarbon ages with depth. Again, however, it is possible only to predict a natural sedimentation rate greater than 0.30 mm y^{-1}. In addition, it is possible that Loch Goil surface sediment losses and disturbances are higher than those of Gare Loch surface sediments during the coring process itself, since Loch Goil sediments are less consolidated (i.e. have higher porosities) than Gare Loch sediments (Tables 3.2, 3.4, 3.5 and 3.6). Indeed, detailed comparisons of radiocaesium, lead-210 and radium-226 in cores collected by the gravity corer used here and by a purpose-built Craib (1965) surface sediment corer have shown that on average the top 8 to 25 cm of material can be lost during gravity coring. This loss is the result of both the impact pressure wave itself and of subsequent loss of the topmost material through vertical channels created along the outside of the core by the teeth of the metal core catcher.

For the upper 35 cm of the Gare Loch sediment and similarly perhaps for the upper 25 cm sediment depth of the Loch Goil sediment LGG-2, no classical sedimentation rate based on decay can be calculated from the C-14 data. At this point it is, therefore, interesting to consider the radiocaesium isotope concentrations and in particular the Cs-134/Cs-137 ratios in the upper sections of these cores. These parameters are useful in defining accurately to what depth mixing of sediment occurs and in providing a guide to the sedimentation rate in the uppermost few cms of sediment. MacKenzie (1977) has shown

(Figure 4.3) that below 4 cm in Loch Goil core LGC-2, Cs-137 concentrations decrease while no Cs-134 is present. This radiocaesium distribution suggests efficient mixing of the upper 4 cm with relatively consolidated sediment below this depth. In addition, X-ray analysis shows "worm holes" contributing to disturbance of the top 4-5 cm of sediments in Loch Goil. The decrease in C-137 concentrations below 4 cm reflect Windscale input of this radioisotope prior to April 1975. Assuming that the first significant input of Cs-137 into sediments occurred in 1955 and that sediment depth of 6 cm has accumulated since then, an approximate sedimentation rate of 3 mm y^{-1} was calculated. (MacKenzie, 1977).

For Gare Loch core GLC-1 (Figure 4.4), however, the presence of Cs-134 was recorded down to 10 cm depth with Cs-137 concentrations increasing towards the surface in accord with the increasing Windscale input. These results are indicative of a high degree of sediment mixing or of radiocaesium mobility and thus no estimation of sedimentation rate for the upper part of Gare Loch sediments can be derived. The higher Cs-137 concentrations in Gare Loch relative to Loch Goil sediments can be explained by different particulate fluxes in the two lochs. Gare Loch is nearer to the Clyde River system and has a mean total suspended solid level of 3.2 mg l^{-1} composed of equal concentrations of organic and inorganic materials. Loch Goil has, however, a mean total suspended solid content of 1.4 mg l^{-1} inorganic material (Leatherland, 1976). It appears that the

Fig.4.3 Loch Goil L.G.C.2

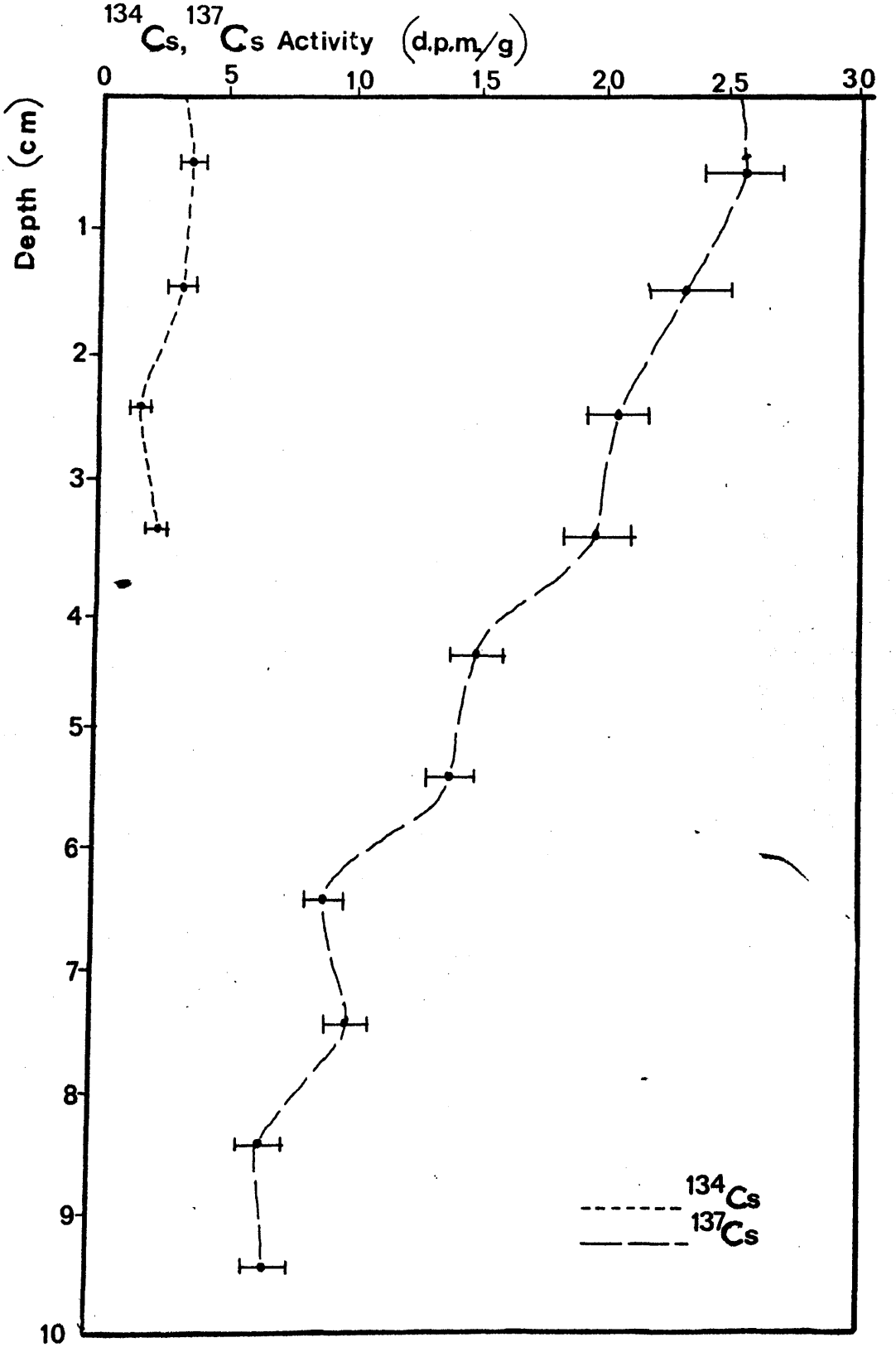

Fig. 4.4 Gare Loch GLC1

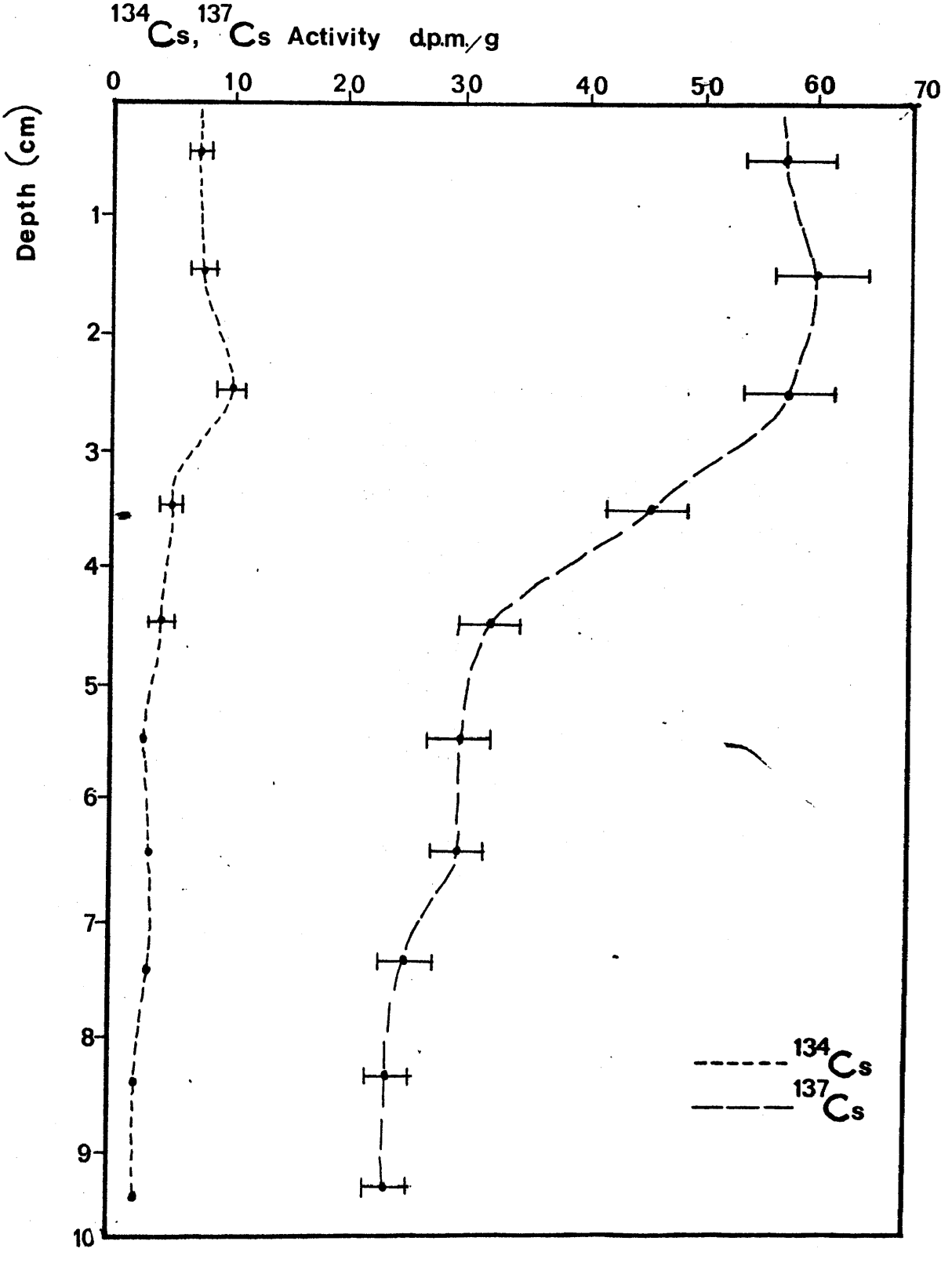

three times greater inorganic specific flux for Gare Loch compares well with the observed enrichment in the sediment.

Perhaps the most definitive information on sedimentation comes from lead-210 profiles obtained by Swan (1977). The Gare Loch and Loch Goil radiometric data, showing Pb-210 concentrations vs. depth, are presented in Figures 4.5 and 4.6. The upper 3 to 4 cm of Gare Loch core GLG-1 show constant Pb-210 activity. This finding is supported by essentially constant Cs-134/Cs-137 ratios, suggesting that physical or biological mixing of sediment occurs down to 4 cm depth. Below this depth an exponential decrease in unsupported (i.e. atmospheric-derived) lead-210 concentrations is observed. At depths below 20 cm constant supported Pb-210 activity is recorded. The data are therefore indicative of a sedimentation rate of 1.75 mm y^{-1} for the upper 20 cm of the Gare Loch sediments (Figure 4.5). Similarly, Pb-210 results for Loch Goil core LGG-5 indicate a mean sedimentation rate of 1.25 mm y^{-1} (Figure 4.6). In Loch Goil an anomaly is recorded in the upper 5 to 6 cm represented by enhanced Ra-226 concentrations and thus increased levels of supported Pb-210. This phenomenon is explained either by a local change in land use (e.g. forestry activity) in recent times, producing an increased input of Ra-rich soil/clays to the loch, or alternatively by an accumulation of biological debris, essentially silicaceous skeleta, at these depths. Radium is well known to correlate with silicate in marine systems (Shannon and Cherry, 1971).

Fig.4.5 Gare Loch Core GLG_1

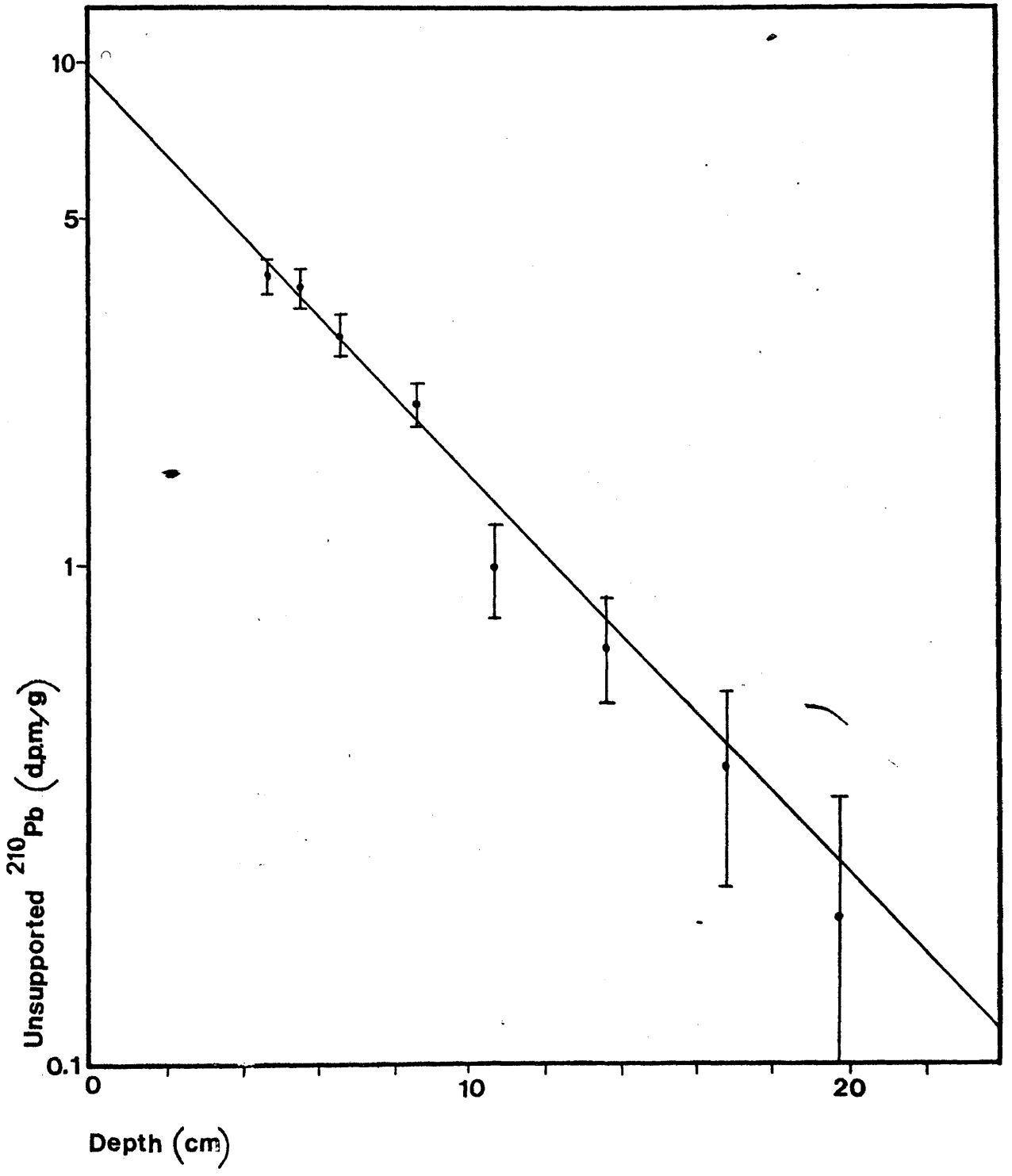

Fig. 4.6 Loch Goil Core L.G.G.5

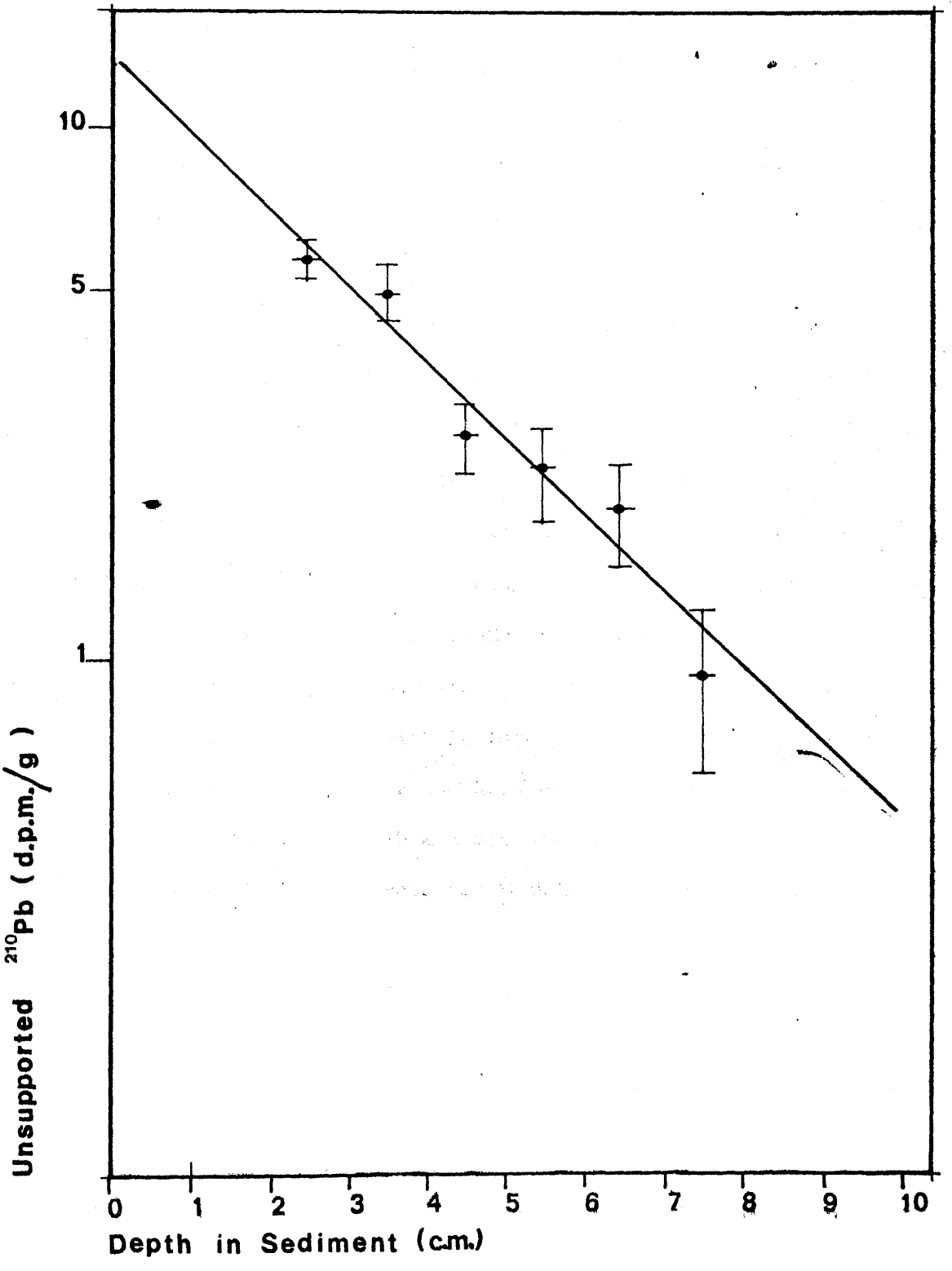

Accepting the industrial era sedimentation rate calculated by the lead-210 method of 1.75 mm y^{-1} for Gare Loch and 1.25 mm y^{-1} for Loch Goil, it is possible to estimate the approximate date of each C-14 inversion point in cores GLG-2 and LGG-2. Thus the increased radiocarbon ages in the upper layers of these sediments imply an admixture of excess fossil carbon in recent sediments which, according to the above Pb-210 sedimentation rates, commenced about 200 years ago in both lochs. An approximate transition age of 200 years is in excellent interval agreement and is consistent with the increase in industrial activities in the mid-18th century. Indeed, the industrial revolution, which started in Dumbartonshire in the 18th century, reached its height in the 19th century, with the two oldest established industries, the textile industry in the Vale of Leven and coal-mining in the eastern part of the county showing great expansion (MacPhail, 1962). Therefore excess fossil carbon in the Clyde sediments was presumably mobilised by industrial activity, which in turn can be traced to $\sim$ 200 years ago in this area. Thus the C-14 profiles in Gare Loch and Loch Goil are consistent with a sedimentation model involving a natural sedimentation rate for both lochs in excess of 0.30 mm y^{-1}. The C-14 inversion, radiocaesium and lead-210 data in the surface sediments are consistent with industrial era sediment accumulation rates of 1.75 mm y^{-1} and 1.25 mm y^{-1} respectively. The onset of industrial impact on the sediments is dated approximately at the early 18th century consistent with

historical records. It is clear, however, that, in these areas, sedimentation rates have not been totally dominated by the industrial component as has been recorded elsewhere. Thus recent and natural rates are of the same order of magnitude consistent with a model involving remobilisation of the artifical component or of a decreasing natural input at the expense of anthropogenic flux. The former possibility is supported by the increasing C-14 ages as a function of depth in the top inversion layers of cores GLG-2 and LGG-2. This trend is most likely the result of preferential oxidation of the less resistant domestic (high Δ) component of the organic carbon material as a function of depth, leaving residual material successively more enriched in the resistant (low Δ) petroleum-derived organic fraction. Thus the domestic carbonaceous matter, perhaps mainly of sewage origin, has been more readily decomposed. If this is the case, an approximate inverse correlation between radiocarbon ages and total organic carbon content would be predicted. Figure 4.7 plots radiocarbon age vs. carbon content for the Gare Loch core GLG-2. Although the data points are few and interpretation therefore is tenuous, an inverse correlation may indeed be implied. Similar realtionships are evident for the other sediment cores.

Besides suggesting an approximate timescale of sedimentary processes, the C-14 data have their major application in assessment of the realtive contributions of natural and fossil carbon to the organic fraction of any sediment sample. It is

Fig. 4.7 Carbon Content Vs C-14 Age (GLG-2)

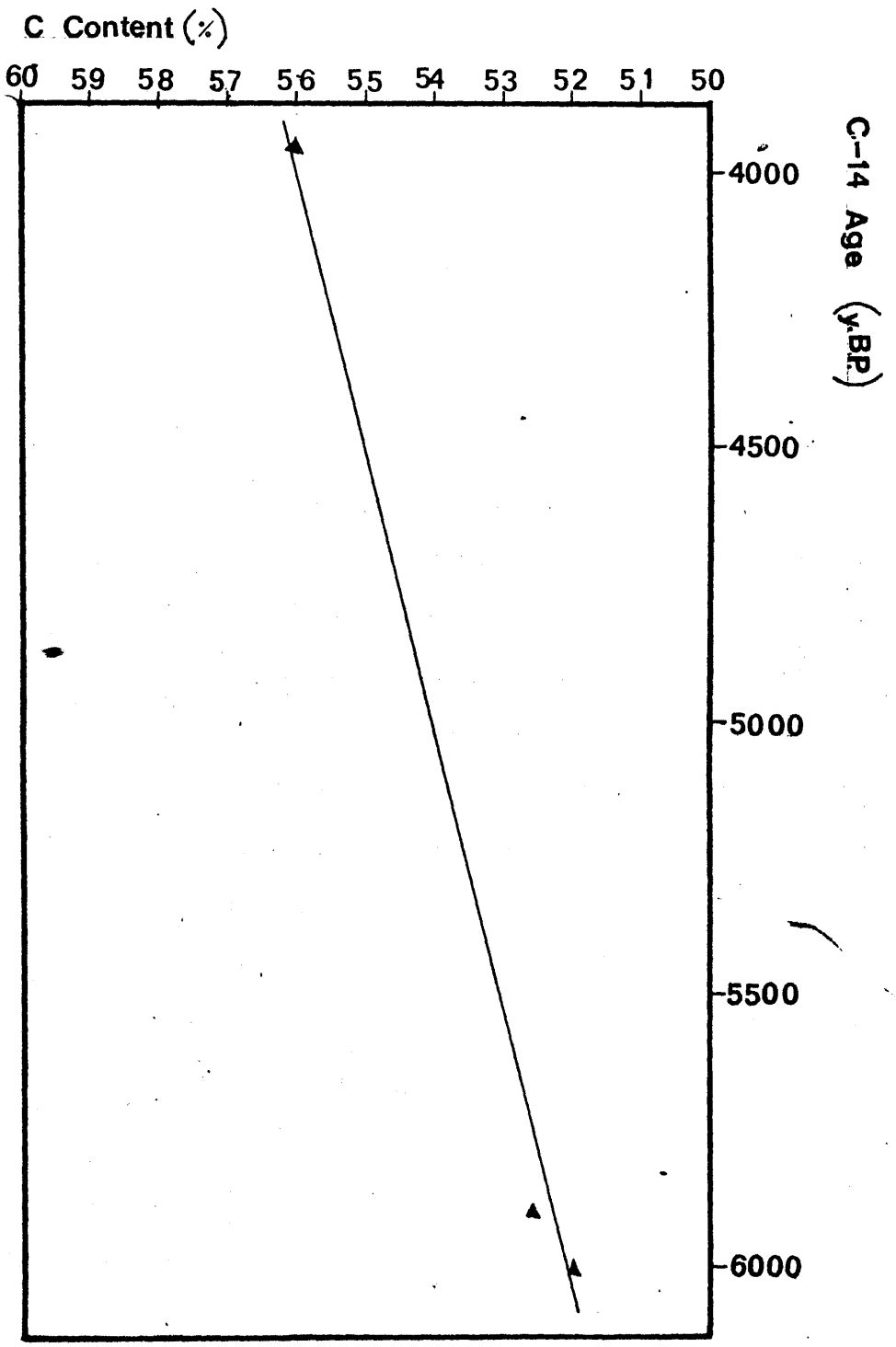

a major characterisitc of the C-14 data that ages for the deeper (pre-industrial) sediment samples are anomalously old. This, as will be discussed, implies a significant natural source of fossil organic carbon in the area. It would therefore be of some value to quantify the total fossil organic carbon "pollution" of the sediments and, if possible, to distinguish recent anthropogenic and natural components of this input. Thus fossil carbon indices have been calculated, based, firstly, on the assumption that "uncontaminated" surface sediment should ideally have the same C-14 activity as the natural atmosphere ($\Delta = 0$) and, secondly, and probably more accurately, on the assumption that such sediments should have an initial activity corresponding to the natural C-14 activity of surface ocean waters ($\Delta = -55$ $^{o}/_{oo}$) (Broecker et al. 1960). These two sets of indices provide an overall assessment of total fossil organic content of the sediments (i.e. both natural and artificial). A third set of indices was then calculated to assess the relative contribution of anthropogenic and natural fossil carbon inputs. Thus if the C-14 dates for depths below 35 cm for Gare Loch and 25 cm for Loch Goil sediments are considered free from the industrial contributions which contaminate the upper sediment layers, an assessment of the natural (but fossil carbon-contaminated) C-14 ages of recent sediments can be made. Extrapolation from 35 cm depth for the Gare Loch sediment core, or simply taking the mean value of C-14 ages below 35 cm, enables a natural surface sediment radiocarbon age of 4710 y B.P. to be estimated (Figure 4.1). This age of surface sediment

cannot be directly measured since it is masked by the anthropogenic effect on the upper recent sediment samples. The sediment surface of core LGG-2 similarly shows a natural radiocarbon age of 1690 y B.P. (Figure 4.2), again by extrapolating from 25 cm sediment depth to the surface. Since these ages are considerably higher than zero, fossil organic carbon of natural origin must be mixed with the sediment. The major fraction of the organic carbon in these sediments originated from two sources, namely primary production and detrital flux. This organic fossil carbon is probably mobilised from glacial marl by erosion of coastal cliffs and coal. The latter detrital flux of fossil carbon is certainly present in the area. Total dissolution of deep sediments by classical strong acid methods is repeatedly unsuccessful, a fine black particulate precipitate remaining. This resistant fraction resembles coal dust and indeed has a carbon content of 60-70%. The Clyde area is well known for its outcrops of coal seams, macroscopic "sea coal" being regularly beached or trawled. It seems reasonable to assume, therefore, that the anomalously high natural C-14 ages for Clyde sediments reflect fossil inputs from such sources.

The calculation of fossil carbon indices was performed via the following equation:

$$\Delta_{obs} = \frac{x}{100} \left(\Delta_{foss.c.}\right) + \frac{100-x}{100} \left(\Delta_{nat.}\right)$$

where x denotes the percentage of fossil carbon in any sample of

measured C-14 content Δ_{obs} ($^{o}/oo$). Δ_{nat} ($^{o}/oo$) is the idealised C-14 content in surface sediments assuming either a) no fossil carbon contribution (i.e. as might be expected in other areas) (Δ = 0 or $-55^{o}/oo$) or alternatively b) that the natural surface age is free from anthropogenic input (i.e. extrapolated from deep layers, Δ variable between lochs). The calculated percentages of fossil carbon for Loch Goil, Gare Loch, Loch Fyne, Loch Etive and Loch Striven in comparison to the three listed natural activity levels ($\Delta_{atm.\ c.}$ = 0, $\Delta_{surf.\ oc.}$ = $-55^{o}/oo$ and $\Delta_{nat.\ sed.}$) are shown in Tables 4.1, 4.2 and 4.3. The data for Loch Fyne, Loch Etive and Loch Striven were obtained by Harkness (1973).

According to these calculations (Tables 4.1, 4.2 and 4.3) Gare Loch shows the highest percentage of fossil carbon with average values GLG (Δ= 0) = 52%, GLG (Δ= $-55^{o}/oo$) = 50% and GLG ($\Delta_{nat.\ sed.}$) = 14%. From these results it is obvious that 36-38% is naturally-derived fossil carbon and only 14% is pollution-derived old carbon. The second loch with high fossil carbon pollution is Loch Fyne with average values LFy (Δ = 0) = 35%, LFy (Δ= $-55^{o}/oo$) = 32% and LFy ($\Delta_{nat.\ sed.}$) = 9.5%; Loch Striven sediments have average values LSt (Δ= 0) = 33%, LSt (Δ= $-55^{o}/oo$) = 29% and LSt ($\Delta_{nat.\ sed.}$) = 8%. Similar anthropogenic pollution ratios i.e. $\frac{1}{3}$ pollution-derived fossil carbon and $\frac{2}{3}$ natural-derived fossil carbon are observed for Gare Loch, Loch Fyne and Loch Striven sediments. Furthermore, Loch Goil with average values

TABLE 4.1 EVALUATION OF FOSSIL CARBON INDICES FOR GARE LOCH, LOCH GOIL, LOCH FYNE, LOCH ETIVE AND LOCH STRIVEN IN COMPARISON TO THE NATURAL C-14 ATMOSPHERIC LEVEL ($\Delta_{nat.} = 0$)

CODE	$\Delta_{obs.}$ (‰)	FOSSIL C INDEX (%)
GLG-2	-524.0	52.40
LGG-1	-374.0	37.40
LGG-2	-340.0	34.00
LGG-3	-251.0	25.10
LF-23B	-281.0	28.10
LF-42	-422.0	42.20
LE-17	-180.0	18.00
LS-7	-333.0	33.30

TABLE 4.2 EVALUATION OF C-14 DEPRESSION FOR THE GARE LOCH , LOCH GOIL , LOCH FYNE , LOCH ETIVE AND LOCH STRIVEN CORES IN COMPARISON TO THE SURFACE OCEAN C-14 NATURAL LEVEL ($\Delta_{nat.}$=-55%)

CODE	$\Delta_{obs.}$(‰)	FOSSIL C INDEX (%)
GLG-2	-524.0	49.63
LGG-1	-374.0	33.75
LGG-2	-340.0	30.16
LGG-3	-251.0	20.74
LF-23B	-281.0	23.92
LF-42	-422.0	38.84
LE-17	-180.0	13.23
LS-7	-333.0	29.42

TABLE 4.3 EVALUATION OF C-14 DEPRESSION IN COMPARISON TO THE ASSUMED NATURAL C-14 LEVELS FOR THE PARTICULAR LOCH WITHIN THE TOP 20 CM DEPTH

CODE	$\Delta_{nat.}$ (°/oo)	$\Delta_{obs.}$ (°/oo)	FOSSIL C INDEX (%)
GLG-2	-447.0	-524.0	14.00
LGG-1	-372.0	-374.0	0.21
LGG-2	-258.0	-340.0	8.70
LGG-3	-196.0	-251.0	5.82
LF-23B	-222.0	-281.0	6.24
LF-42	-303.0	-422.0	12.60
LE-17	-178.0	-180.0	0.21
LS-7	-259.0	-333.0	7.83

LGG ($\Delta = 0$) = 32%, LGG ($\Delta = -55^{o}/oo$) = 28% and LGG ($\Delta_{nat.sed.}$) = 5%, appears less polluted than the three lochs listed above. Indeed, Loch Goil sediments show only 1/5 pollution-derived fossil carbon. The lowest carbonaceous pollution is observed for Loch Etive, the average depressions LEt ($\Delta = 0$) = 18%, LEt ($\Delta = -55^{o}/oo$) = 13% and LEt ($\Delta_{nat. sed.}$) = 0.21% and ~1/60 pollution-derived fossil carbon. As expected, indeed, Gare Loch, which is nearest to the River Clyde, shows in absolute terms the highest fossil carbon pollution. Loch Fyne and Loch Striven have approximately the same fossil carbon indices. Loch Etive which is not connected with the Clyde estuary or with major industrial inputs shows an approximately 2 to 3 times lower natural fossil carbon index and 25 to 60 times lower fossil carbon pollution index relative to the Clyde sea area lochs.

The admixture of fossil carbon should be noticed also in the δC-13 data, with lower values for fossil carbon contaminated samples (the three top layers of the sediments) (for GLG-2: $-29.41^{o}/oo$, LGG-1: $-27.19^{o}/oo$, LGG-2: $-27.63^{o}/oo$ and LGG-3: $-29.48^{o}/oo$) than for more natural sediment (for GLG-2: $-29.09^{o}/oo$, LGG-1: $-26.27^{o}/oo$, LGG-2: $-27.01^{o}/oo$ and LGG-3: $-27.84^{o}/oo$). Such differences result from the greater depletion of C-13 in fossil fuels relative to organic sediments (δC-13 values: marine crude oils: from -20 to $-32^{o}/oo$; organic carbon of marine sediments: $-24.75^{o}/oo$; organic carbon of freshwater sediments: -22.0 to $-28^{o}/oo$) (Craig, 1953). Thus an admixture

of C-14 free material could agree with both the δC-13 and δC-14 results. However, the δC-13 effect is not sensitive to the mixing ratio since the δC-13 difference of the components is small and since the δC-13 data for the sediments show a large spread due to natural fractionation effects (and laboratory pretreatment).

Considerable concentrations of heavy metals, along with fossil fuel carbon are carried by aerosols and organic effluents released by fuel burning and by industry. Thus pure anthropogenic sediment consisting of coal-ash, of aerosol particles (slag) and residues from oil would contain heavy metals in far larger specific concentrations than in natural sediments. Metals such as Cd, Pb, Zn and Cu are mobilised through burning of fossil fuels (coal and oil), with coal the more important source (Erlenkeuser et al., 1973). Leatherland (1977) has shown conclusively that in Clyde estuarine sediments there is an obvious correlation of trace metals with organic carbon content.

Unfortunately, only one core, Loch Goil core LGG-3, has so far been fully analysed for metals. Thus from the micro-analytical data for Loch Goil core LGG-3, shown in Table 3.7, it is obvious that Fe and Al concentrations do not vary considerably with depth in the sediment. The concentrations of Fe and Al throughout the core are much higher than for Pb and Cr, reflecting the fact that the former pair occur naturally in sediments through mobilisation from rock weathering, soil erosion and

rainfall. Stable lead, a good indicator of industrial induced pollution into sediments, shows constant levels (0.04%) below the sediment surface until concentrations increase (0.7%) in the 20 to 30 cm interval. This observation is in agreement with the 25 cm natural/industrial transition observed in the C-14 data and confirms the onset of major pollution in the area at ~200 years ago. In addition, recent data obtained by Farmer (1977) have shown that stable lead starts increasing towards the surface at 25 cm sediment depth for a Loch Goil core LGG-5. Surface concentrations of stable lead are ~420 ppm, while below 25 cm depth lead concentrations are almost constant around 20 ppm. For Gare Loch core GLG-1, however, constant concentrations of stable lead (~500 ppm) through the entire length (35cm) of the core have been observed. A longer core is therefore required to determine if C-14 and metal profiles are mutually consistent with the 35 cm industrial/natural boundary implied by C-14 alone. The concentrations of Cr are essentially constant with depth in the LGG-3 core (Table 3.7).

4.2 Loch Lomond sediments.

The sediment accumulation rate in Loch Lomond was determined by plotting the radiocarbon ages of various levels in the core against depth (Figure 4.8). The radiocarbon age calculation was again based on the Libby half-life, 5570 ± 30 y B.P. The error bars in Figure 4.8 have the same significance as those in the Clyde sediment plots. Zero on

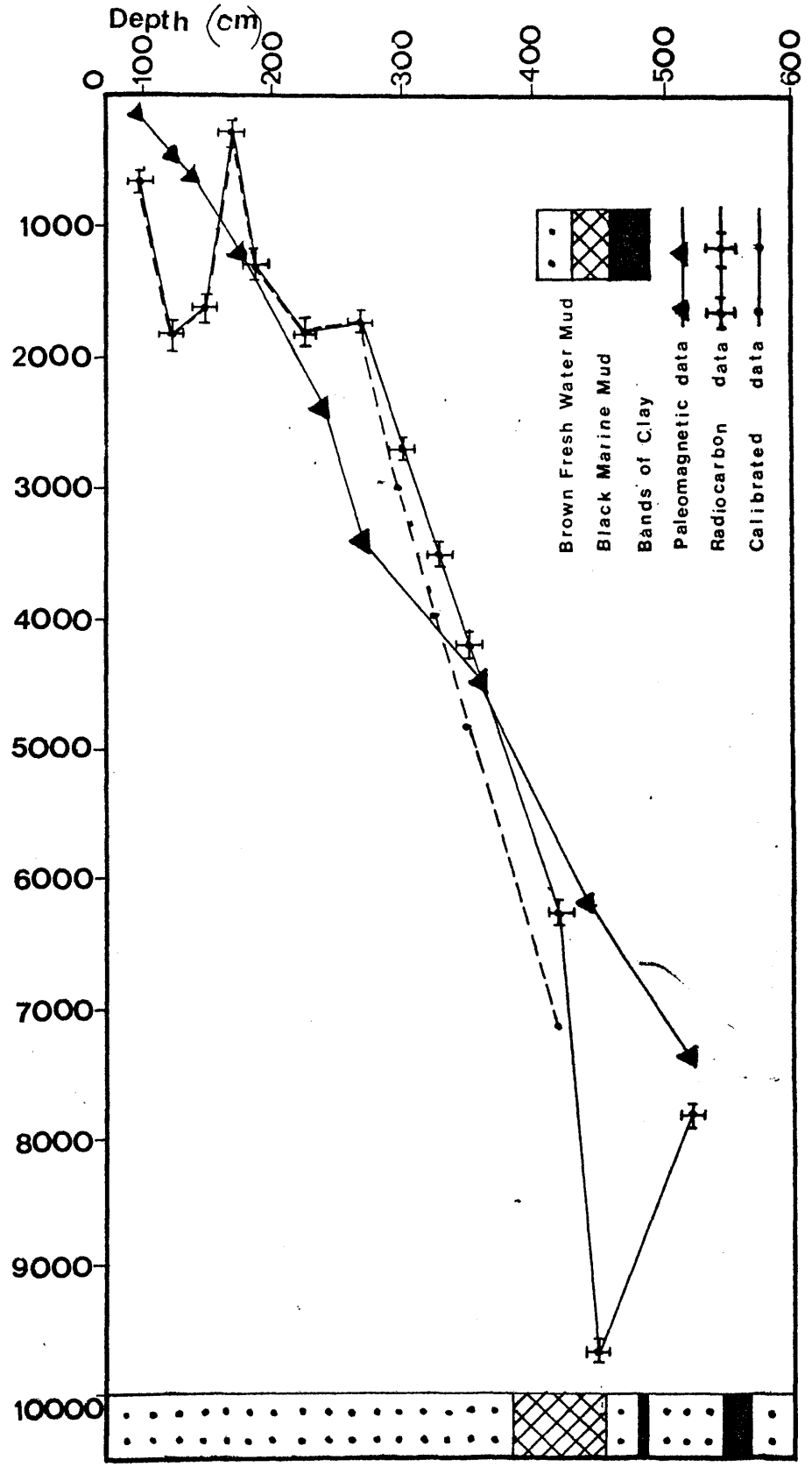

Fig. 4.8 Radiocarbon Age, Calendar Age and Paleomagnetic Age Vs Depth
Age (y)

the depth axis corresponds to the top of the plastic core liner and not to the sediment/water interface. This system was employed by all collaborating laboratories to ensure a consistent treatment. The sediment surface in fact lies at 80 cm depth on this scale. Thus first sample for C-14 dating which was collected at 95-105 cm depth actually lies 15 to 25 cm below the sediment surface.

On the left of the diagram a preliminary stratigraphy of the sediment core is presented. Well differentiated layers of variable colour and consistency were clearly apparent. A major observation here is conclusive evidence of marine incursion into Loch Lomond, as indicated by marine muds between 385 and 455 cm. These contain dinoflagellate and shell remains. Accurate dating of this event is obviously of considerable interest. Above and below the zone of marine muds there are brown fresh water muds, interrupted by two thin layers of grey clay, the first 2 cm thick at 470 cm and the second 24 cm thick at 550 cm depth. The brown colour of the sediment is presumably imparted by its humic components. In the zone of marine muds the colour changes to black, with a corresponding increase in water content and a visible change to wetter and less firm material. Organic carbon content is an additional and useful indicator of humus accumulation and soil biological activity. The carbon and nitrogen concentrations vs. sediment depth are shown in Figure 4.9. According to the diagram maximum carbon and nitrogen levels are recorded within the depth

Fig. 4.9 Carbon Plus Nitrogen Content Vs Depth. ($LLRD_1$)

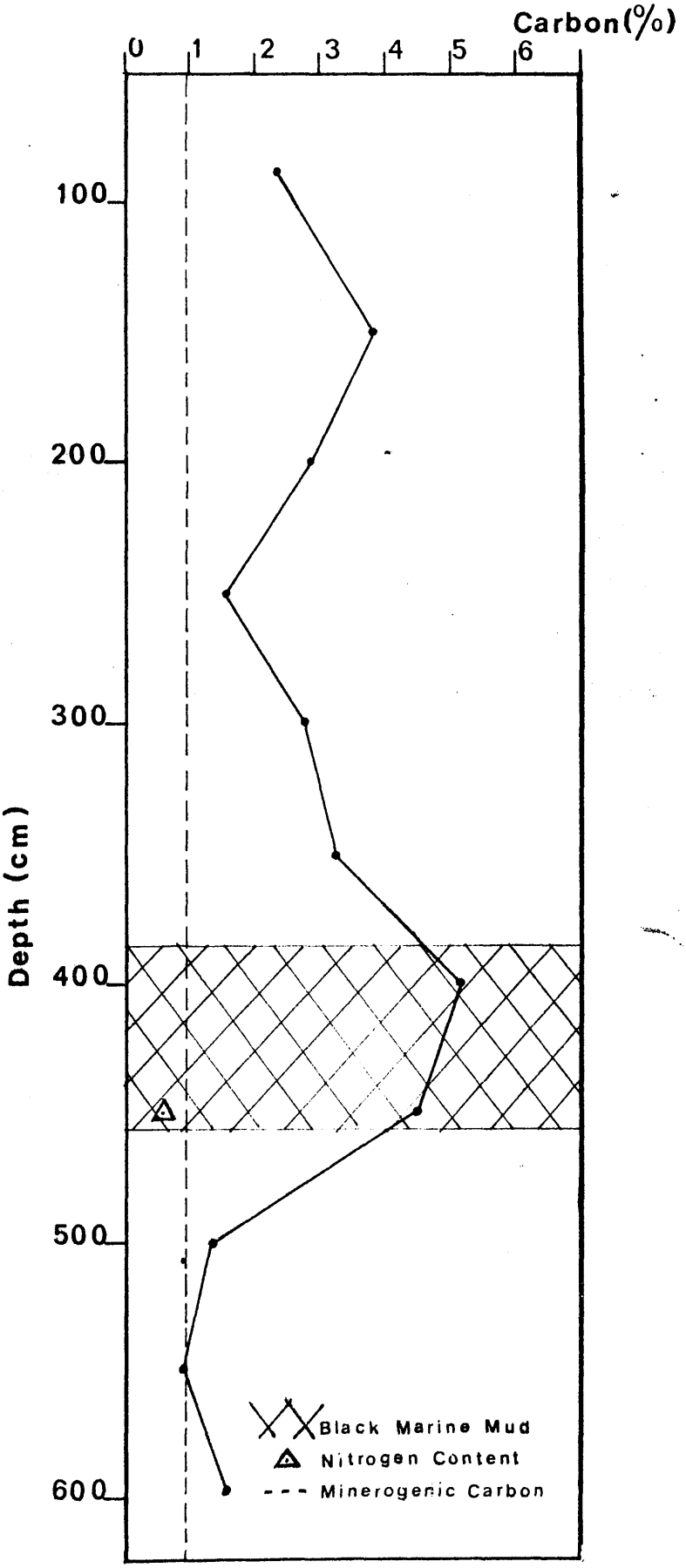

interval 385 to 455 cm i.e. in the zone of marine muds. Indeed, these levels approach carbon and nitorgen concentrations recorded for the sea water lochs (Gare Loch and Loch Goil). Presumably the marine transgression stage of Loch Lomond transformed it to a system extremely similar to these present sea lochs. In the zone of fresh water muds there are smaller variations in carbon content with depth, while nitrogen levels at other depths lie below detectable limits (Figure 4.9). The baseline carbon content of 0.95% within the grey clay band probably indicates inorganic (minerogenic) carbon concentration.

From the overall non-linearity of the C-14/depth plot (Figure 4.8), fluctuations in sedimentation rate appear to have occurred from time to time. Table 4.4 lists a) conventional C-14 ages, b) those based on the half-life value 5730 ± 40 y B.P., c) corrected (calendar) ages calculated via the correction curve of Ralph et al (1973) d) paleomagnetic age data. Furthermore, corrected (calendar) ages and paleomagnetic ages are plotted in the diagram (Figure 4.8). Since any reasonable correction of radiocarbon ages does not remove non-linearity from the age/depth plot the deviations cannot be attributed to past fluctuations of atmospheric C-14 in the atmosphere. A more reasonable hypothesis is therefore that the C-14 results reflect a pattern of disturbances in the orderly transfer of "stable organic residues" (Mackereth, 1966) from catchment soils to sediments by erosion, consequent on marine incursion, deforestation and agricultural development in the area.

TABLE 4.4 TIMESCALE FOR LOCH LOMOND SEDIMENTS

DEPTH (CM)	5570($T_{\frac{1}{2}}$)	5730($T_{\frac{1}{2}}$)	CALIB. AGE (Y)	PALEOMAG AGE (Y)
100	643±52(1307 AD)	662±54(1288 AD)	665	150
125	1894±68(56 AD)	1954±70(1 BC)	1880	450
140				600
150	1627±51(323 AD)	1676±53(274 AD)	1600	
170	231±55(1719 AD)	238±57(1712 AD)	255	
175				1200
188	1373±57(577 AD)	1414±59(536 AD)	1345	
225	1832±59(112 AD)	1893±61(57 AD)	1825	
240				2400

270	1730±59(220 AD)	1782±61(168 AD)	1715	3400
299	2791±67(841 BC)	2875±69(925 BC)	2960	
325	3542±65(592 BC)	3648±57(1698 BC)	3980	
350	4205±59(2255 BC)	4331±61(2381 BC)	4860	
360				4500
420	6293±102(4343 BC)	6482±105(4532 BC)	7150	
440				6200
450	9694±156(7744 BC)	9985±161(8035 BC)		
500				7400
520	7927±127(5977 BC)	8165±131(6215 BC)		

The first deviation from linearity appears to be at 450 cm depth. This point corresponds to the core section where black marine muds are recorded (Figure 4.8). The second deviation from linearity is observed at 270 cm depth. As already shown, an increase of C-14 age is in general caused by introduction of fossil or at least "old" organic carbon into the sediments. In this case, however, both data points (270 cm and 225 cm depth) correspond to uniform stratigraphy of the core i.e. to the section of brown fresh water muds. Therefore, this deviation is not associated with marine incursion into the loch but must be attributed to increased erosion of soil carbon in the catchment. Between 420 cm and 270 cm, perfect linearity is recorded. Two further deviations from the linear sedimentary trend are observed at 170 cm and 125 cm depth. These deviations, again caused by enrichment of sediments by soils introduced by erosion of catchment soil can be fully confirmed by pollen analysis as shown later.

The paleomagnetic ages (also listed in Table 4.4 and plotted in Figure 4.8) are based on observatory records (declination at 100 cm depth), on archaeomagnetic curves (declinations at 125 cm and 140 cm depth) and on Lake District paleomagnetic calibration curves (declinations at 175, 240, 270, 360, 440 and 500 cm sediment depth) (Thompson, 1977). Significant discrepancy between radiocarbon and paleomagnetic data, especially for the upper 200 cm depth interval is evident. It is certain that the prime reason for the surface discrepancies is the artificial depression of radiocarbon ages by man-induced

modifications of agricultrual and erosion patterns in the area with corresponding increases in "old" carbonaceous soils. Between 150 and 240 cm depth a massive increase in soil input is evident and, since there is no possible mechanism for producing an anomalously young age for the 170 cm sample, it must be deduced that this extensive input occurred since ~230 years ago. Therefore it is reasonable to postulate an agriculturally related perturbation in the 270 to 225 cm depth increment followed by a restabilisation from 190 to 170 cm, the latter depth corresponding to an age of 230 years. Above this, marked C-14 depression occurs presumably through massive agricultural/industrial fossil carbon inputs with slight recovery at 100 cm depth. The paleomagnetic age for this level, based on the 175 cm easterly maximum declination drift (D, Figure 4.10), is 1200 years. Below 200 cm in the core paleomagnetic ages based on declination turning points continue to deviate from the C-14 record as shown in Figure 4.8 and Table 4.4. The relative trends at depth, however, are similar.

Figure 4.10 also plots paleomagentic intensity and susceptibility against sediment depth. However, intensity as a paleomagnetic parameter is not primarily related to the past intensity of the geomagnetic field but is controlled by the physico-chemical environmental conditions in which the magnetic grains were deposited. It has been observed that some recent sediments have not retained a stable magnetic remanence formed

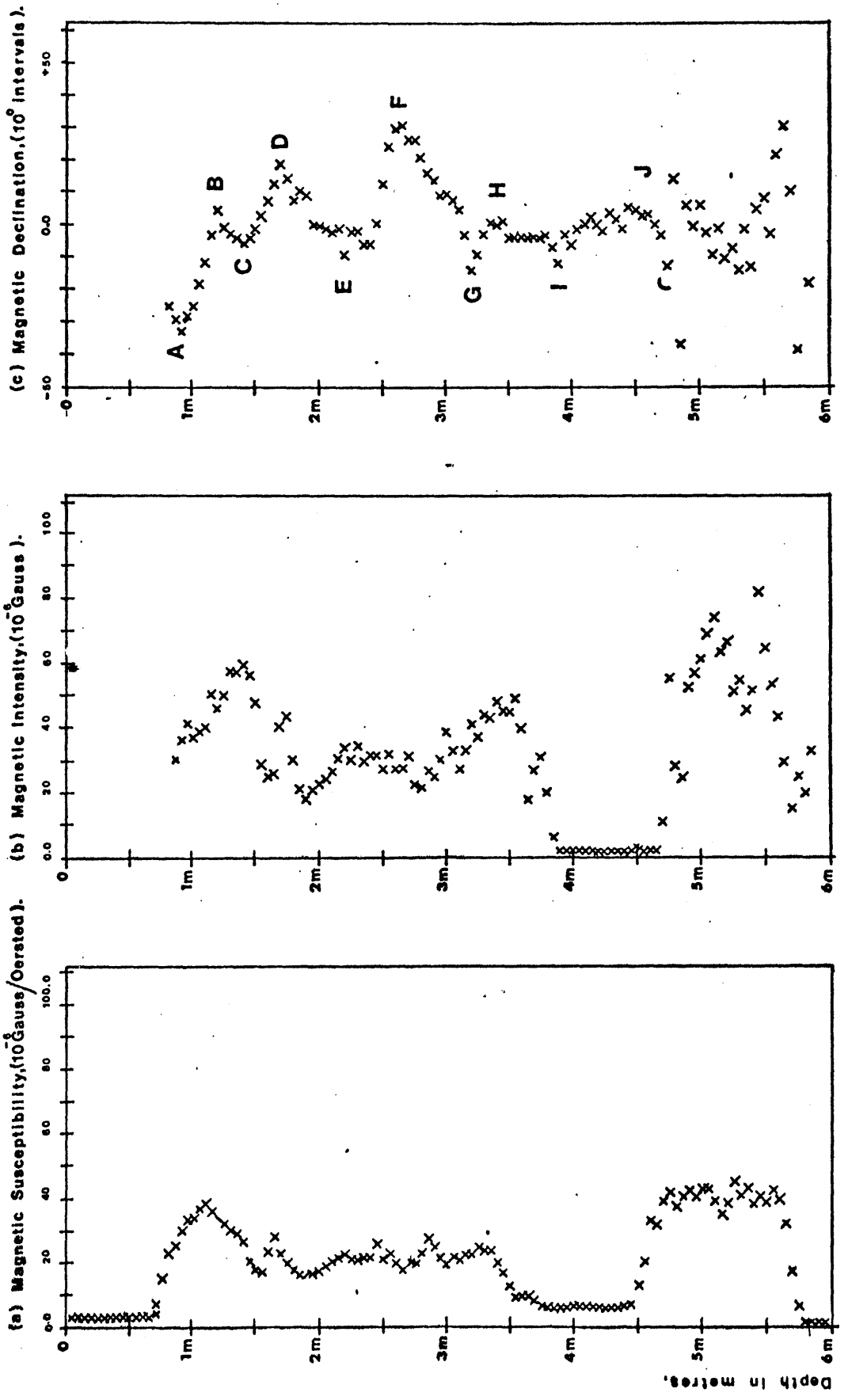

Fig. 4.10
Palaeomagnetic Records for Loch Lomond Sediment Core (LLRD$_1$).

in the geomagnetic field direction at the time of deposition (Thompson, 1977). It is difficult to date sediments in which the rate of sedimentation changed considerably and frequently. Geomagnetic secular direction changes, however, cover a wide frequency spectrum and different parts of the spectrum will dominate the geomagnetic parameter recorded in sediments of different deposition rates. When the remanence is of a chemical origin, smoothing of geomagnetic fluctuations occurs. Thus only with correctly defined sedimentation rates can confusion of various geomagnetic oscillations, with similar amplitudes and periods, be avoided. Magnetic susceptibility (Figure 4.10) peaks, however, are obtained at 270, 170 and 125 cm depth. The higher proportions of detrital magnetic minerals in sediments correspond to higher susceptibilities. Thus suceptibility data are in accord with the radiocarbon results, each susceptibility maximum corresponding to a radiocarbon deviation from the linear sedimentary trend. Magnetic susceptibility is, therefore, a useful indicator of changes in surrounding land-use for agricultural purposes reflecting varying inwash of particulate material and clay minerals.

Through the radiocarbon data points three best fitting straight lines have been drawn by computer in an attempt to define natural sedimentation rates in the lochs (Figure 4.11). Thus, consideration of the total number of data points (13) yields a mean sedimentation rate of 0.5 mm y^{-1} (Figure 4.11, line $y_{13} = 0.05x + 115$ where x represents C-14 age years and y depth in cm). Rejection of the three topmost points of the

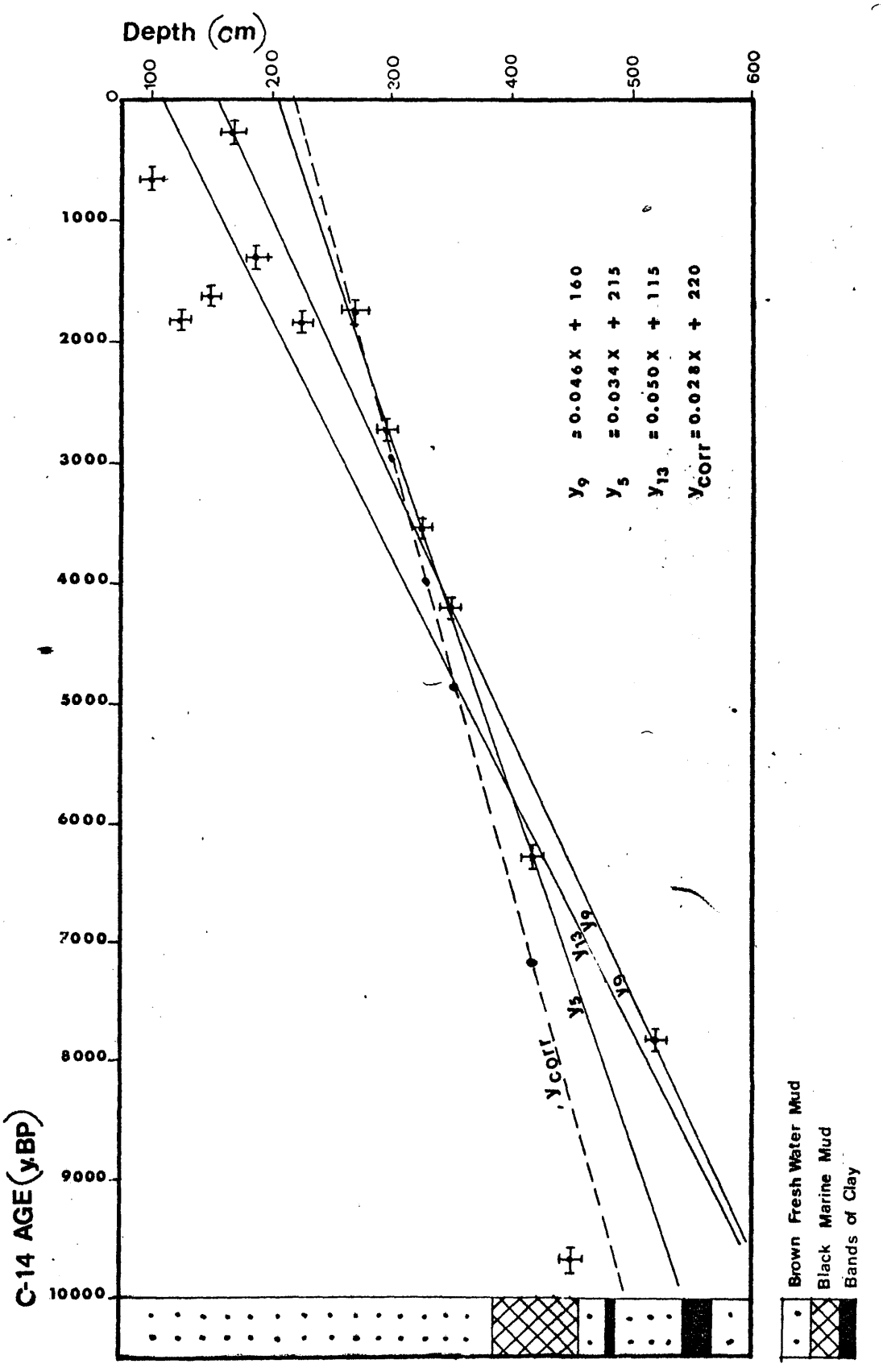

Fig 4·11 Radiocarbon Age Vs Depth For Loch Lomond Core ($LLRD_1$)

sediment core (i.e. those most influenced by anthropogenic effects) and of the deviant point at 450 cm depth (presumably influenced by fossil carbon inwash during the main phase) gives a sedimentation rate of 0.46 mm y^{-1} (Figure 4.11, line $y_9 = 0.046X + 160$). By including only the five data points within the intermediate section of perfect linearity a sedimentation rate of 0.34 mm y^{-1} is obtained (Figure 4.11, line $y_5 = 0.034X + 215$). Finally the best fitting line through the same five but calibrated data points yields a sedimentation rate of 0.28 mm y^{-1} (Figure 4.11 dotted line $y_{corr.} = 0.028X + 220$). The differences between these various estimates of sedimentation rate are relatively minor and should perhaps be considered a normal margin of error for this study. It can be concluded therefore that the natural sedimentation rate for Loch Lomond falls in the range 0.40 ± 0.12 mm y^{-1}. An independent though partial timescale derives from the pollen data, the main markers here being the alder rise ($\sim$6100 to 6300 y B.P.) and elm decline ($\sim$5100 y B.P.) established by pollen spore spectra analyses. According to these data (Table 4.5) the alder rise is recorded at 435 cm depth and the elm decline between 380 — 385 cm. Since the accepted pollen ages are based on conventional radiocarbon dates from other samples and locations, it is necessary to consider uncalibrated data for Loch Lomond only. Best agreement is observed using the $y_9 = 0.046X + 160$ line with values of 6050 y B.P. and 5000 y B.P. for the alder rise and elm decline

TABLE 4.5 POLLEN DATA

DEPTH(CM)	C-14 AGE (YR. B.P.)	TYPE AND PERCENTAGE OF TOTAL POLLEN
435 - 385	6050	ALDER,RISE FROM 2 TO 15
		PINE,DECLINE TO 2
		BIRCH,MAX.VALUE, 16
		OAK,MAX.VALUE, 19
		HAZEL,MAX.VALUE, 40
	6500-4950	MARINE DINOFLAGELLATES
	5000	ELM,DECLINE, FROM 7 TO 1
380 - 260	5000	ELM,DECLINE TO 0
	4750	OAK,SPREADS
	4400	PLANTAGO LANCEOLATA, TRACES
	4200	PINE,RISES TO 11
	3100	PTERDIUM,MAX.VALUE, 20
260- 80		GRAMINEAE,RISES FROM 10 TO 20
		CALLUNA,RISES FROM TRACES TO 12
		PTERIDOPHYTES,RISE
		BIRCH,DECLINE FROM 12 TO 7
		PINE,TRACES
		OAK,DECLINE FROM 10 TO 1
80		PINE,OAK,RISE TO 5

respectively. Thus pollen dates and radiocarbon dates appear to be in accord. From the paleomagnetic data (Table 4.4 and Figure 4.8) the following estimates of sedimentation rate have been made: a) 2 mm y^{-1} to 100 cm sediment depth, b) 1 mm y^{-1} between 100 and 150 cm depth and c) 0.52 mm y^{-1} below 150 cm depth (Thompson, 1977A). The upper 150 cm show increased sedimentation rates presumably reflecting anthropogenic effects. In addition to the long core discussed this far, a one metre long "mini" Mackereth corer (1969) was used to collect the uppermost sediments. This "mini" core collected from the same site as core $LLRD_1$ was analysed for lead-210 and caesium-137 isotopes. Thus, the recent sedimentation rate in the loch, derived by the Pb-210 method for the upper 30 cm sediment depth was 0.7 mm y^{-1} (Swan, 1977). Figure 4.12 plots Cs-137 concentrations vs depth (McKinley, 1977). Unlike the marine system of the Clyde area, the Loch Lomond freshwater catchment has only one source of radiocaesium, namely from nuclear weapons testing which produced maximum fallout around 14 years ago. Assuming that the topmost sediments were sampled and preserved undisturbed, Cs-137 levels are almost constant to 2 cm depth, indicating fairly efficient mixing of surface sediments (Figure 4.12). At 3 cm depth, Cs-137 concentrations decrease rapidly so that, below 6-7 cm, levels lie beneath detectable limits. It is believed that radiocaesium from 3 cm to 6 cm depth is transferred by diffusion. Assuming that 14 years ago bomb Cs-137 was introduced into the

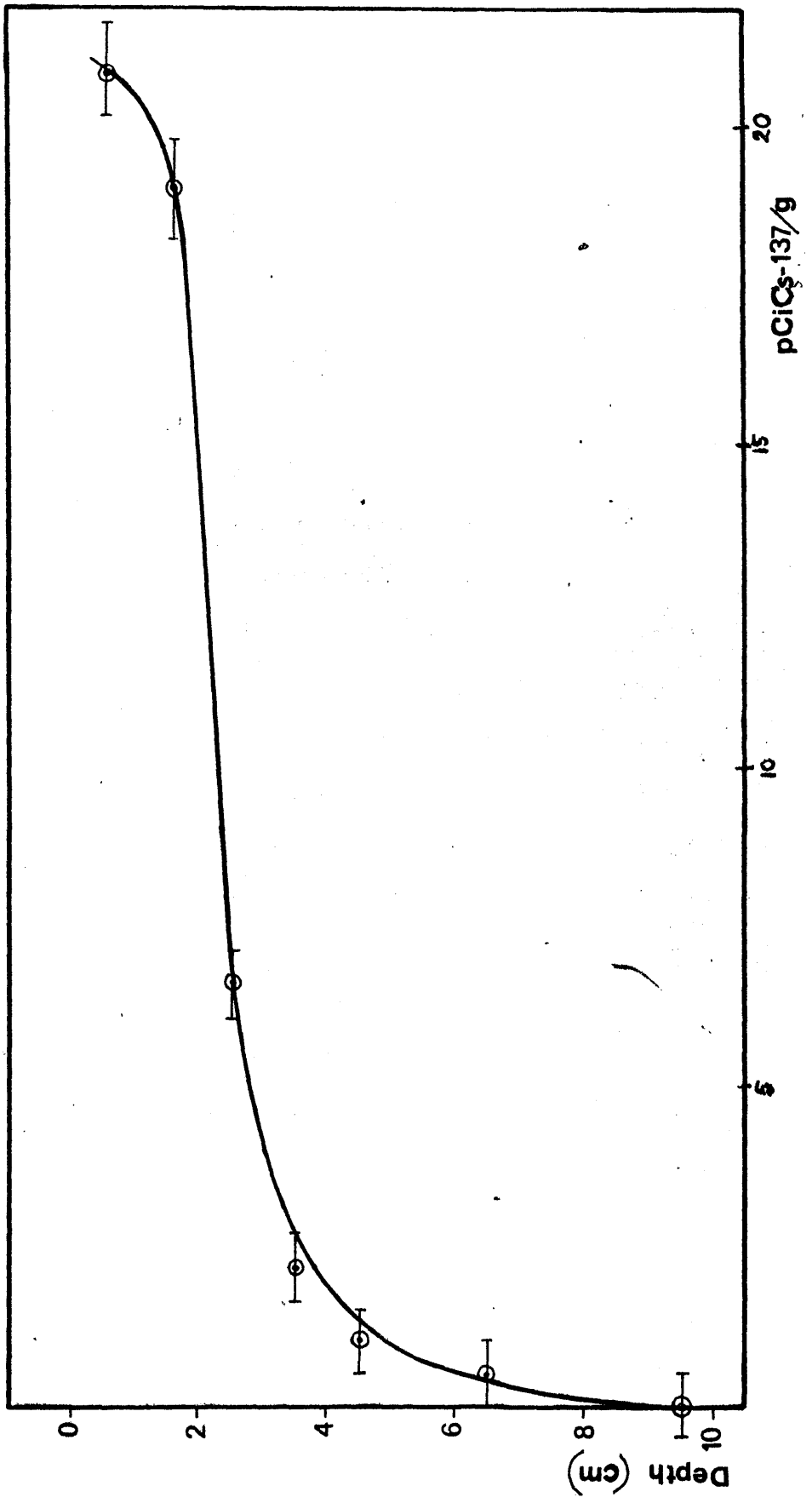

Fig. 4.12 LLRP Core:Cs-137 Concentrations Vs Depth

upper sediments and then carried by pronounced mixing to 2 cm depth in the mixed layer an approximate estimate of accumulation rate for the uppermost sediments would be 0.5 mm y^{-1}, in good agreement with Pb-210 but again quite inconsistent with paleomagentic data. However, the evidence from radiocaesium of the existence of a 2 cm mixed layer can perhaps explain the discrepancy between paleomagentic and radiocarbon dates. It is necessary that grains carrying their paleomagnetic marker, while precipitating through the water column, preserve their original orientation. It is conceivable that rapid surface mixing of sediments tends to randomise orientations producing erroneous date. Another possible explanation of the discrepancy is that a hard water effect exists either in Loch Lomond or in the Lake District loch on which the paleomagentic data are primarily based. Thus if higher concentrations of fossil carbonates exist in one or the other, systematically older C-14 ages will result. This possibility highlights the fact that C-14 ages of sediments are best regarded as relative rather than absolute ages such are the uncertainties i.e. C-14 input and the "open" chemical nature of the systems involved.

As mentioned earlier, the same Loch Lomond core ($LLRD_1$) was analysed for pollen spore spectra (Stewart, 1977). The pollen data divided into three zones are presented in Table 4.5 and show a clear relationship between sediment composition and environmental changes in the catchment. Thus the first pollen zone is defined by the alder rise (at 435 cm sediment depth)

which is generally attributed a C-14 age, as already mentioned, of 6100 to 6300 y B.P., in accord with the observed date in this study of ~ 6050 y B.P. Secondly, the elm decline (at 380-385 cm depth) has a C-14 age here of 5000 y B.P., again in agreement with the classical pollen date of ~5100 y B.P. Within the same pollen zone a pine decline is recorded reflecting a change to wetter climate, while birch, oak and hazel spores reach their maximum values. The presence of marine dinoflagellates in this zone (in the 385 to 455 cm increment) proves that marine incursion into Loch Lomond occurred. This event can thus be dated. Marine incursion therefore began at ~ 6500 y B.P. and ended shortly after the elm decline at 4950 y B.P. This timescale agrees well with accepted theory of sea -level variations with maximum sea-level in this area occurring around 3000-4000 y B.C (Heyworth, 1977). The second pollen zone starts with the elm decline (at 380-385 cm sediment depth). The elm decline phenomenon is generally interpreted as being indicative of anthropogenic deforestation episodes and also of climate disturbances which modify the erosion rate of the catchment either directly or through changes in vegetation. This pollen zone also contains Plantago lanceolata and Pterdium pollen spores, both indicative of these effects. Throughout the third pollen zone (Table 4.5) an increase of grass and Calluna pollen spores is recorded. These are undoubtedly indicative of anthropogenic deforestation, since these species are more desirable plants for grazing animals.

Therefore, both C-14 and pollen methods indicate man-induced changes in sediment composition for any deforestation inevitably increases soil erosion and introduces "old" soil carbon inwash to the loch and its sediments. Thus the deviations in C-14 age/depth profile which occur, particularly at 170 cm and perhaps also at 225 to 270 cm are almost certainly the effect of agricultural modifications in the catchment area. These depth intervals are indeed associated with enhanced grass and Calluna pollen levels and with magnetic susceptibility maxima, both these being indicators of agricultural change. The most noticeable deviant point in the C-14 age/depth profile is perhaps that at 450 cm depth within the marine incursion layer. It is probable that the anomalously old age of this sample can be explained in exactly the same manner as the "old" C-14 ages observed in natural marine sediments from the Clyde sea lochs. These were previously attributed to a natural fossil carbon source in the Clyde catchment area and it seems reasonable to assume that, in tis marine phase, Loch Lomond was an extremely similar system to the present Clyde sea lochs with a similar depression of C-14 levels resulting from natural fossil carbon inwash via Clyde/Leven valley. After the marine stage, sedimentation and C-14 levels restabilised to produce a natural fresh water equilibrium system which remained undisturbed until the effects of man disrupted it. This latter perturbation, according to the C-14 record, occurred shortly after 230 years ago when there was a major input of

"old" soil-derived organic carbon which introduced the majority of the overlying sediment in a very short time interval. Such an extensive and short-term input of soil has been observed frequently elsewhere. For example, Pennington et al. (1976) have observed a single event input of more than 50 cm of Lake District sediments and quote Likens et al. (1969) who showed that deforestation and ploughing in an experimental catchment area increased stream flow by 39% and suspended particulate matter by 400%. The uppermost sediment levels indicate a trend towards a restabilisation of sediment input with, according to Pb-210 data, a recent sedimentation rate of 0.7 mm y^{-1} compared to the natural level of around 0.4 mm y^{-1}.

APPENDIX 1. LINEAR REGRESSION ANALYSIS.

```
C     THIS PROGRAMME IS A LINEAR LEAST SQUARES REGRESSION FIT WITH A
C     CONFIDENCE INTERVAL ESTIMATE FOR THE LINE AS A WHOLE USING THE
C     METHODS AS DESCRIBED IN THE NBS SPECIAL PUBLICATION 300 VI
C     "PRECISION, MEASURMENT AND CALIBRATION". THE CONFIDENCE INTERVAL
C     ESTIMATE (+ OR -W) IS NORMALLY TAKEN TO BE 95% (2 SIGMA) AND IS
C     DETERMINED BY THE F VALUE SUPPLIED WITH EACH DATA SET, WHICH
C     ITSELF IS DETERMINED BY THE NUMBER OF (X,Y) DATA POINTS (N), WHERE
C     F(2,N-2) IS THE VALUE SELECTED FROM THE F TABLE.
C     THIS WILL PRINT OUT, IN COLUMNS, X OBSERVED, Y OBSERVED Y
C     CALCULATED, THE DEVIATION, THE ERROR ON THE LINE (W) AND THE DATE
C     OF THE DATA POINT WHICH IS CALLED "IDENT" AND IS ENTERED IN
C     COLUMNS 73-80
C
      DIMENSION DEV(200)
      COMMON /PLT PGM/X(200), Y(200), YC(200), W(200), E(200),
     1TITLE(20), B0,B1,N,XMA,XMIN, WU(200), WL(200),YMIN,YMAX
      INTEGER P
    1 READ(5,5)  (TITLE(I),I=1,20)
      WRITE(6,5)  (TITLE(I),I=1,20)
    5 FORMAT(20A4)
      READ(5,7) N, F
    7 FORMAT(I3,F10.0)
      READ(5,10) (X(I), Y(I), E(I), I=1,N)
   10 FORMAT(3F10.0)
      SX=0
      SY=0
      SXY=0
      SXSY=0
      SX2=0
      SY2=0
      DO 20 I=1,N
      XI=X(I)
      YI=Y(I)
      SX=SX+XI
      SY=SY+YI
      SXY=SXY+XI*YI
      SX2=SX2+XI*XI
      SY2=SY2+YI*YI
   20 CONTINUE
      AVE X=SX/N
      AVE Y=SY/N
      SXSY=SX*SY
      SSXY=SXY-SXSY/N
      SSX2=(SX*SX)/N
      SXX=SX2-SSX2
      SSY2=(SY*SY)/N
      SYY=SY2-SSY2
      B1=SSXY/SXX
      B0=AVE Y-B1*AVE X
```

```
      SXY2SX=(SSXY*SSXY)/SXX
      S2Y=(SYY-SXY2SX)/(N-2)
      SSY=SQRT(S2Y)
      RMS ERR=SQRT((SY2-SY*B0-SXY*B1)/(N-2))
C     ESTIMATED VARIANCE ON SLOPE
      S2B1=S2Y/SXX
C     ESTIMATED VARIANCE OF THE INTERCEPT
      AN=N
      S2B0=S2Y*((1/AN+(AVE X*AVE X))/(SXX))
      XY=0.0
      VX=0.0
      VY=0.0
      DO 30 I=1,N
      XI=X(I)
      YI=Y(I)
      VX=VX+(XI-AVE X)*(XI-AVE X)
      VY=VY+(YI-AVE Y)*(YI-AVE Y)
      XY=XY+(XI-AVE X)*(YI-AVE Y)
   30 CONTINUE
      CC=(XY)/(SQRT(VX*VY))
      DO 40 I=1,N
      XI=X(I)
      YC(I)=AVE Y+B1*(XI-AVE X)
      W(I)=SQRT((1/AN+((XI-AVE X)**2)/(SXX))))*SSY*(SQRT(2*F))
      DEV(I)=Y(I)-YC(I)
   40 CONTINUE
      WRITE(6,60) (X(I), Y(I), YC(I), DEV(I), W(I), E(I), I=1,N)
   60 FORMAT('1',9X,'X OBS',17X,'Y OBS',15X,'Y CALC',11X,'DEVIATION',9X,
     1'ERROR ON LINE',9X,'ERROR ON POINT'//(' ',6E20.8))
      WRITE(6,50) B1, S2B1,B0,S2B0,RMS ERR
   50 FORMAT(///,' SLOPE=',E15.8,5X,' ESTIMATED VARIANCE OF THE SLOPE=',
     1E15.8,/' INTERCEPT=',E15.8,5X,' ESTIMATED VARIANCE OF THE
     2INTERCEPT=',E15.8,/' RMS ERROR=',E15.8)
      WRITE(6,55) SX2,SX,SXY,N,SY,SY2,AVE X,AVE Y,F
   55 FORMAT(///,' LEAST SQUARES TOTALS   X2   X   XY   N   Y   Y2'//,
     1' SUM X2 =',E15.8,/' SUM X=',E15.8,/' SUM XY =',E15.8,/' N =',I4/
     2 ' SUM Y =',E15.8,/' SUM Y2 =',E15.8,//'AVE X=',E15.8,/' AVE Y=',
     3E15.8,//' F VALUE FOR 95% CONFIDENCE INTERVAL,    F(2,N-2)=',F5.2)
      WRITE(6,56) CC
   56 FORMAT(/,' CORRELATION COEFFICIENT=',F6.3)
C     IF ANOTHER SET OF DATA IS TO FOLLOW PUNCH 1 OTHERWISE 0
      READ(5,70) P
   70 FORMAT(I1)
      IF (P.EQ.1) GO TO 1
      STOP
      END
```

APPENDIX 2. MULTIPLE (TRIGONOMETRIC) REGRESSION ANALYSIS

```
STATISTICAL PACKAGE FOR THE SOCIAL SCIENCES SPSSH - VERSION 6.02

SPACE ALLOCATION FOR THIS RUN ..

   TOTAL AMOUNT REQUESTED                          22000 BYTES

   DEFAULT TRANSPACE ALLOCATION                     2748 BYTES

     MAX NO OF TRANSFORMATIONS PERMITTED    27
     MAX NO OF RECODE VALUES                108
     MAX NO OF ARITH.OR LOG.OPERATIONS      216

   RESULTING WORKSPACE ALLOCATION .                19252 BYTES

     RUN NAME           REGRESSION FOR CARBON VALUES
     VARIABLE LIST      TIME, CARBON
     INPUT MEDIUM       CARD
     INPUT FORMAT       FIXED (F12.6, F12.6)

   ACCORDING TO YOUR INPUT FORMAT, VARIABLES ARE TO BE
   READ AS FOLLOWS

   VARIABLE    FORMAT    RECORD    COLUMNS

   TIME        F12.6     1          1- 12
   CARBON      F12.6     1         13- 24

THE INPUT FORMAT PROVIDES FOR 2 VARIABLES.  2 WILL BE READ
IT PROVIDES FOR 1 RECORDS ('CARDS') PER CASE.  A MAXIMUM OF
24 'COLUMNS' ARE USED ON A RECORD.

   N OF CASES      25
   COMPUTE         SINT=SIN(0.6283*TIME)
   COMPUTE         COST=COS(0.6283*TIME)
   REGRESSION      VARIABLES=CARBON,SINT,COST,TIME/
                   REGRESSION=CARBON WITH SINT,COST,TIME(2)
                   RESID=0
   STATISTICS      ALL

REGRESSION PROBLEM REQUIRES  512 BYTES WORKSPACE, NOT
INCLUDING RESIDUALS

   READ INPUT DATA
```

REFERENCES

Alekseev, V.A., Lavrukhina, A.K., Milinkova, Z.K., Smirnov, T.V. and Sulerzhitsky, L.D., 1974, 5th National Proceeding of Meeting on "Astrophysical phenomena and radiocarbon", Tbilisy, 47.

Anderson, E.C., Libby, W.F., Weinhouse, S., Reid, A.F., Kirschenbaum, A.D. and Grosse, A.V., 1974, Phys. Rev., 72, 931; or Science 105, 576.

Averdieck, F.R., Erlenkeuser, H., and Willkomm, H., 1972, Schriften Naturw. Ver. Schleswig-Holstein, 42, 47.

Baxter, M.S., 1969, Ph.D. thesis, University of Glasgow.

Baxter, M.S. and Walton, A., 1970, Proc. Roy. Soc. Lond. A 318, 213.

Baxter, M.S. and Walton, A., 1971, Proc. Roy. Soc. Lond. A 321, 105.

Baxter, M.S., 1974, Nature, 249, 93.

Baxter, M.S. and Harkness, D.D., 1975, Proc. I.A.E.A. and FAO Conf. "Isotope ratios as pollutant source and behaviour indicators", 135.

Becker, B., 1975, unpublished manuscript.

Berger, R., 1970, Phil. Trans. Roy. Soc. Lond. A269, 23.

Bolin, B. and Bischof, W., 1970, Tellus, 22, 431.

Bortleson, G.C. and Lee, G.F., 1972, Environ. Sci. Technol., 6, 799.

Brannon, H.R., Daughtry, A.C., Perry, D., Whitaker, W.W. and Williams, M., 1957, Trans. Am. Geophys. Union, 38, 643.

Bray, J.R., 1965, Nature, 205, 440.

Bray, J.R., 1966, Nature, 209, 1065.

Bray, J.R., 1967, Science, 156, 640.

Brinkmann, R., Münnich, K.O. and Vogel, J.C., 1959, Naturwiss. 46, 10.

Broecker, W.S. and Olson, E.A., 1959, Am. J. Sci. Radiocarbon Suppl. 1, 111.

Broecker, W.S. and Walton, A., 1959, Science 130, 309.

Broecker, W.S. and Olson, E.A., 1960, Science, N.Y. 132, 712.

Broecker, W.S., Gerard R., Ewing M. and Heezen, B.C., 1960, J. of Geophys. Res., 65, 2903.

Broecker, W.S. and Olson, E.A., 1961, Radiocarbon 3, 176.

Brown, H., 1957. The carbon cycle in nature, in "Fortschritte der Chemie organischer Naturstoffe" (ed. Zechmeister, L.) 14, 317.

Brunnée, C. and Voshage, H., 1964, Massenspektrometrie, München, Thieming, (1964).

Bucha, V., 1963, Travaux de l'Inst. Geophys. Prague, No. 170, 207.

Bucha, V., 1967, Nature, 213, 1005.

Bucha, V., 1970, Radiocarbon variations and absolute chronology, 12th Nobel Symp. (ed. Olsson, I.U.), Wiley, New York, 501.

Burke, W.H. and Meinschein, W.G., 1955, Rev. Sci. Instr., 26, 1137.

Cain, W.F. and Suess, H.E., 1976, J. Geophysical Res., Vol. 81, No. 21, 3688.

Callendar, G.S., 1938, Quart. J. Roy. Met. Soc., 64, 223.

Callendar, G.S., 1958, Tellus, 10, 243.

Callow, W.J., Baker, M.J. and Hassall, G.I., 1965, 6th Internat. Conf. Radiocarbon and Tritium Dating Proc., Pullman, 393.

Calvert, S.E. and Price, N.B., 1970, Contr. Miner. Petrol., 29, 215.

Cambray, R.S., Jefferies, D.F. and Topping, G., 1975, U.K.A.E.A. Publication A.E.R.E.-R 7733, H.M.S.O.

Campbell, J.A., 1977, pers. comm.

Clark, R.M., 1975, Antiquity, 49, 251.

Clyde River Purification Board, 1974, 19th Annual Report.

Clyde River Purification Board, 1975, 20th Annual Report.

Clyde River Purification Board, 1976, 21st Annual Report.

Cowan, C., Atluri, C.R. and Libby, W.F., 1965, Nature, 206, 861.

Cox, A., 1969, Science, 163, 237.

Craib, J.S., 1965, J. Cons. Perm. Int. Explor. Med., 1, 34.

Craig, H., 1953, Geochim. et Cosmochim. Acta, 3, 59.

Craig, H., 1954, J. Geol., 62, 115.

Craig, H., 1957, Geochim. et Cosmochim. Acta, 12, 133.

Craig, R.E., 1959, Mar. Res., 20, 30.

Damon, P.E., Long, A. and Grey, D.C., 1966, J. Geophys. Res. 71, 1055.

Damon, P.E., 1968, Meteorol. Monogr., 8, 151.

Damon, P.E., 1970, Radiocarbon variations and absolute chronology, 12th Nobel Symposium (ed. Olsson, I.U.,) , Wiley, New York, 571.

Damon, P.E. and Wallick, E.I., 1971, presented paper, American Geophys. Union, Washington.

Damon, P.E., Long, A. and Wallick, E.I., 1973, Earth and Planet Sci. Lett. 20, 300

Deegan, C.E., Kirby, R., Rae, I. and Floyd, R., 1973, Institute of Geological Sciences Report No. 73/9, H.M.S.O.

de Geer, G., 1940, Kungl. Sv. Vetensk. Akad. Handl. Ser. 3, 18, No.6.

Dergachev, V.A., Kocharov, G.E., and Rumyantsev, S.A., 1974, 5th National Meeting on "Astrophysical phenomena and radiocarbon", Tbilisy, Proc. , 9.

Dergachev, V.A., Tleugaliev, S. Kh., Zhitorchuk, Iv. V., 1976, Akad. Nauk S.S.S.R., Lenin's Physics-Techn. Institut, A.F.I.O.F.F.E., 1.

de Vries, Hl. and Barendsen, G.W., 1953, Physica 19, 987.

de Vries, Hl., 1958, Koninkl. Ned. Akad. Wetensch. Proc. B61, 94.

Dolctov, V.A., 1968, Solnechuyye dannyye, 9, 69.

Dyck, W., 1965, Radiocarbon and tritium dating, Proc. 6th Intern. Conf., Pullman, 440.

Eddy, J.A., 1976, Science, Vol. 192, No. 4245, 1189.

Elsasser, W.E., Ney, P. and Wincler, J.R., 1956, Nature 178, 1226.

Erlenkeuser, H., Suess, E. and Willkomm, H., 1973, Geochim. et Cosmochim. Acta, Vol. 38, 823.

Fairhall, A.W., Schell, W.R. and Takashimo, Y., 1961, Rev. Sci. Instr. 32, 323.

Fairhall, A.W. and Young, J.A., 1970, Radiocarbon in the environment, radionuclides in the environment, Am. Chem. Society, Washington D.C., 401.

Farmer, J.G., 1972, Ph.D. thesis, University of Glasgow.

Farmer, J.G. and Baxter, M.S., 1973, Earth and Plan. Sci. Lett., 20, 295.

Farmer, J.G., 1977, pers. comm.

Ferguson, C.W., 1968, Science, 159, 839.

Ferguson, C.W., 1969, Tree Ring Bull., 29, 1.

Fergusson, G.J., 1955, Nucleonics, 13 (1), 18.

Fergusson, G.J., 1958, Proc. Roy. Soc. Lond., A 243, 561.

Fergusson, G.J., 1963, J. Geophys. Res., 68, 3733.

Firbas, F., 1949, Spat -und nacheiszeitliche Wald-geschichte Mitteleuropas nordlich der Alpen, (ed. V.G. Fisher), 480.

Godwin, H., 1962, Nature, 195, 943.

Grey, D.C., 1969, J. Geophys. Res., 74, 6333.

Grey, D.C., Damon, P.E., Haynes, C.V. and Long, A., 1969, Radiocarbon, 11, 1.

Hagemann, F.T., Gray, J. Jr., Machta, L. and Turkevich, A., 1959, Science, 130, 542.

Harkness, D.D., 1970, Ph.D. thesis, University of Glasgow.

Harkness, D.D., 1973, pers. comm.

Harrison, C.G.A. and Funnell, B.M., 1964, Nature, 204, 566.

Hayes, F.N., Anderson, E.C. and Arnold, J.R., 1955, Internat. Conf. on the Peaceful Uses of Atomic Energy, 14, Proc., Geneva, 188.

Hill, K.J. and Winter, E.R.S., 1956, J. Phys. Chem., 60, 1361.

Houtermans, J., 1966, Z. fur Physik, 193, 1.

Jansen, H.S., 1970, Radiocarbon variations and absolute chronology, 12th Nobel Symp., (ed. Olsson, I.U.), Wiley, New York, 261.

Jenkinson, D.F., 1966, J. Soil Sci., 17, 280.

Kaplan, L.D., 1960, Tellus, 12, 204.

Karlen, J., Olsson, I.U., Kalberg, P. and Killicci, S., 1964, Arkiv. Geophysik, 4, 465.

King, J.W., 1973, Nature, 245, 443.

Kocharov, G.E., Arslanov, Kh.A., Dergachev, V.A., Rumyantsev, S.A., Chernov, S.B. and Goucharov, V.F., 1974, 5th National Meeting on "Astrophysical phenomena and radiocarbon", Tbilisy, Proc. (1974), 19.

Koide, M., Soutar, A and Goldberg, E.D., 1972, Earth Planet. Sci. Lett., 14, 442.

Konstantinov, B.P. and Kocharov, G.E., 1965, Dokl. Akad. Nauk S.S.S.R., 165, 63.

Labeyrie, J., Delibrias, G. and Duplessy, J.C., 1970, Radiocarbon variations and absolute chronology, 12th Nobel Symp., (ed. Olsson, I.U.), Wiley, New York, 539.

Lal, D. and Rama, J., 1966, J. Geophys. Res., 71, 2865.

Lal, D. and Suess, H.E., 1968, Ann. Rev. Nuclear Sci., 18, 407.

Lal, D. and Venkatavaradan, V.S., 1970, Radiocarbon variations and absolute chronology, 12th Nobel Symp., (ed. Olsson, I.U.) Wiley, New York, 549.

Lamb, H.H., 1961, Ann. New York Acad. Sci., 95, 124.

Lamb, H.H., 1965, Quart. J.R. Met. Soc., 91, 546.

Lamb, H.H., Lewis, R.P.W. and Woodroffe, A., 1966, Roy. Meteorol. Soc. Proc. Intern. Symp. on World Climate 8000 to 0 B.C., 174.

Lavrukhina, A.K., Alekseev, V.A., Galinov, E.N. and Sulerzhitsky, L.D., 1973, Doklady Akad. Nauk S.S.S.R., 210, 941.

Leatherland, T.M., 1976, pers. comm.

Leatherland, T.M., 1977, pers. comm.

Lerman, J.C., Mook, W.G. and Vogel, J.C., 1970, Radiocarbon variations and absolute chronology, 12th Nobel Symp. (ed. Olsson, I.U.), Wiley, New York, 275.

Libby, W.F., 1946, Phys. Rev., 69, 671.

Libby, W.F., 1955, Radiocarbon dating, University of Chicago Press.

Libby, W.F., 1965, Radiocarbon dating, University of Chicago Press, 175.

Likens, G.E., Bormann, F.H., Johnson, N.M., Fisher, D.W. and Pierce, R.S., 1969, Ecol. Monogr., 40, 23.

Lingenfelter, R.E., 1963, Rev. Geophy., 1, 35.

Lingenfelter, R.E. and Ramaty, R., 1970, Radiocarbon variations and absolute chronology, 12th Nobel Symp., (Olsson, I.U., ed.), Wiley, New York, 496.

Lomenick, T.F. and Gardiner, D.A., 1965, Health Phys., 11, 567.

Long, A., 1965, Radiocarbon and tritum dating, Proc. 6th Intern. Conf., Pullman, 1965, 37.

Machta, L., 1959, Hearings of the Joint Comm. on Atomic Energy Congress of the U.S.A., 3, 2191.

MacKenzie, A.B., 1977, pers. comm.

Mackereth, F.J.H., 1958, Limnol. Oceanog., 3, 181.

Mackereth, F.J.H., 1966, Phil. Trans. Roy. Soc., B 250, 165

MacPhail, I.M.M., 1962, A short history of Dumbartonshire, ed. Bennett and Thomson, Dumbarton.

McCrea, J.M., 1950, J. Chem. Phys., 18, 849.

McKinley, I.G., MacKenzie, A.B., Jack, W. and Baxter, M.S., 1976, Paper presented to 3rd E.G.S. Meeting, Amsterdam.

McKinley, I.G., 1977, pers. comm.

Mill, H.R., 1892, Trans. Roy. Soc. Edinburgh, 36, 641.

Moore, H.B., 1931, J. Mar. Biol. Assoc. U.K., 17, 325.

Münnich, K.O. and Roether, W., 1967, Radioactive dating and methods of low-level counting, Proc. Symp., I.A.E.A., Vienna, 93.

Münnich, K.O., 1968, Naturwissenschaften, 55, 158.

Murdoch, J.D. and Barnes, J.A., 1974, Statistical tables for science, engineering, management and business studies, Macmillan, London.

Murdoch, J.D., 1974, pers. comm.

Natural Environment Research Council, 1974, "Pollution in Clyde", Publ. Ser. C, 11, 10.

Nilsson, T., 1964, Publ. 124, Inst. of Mineralogy, Paleontology and Quaternary Geol., Univ. of Lund, Publ. 124, 52pp.

Nydal, R., 1963, Nature, 200, 212.

Nydal, R., 1966, Tellus, 18, 172.

Olsson, I.V., Karlen, I., Turnbull, A.H. and Prosser, N.J.D., 1962, Arkiv Fysik, 22, 3.

Opdyke, N.D., Glass, B., Hays, J.D. and Foster, J.H., 1966, Science, 154, 349.

O'Sullivan, P.E., Oldfield, F. and Battarbee, R.W., 1973, Quaternary plant ecology (ed. Birks, H.J.B. and West, R.G.), 267.

Overbeck, F., 1950, Geologie und Lagerstatten Niedersächsens, 3, 4.

Pendleton, R.C. and Hanson, W.C., 1958, Proc. Intern. Conf. Peaceful Uses of Atomic Energy, Geneva, 18, U.N., New York, 419.

Pennington, W., Cambray, R.S., Eakins, J.D., Harkness, D.D., 1976, Freshwater Biology, 6, 317.

Plato, P. and Goldman, G.C., 1972, Radiation Data and Reports, 13, 12, 653.

Plass, G.N., 1956, Tellus, 8, 140.

Rafter, T.A., 1965A, New Zealand J. Sci., 8, 451.

Rafter, T.A., 1965B, New Zealand J. Sci., 8, 472.

Rafter, T.A. and Stout, J.D., 1970, Proc. 12th Nobel Symp. on Radiocarbon Variations and Absolute Chronology (ed. Olsson, I.U.), Wiley, New York, 401.

Rafter, T.A. and O'Brien, B.J., 1970, Proc. 12th Nobel Symp. on Radiocarbon Variations and Absolute Chronology (ed. Olsson, I.U.), Wiley, New York, 355.

Ralph, E.K., Michael, H.N. and Han, M.C., 1973, MASCA Newsletter, 9, 1.

Reiter, R., 1973, J. Geophys. Res., 78, 6167.

Revelle, R. and Suess, H.E., 1957, Tellus, 9, 18.

Revelle, R., 1965, Atmospheric CO_2, Appendix Y4 of Restoring the Quality of the Environment, Report of the Envir. Pollution Panel, President's Sc. Adv. Comm., 111.

Ritchie, J.C., McHenry, J.R., Gill, A.C. and Hawks, P.H., 1971, Proc. 3rd Nat. Symp. Radioecol., U.S.A.E.C. Conf. - 710501.

Roberts, W.O., 1960, J. Geophys. Res., 65, 2.

Roberts, W.O., 1962, Proc. Internat. Symp. on Stratospheric and Mesopheric Circulation, Berlin, 341.

Roberts, W.O. and Olson, R.H., 1973, J. Atmosph. Sci., 30, 135.

Schell, W.R., Fairhall, A.W. and Harp, G.D., 1965, 6th Intern. Conf. Radiocarbon and Tritium Dating, Proc., Pullman, 397.

Schmitz, J., 1968, Studien zur europaischen Vor -und Fruhgeschichte (ed. Claus, M., Haarnagel, W., Raddatz, K.), 409.

Schove, D.J., 1955, J. Geophys. Res., 60, 127.

Schuurmans, C.J.E., 1969, Meded. Verh. Kon. Nederl. Meteorol. Inst., 92.

Shannon, L.V. and Cherry, R.D., 1971, Earth Plan. Sci. Lett., 11, 339.

Shapiro, R., 1959, J. Meteorol., 16, 569.

Shapiro, R. and Ward, F., 1962, J. Atmsoph. Sci., 19, 60.

Sissons, J.B., 1967, The evolution of Scotland's scenery, Oliver and Boyd, Edinburgh, 451.

Starka, H., 1970, Pollenanalyse und Vegetationsgeschichte, 109.

Stenhouse, M.J., 1974, Ph.D. Thesis, University of Glasgow.

Stenhouse, M.J. and Baxter, M.S., 1976, Radiocarbon, 18, 161.

Stewart, D.R., 1977, pers. comm.

Stolov, H.L. and Shapiro, R., 1974, J. Geophys. Res., 79, 2161.

Stuiver, M.J., 1961, J. Geophys. Res., 66, 273.

Stuiver, M.J., 1965, Science, 149, 533.

Stuiver, M.J., 1967, Radioactive dating and methods of low-level counting, Proc. Conf. I.A.E.A., Vienna, 27.

Stuiver, M.J., 1969, Radiocarbon, 11, 545.

Stuiver, M.J., 1970, Proc. 12th Nobel Symp. on Radiocarbon Variations and Absolute Chronology (ed. Olsson, I.U.),

Wiley, New York, 197.

Stuiver, M.J., 1970A, Nature, 228, 454.

Stuiver, M.J., Robinson, S.W., Osthund, H.G. and Dorsey, H.G., 1974, Earth and Planet. Sci. Lett., 23, 65.

Stuiver, M.J., 1976, pers. comm.

Suess, H.E., 1954, Science, 120, 1.

Suess, H.E., 1955, Science, 122, 415.

Suess, H.E., 1965, J. Geophys. Res., 70, 5937.

Suess, H.E., 1967, Radioactive dating and methods of low-level counting, Proc. Conf. I.A.E.A., Vienna, 143.

Suess, H.E., 1968, Met. Monogr., 8, 146.

Suess, H.E., 1969, Bild der Wissenschaft (ed. Haber, H.), Stuttgart, 121.

Suess, H.E., 1970, Proc. 12th Nobel Symp. on Radiocarbon Variations and Absolute Chronology (ed. Olsson, I.U.), Wiley, New York, 303, 595.

Swan, D.S., MacKenzie, A.B., Jack, W. and Baxter, M.S., 1976, Paper presented to 3rd E.G.S. Meeting, Amsterdam.

Swan, D.S., 1977, pers. comm.

Tamura, T. and Jacobs, D.G., 1960, Health Phys., 2, 391.

Tauber, H., 1960, Science, 131, 921.

Tauber, H., 1970, Proc. 12th Nobel Symp. on Radiocarbon Variations and Absolute Chronology (ed. Olsson, I.U.), Wiley, New York, 173.

Telegades, K., 1971, U.S.A.E.C. Health Safety Lab. Report, HASL-243.

Thompson, R., 1975, Geophys. J. Roy. Astr. Soc., 43, 847.

Thompson, R., 1977, J. Geol. Soc., 133, 51.

Thompson, R., 1977A, pers. comm.

Twitchell, P.F., 1963, Bull. Geophys., 13, 69.

Urey, H.C., Lowenstam, H.A., Epstein, S. and McKinney, C.R., 1951, Bull. Geol. Soc. Amer., 62, 399.

Vinogradov, A.P., Devirts, A.L. and Dobkina, E.I., 1966, Dokl. Akad. Nauk S.S.S.R., 168, 900.

Vogel, J.C., 1970, Proc. 12th Nobel Symp. on Radiocarbon Variations and Absolute Chronology (ed. Olsson, I.U.), Wiley, New York, 313.

Walton, A., Ergin, M. and Harkness, D.D., 1970, J. Geophys. Res., 75, 3089.

Willis, E.H., 1960, Nature, 185, 552.

Willis, E.H., Tauber, H. and Munnich, K.O., 1960, Amer. J. Sci. Suppl. Radiocarbon, 2, 1.

Wilson, A.T., 1961, Nature, 191, 714.

Wilson, A.T., 1963A, Nature, 197, 711.

Wilson, A.T., 1963B, Nature, 198, 500.

Young, J.A. and Fairhall, A.W., 1968, J. Geophys. Res., 73, 1185.